NASA Conference Publication 2381

Structural Integrity and Durability of Reusable Space Propulsion Systems

Proceedings of a conference held at NASA Lewis Research Center Cleveland, Ohio June 4–5, 1985

NASA

NASA Conference Publication 2381

Structural Integrity and Durability of Reusable Space Propulsion Systems

Proceedings of a conference
sponsored by the NASA Office of Aeronautics and
Space Technology and Office of Space Flight
and the NASA Lewis Research Center
and held at NASA Lewis Research Center
Cleveland, Ohio
June 4–5, 1985

NASA
National Aeronautics
and Space Administration

Scientific and Technical
Information Branch

1985

FOREWORD

The space shuttle main engine, a reusable space propulsion system, is the most sophisticated rocket engine in use today. However, on the premise that the United States will depend on the shuttle and its derivatives as its principal Earth-to-orbit transportation system for the next several decades, the National Aeronautics and Space Administration (NASA) has decided to continually upgrade SSME capabilities. Therefore, NASA has initiated a research and technology program for advanced high-pressure oxygen-hydrogen rocket technology. This program is intended to establish the basic discipline technology and to develop new analytical tools for an orderly evolution of reusable rocket systems.

A substantial portion of this technology program is devoted to the structural integrity and durability aspects of reusable space propulsion systems. This effort will improve the understanding of aerothermodynamic loads, structural dynamics, and fatigue, fracture, and life issues in the SSME and its derivative engines. The overall approach is to examine and modify existing analytical methods, to develop new methods where needed, and to verify them in systematic test programs. The research is conducted through industrial contracts, university grants, and in-house activities at the Lewis Research Center.

To provide a forum for representatives from government, industry, and academia to learn about and discuss the latest findings and progress toward improved structural integrity and durability of reusable space propulsion systems, a two-day conference was held at Lewis in June 1985. This publication contains extended abstracts of the papers presented at that conference.

Stanley J. Marsik
Conference Chairman

CONTENTS

OAST TECHNOLOGY PROGRAM - DURABILITY EFFORT

F.W. Stephenson, Jr.
NASA Headquarters
Washington, D.C. 20546

The NASA Office of Aeronautics and Space Technology has in place a program directed toward technology advances needed to improve service life, performance, and operations of reusable rocket engines such as the space shuttle main engine (SSME), its derivatives, and advanced engines of this class. The program is focused on the development of (1) accurate analytical models for describing flow fields, aerothermodynamic loads, structural response rotordynamics, bearing characteristics, etc., from which life predictions codes can be evolved; (2) the technology for longer life components such as bearings, seals, turbine blades, and combustors; and (3) advanced instrumentation to better measure the engine internal operating environments and to develop diagnostic sensors for real-time condition monitoring of critical engine components. The program is supported by a strong effort in materials and processes development and evaluation.

An integral part of the reusable rocket engine technology program is the structural integrity and durability effort, which is the subject of this conference and which is focused on the hot-gas flow system of staged combustion engines like the SSME. This presentation provides a brief overview of the overall technology program and the relationship between the overall program and the structural integrity and durability effort.

OVERVIEW OF AEROTHERMODYNAMIC LOADS DEFINITION STUDY

Louis A. Povinelli
National Aeronautics and Space Administration
Lewis Research Center
Cleveland, Ohio 44135

The objective of the Aerothermodynamic Loads Definition Study* is to develop methods to more accurately predict the operating environment in the space shuttle main engine (SSME) components. Development of steady and time-dependent, three-dimensional viscous computer codes as well as experimental verification and engine diagnostic testing are considered to be essential in achieving that objective. The steady, nonsteady, and transient operating loads must all be well defined in order to accurately predict powerhead life. Improvements in the structural durability of the SSME turbine drive systems will depend on our knowledge of the aerothermodynamic behavior of the flow through the preburner, turbine, turnaround duct, gas manifold, and injector post regions.

The study was begun in October 1983. The various elements in the study were described in December 1983 at the initial meeting of the SSME Durability Activity at Lewis. During the first year, emphasis was placed on the computations of the turbine losses, the redistribution of the radial temperature profile through the turbines, and the flow behavior in the turnaround duct. A viscous computation was also carried out for the fuel turbine rotor, and work was begun on a time-dependent turbomachinery code. Experimentally, an unsteady heat transfer apparatus was designed, and instrumentation was fabricated for installation in a low-aspect-ratio turbine. Highlights of the first year's accomplishments were as follows:

(1) Computations of the fuel turbine losses indicated a potential improvement of 8 to 10 points by reducing blade roughness and platform leakage.

(2) Oxidizer turbine loss could be reduced 5 to 7 points by redesigning for correct rotor incidence angles.

(3) Turbine inlet temperature profiles were not significantly changed through the turbines. It was concluded that the high solidity led to relatively lightly loaded surfaces and reduced secondary flow generation. Hence temperature redistribution was reduced.

(4) Viscous computations of the first-stage rotor profile, using flow conditions supplied by Rocketdyne, revealed a flow separation on the pressure side. Subsequent computations, using newly computed stator exit conditions, did not reveal any separation.

(5) The first manned orbital flight (FMOF) and full power level (FPL) turnaround ducts were analyzed by using a viscous computation. After a detailed study of the pressure losses, flow separation, diffusion, and

*This study is part of the activity of the Fluid and Gas Dynamic Working Group of the SSME Technology Program.

acceleration through the turn, a new geometry was computationally defined within the available space envelope. The modified design of the turnaround duct had minimum pressure loss and reduced the potential for flow separation.

(6) Substantial effort was devoted to fabricating and installing high-response heat flux gauges on a low-aspect-ratio turbine. This apparatus will be used to determine the response of the blade surfaces to temperature variations introduced by upstream disturbances.

The results obtained during the first year of the study were presented in two workshops (March and November 1984) and at the Advanced High Pressure O_2/H_2 Technology Conference (June 1984), all held at the Marshall Space Flight Center. A summary of the results was also presented at the SAE Aerospace Congress Meeting (November 1984). A list of references is included. The material to be presented in this session will update these results. It represents the effort since October 1984 and is focused on the turbine components. It is anticipated that the upcoming year's effort will be directed toward the unsteady aspects of the turbine flows.

REFERENCES

1. Chima, R.V., Analysis of Inviscid and Viscous Flows in Cascades with an Explicit Multiple-Grid Algorithm - Application to an SSME Fuel Pump Turbine Rotor. Presented at the Computational Fluid Mechanics Workshop, Marshall Space Flight Center, March 14-15, 1984.

2. Haas, J.E.: Turbine Loss Assessment Using Quasi 3-D Flow and Boundary Layer Analysis Methods. Presented at the Computational Fluid Mechanics Workshop, Marshall Space Flight Center, March 14-15, 1984.

3. McFarland, E.R.: A Rapid Blade-to-Blade Solution for Use in Turbomachinery Design - Application to the SSME Fuel Pump Turbines. Presented at the Computational Fluid Mechanics Workshop, Marshall Space Flight Center, March 14-15, 1984.

4. Povinelli, L.A.: Overview of the LeRC CFM Activity in the Aerodynamics Loads Program. Presented at the Computational Fluid Mechanics Workshop, Marshall Space Flight Center, March 14-15, 1984.

5. Haas, Jeffrey E.: Fuel and Oxidizer Turbine Loss Analysis. Proceedings of Marshall Space Flight Center Advanced High Pressure O_2/H_2 Technology Conference. S.F. Morea and S.T. Wu, eds., Marshall Space Flight Center, 1984. pp. 288-293.

6. McLallin, Kerry L.: Analytical Study of Flow Phenomena in SSME Turnaround Duct Geometries. Proceedings of Marshall Space Flight Center Advanced High Pressure O_2/H_2 Technology Conference. S.F. Morea and S.T. Wu, eds., Marshall Space Flight Center, 1984. pp. 298-308.

7. Schwab, John R.: Redistribution of the Inlet Temperature Profile Through the SSME Fuel Turbine. Proceedings of Marshall Space Flight Center Advanced High Pressure O_2/H_2 Technology Conference. S.F. Morea and S.T. Wu, eds., Marshall Space Flight Center, 1984. pp. 294-297.

8. Povinelli, L.A., et al.: Application of Viscous and Inviscid Computational Methods for Rocket Turbopump Systems. Space Propulsion - Advanced Concepts Systems and Technology, SAE SP-593, SAE, 1985.

9. Adamczyk, John J.; and Celestina, Mark L.: Three-Dimensional Euler Solver for Turbomachinery. Computational Fluid Dynamics Workshop, Marshall Space Flight Center, Nov. 1984.

10. Chen, S.S.: Flow-Induced Vibration of the SSME LOX Posts. Computational Fluid Dynamics Workshop, Marshall Space Flight Center, Nov. 1984.

11. Jorgenson, Philip C.E.: Viscous Turbine Computations. Computational Fluid Dynamics Workshop, Marshall Space Flight Center, Nov. 1984.

12. Schwab, John R.: Turbine Temperature Redistribution Effects. Computational Fluid Dynamics Workshop, Marshall Space Flight Center, Nov. 1984.

13. VanOverbeke, T.; and Claus, R.: Numerical Accuracy Considerations in a Turn-Around Duct Geometry. Computational Fluid Dynamics Workshop, Marshall Space Flight Center, Nov. 1984.

14. Chen, S.S.; and Jendrzejcyk, J.A.: Flow-Induced Vibration of the SSME LOX Posts. ANL-84-75, Argonne National Lab. Sept. 1984.

15. Huff, Ronald G.: A Theoretical Prediction of the Acoustic Pressure Generated by Turbulence-Flame Front Interaction. NASA TM-83567, 1984.

16. Civinskas, K.C.: Quasi-3D and STAN5 Analysis of LART Stage and Comparison with CALSPAN Data. Presented at the Turbine Heat Transfer Mini-Symposium, February 26-27, 1985, CALSPAN Advanced Technology Center, Buffalo, New York.

SSME FUEL PREBURNER TWO-DIMENSIONAL ANALYSIS

Thomas J. VanOverbeke
National Aeronautics and Space Administration
Lewis Research Center
Cleveland, Ohio 44135

The durability of the SSME turbine is strongly affected by the temperature profile leaving the preburner. Experimental measurements of this temperature profile are difficult to obtain because of the severe operating environment within the SSME. Therefore a designer attempting to tailor the flow entering the preburner to conform to acceptable temperatures must either engage in an expensive and difficult experimental effor or be overly conservative in the design. With recent advances in computational capabilities, a more promising design approach is to use a reacting flow computer model to predict the turbine inlet temperature profile. This is the objective of the current study. A series of calculations were made, using a reacting flow code, to assess the sensitivity of the turbine inlet temperature profile to variations in the flow entering the SSME preburner.

A two-dimensional teaching type of combustion code was modified to work with preburner geometry. The program solves the fully elliptic, steady-state equations of motion. Either hybrid or bounded skew upwind differencing can be used. The pressure distribution was found by the pressure-implicit split operator (PISO) predictor-corrector technique. Closure for the equations of motion was provided by using the turbulent kinetic energy k and energy dissipation to obtain an effective eddy viscosity. The density was calculated from the ideal-gas law. Combustion was modeled by using the eddy breakup model of Magnussen and Hjertager. This model relates fuel combustion to turbulence. Combustion depends on the mixing of species and the dissipation of energy from hot combustion products. Combustion of the fuel in the code occurs as a negative source term for the fuel fraction depending on the dissipation of turbulent eddies (mixing) and the concentration of fuel, oxygen, and product in each grid cell.

The preburner was modeled as a series of coaxial nozzles injecting into a chamber. The walls were approximated by a fine rectangular mesh. Thus the rear wall of the prechamber model is a series of steps over which the gases flow to the powerhead turbine. A 70-by-53 grid was used. The density of the radial grid points was increased for the igniter and for the exit flow to ensure an accurate solution. The turbine inlet temperature profile was taken at 0.33 m, but calculations were performed to 0.5 m to ensure that exit boundary conditions for the code would not affect the temperature profile. The cooling flow along the outside wall, which eventually enters the prechamber, was included in the nozzle flow nearest the outside wall.

For most of the calculations the preburner inlet was divided into five regions of premixed reactants. The igniter was modeled as an inlet with a mixture of hydrogen and oxygen at low temperatures or a mixture of hydrogen and water at 1000 K. Changing the inlet condition produced little change in the turbine inlet temperature profile even though the flow was greatly changed in the inlet computational area. Also, changing the equivalence ratio of the inlet corresponding to the igniter did not change the turbine inlet temperature profile to any appreciable degree. One reason is that the igniter takes up the

smallest area of the inlet flow and contributes the smallest part of the flow. Changing larger areas of the flow than that of the igniter did change the temperature profile. Decreasing the equivalence ratio of any of the other inlet conditions produced temperature increases in the flow corresponding to that portion of the total inlet. Changing the inlet condition for the largest area had the greatest effect on the turbine inlet temperature profile. Also, increasing equivalence ratios decreased temperatures: the fuel-side SSME preburner operates so fuel rich that increasing the fuel flow decreases temperatures and decreasing the fuel flow increases temperatures. Decreasing just the outer inlet equivalence ratio resulted in a series of inlet boundary conditions with decreasing equivalence ratio toward the outer preburner wall. This run generated a temperature profile with temperatures increasing from the inner wall to the outer wall. A comparison calculation was made with increasing equivalence ratios toward the outer wall, keeping the overall mass flow similar. The resulting temperature profile was skewed in the opposite direction from the previous calculation.

The inlet turbulence was increased to 30 percent from 5.5 percent and decreased to 0.55 percent to see if the inlet turbulence had an effect on the temperature profile. Calculated temperatures differed only for a few grid points downstream of the nozzle inlets, and the turbine inlet temperature profile was essentially the same. The code was also run with five burned inlet conditions. That is, the combustion had already occurred, the reaction was not needed, and the temperature was a function of mixing. The turbine inlet temperature profile was essentially unchanged, even though inlet flow conditions were vastly different.

Finally, the number of inlet boundary conditions was increased to represent a coaxial series of alternating pure hydrogen and oxygen nozzles along with the igniter. The turbine inlet temperature profile was changed but only for a few of the outer grid points. Most of the turbine inlet temperature profile was unchanged even though temperatures varied widely downstream of the inlet nozzles because of the extreme variation in local equivalence ratios. Since the actual inlet for the preburner is a collection of more than 200 nozzles rather than a small number of coaxial nozzles, the calculation with alternating pure hydrogen or oxygen coaxial nozzles corresponds to a worst case. Thus the actual temperature profile should be closer to that generated with the five premixed inlet conditions.

The temperature profiles generated by these calculations with the eddy breakup combustion model show that the turbine inlet temperature profile is affected by changing the equivalence ratio (if the affected area is large enough) but that other aspects of modeling, such as modeling separate oxygen and hydrogen nozzles or modeling the inlet conditions as burned or unburned, have minor effects.

COMBUSTION MODEL

THE PRESENT CODE USES THE EDDY BREAKUP COMBUSTION MODEL WHICH RELATES COMBUSTION TO THE DISSIPATION OF TURBULENT EDDIES AND THE CONCENTRATION OF SPECIES.

$$H_2 + \frac{1}{2} O_2 \text{ ---- } H_2O + 1.21 \times 10^8 \text{ J/kg}$$

$$h = m_f H_R + C_{p,m} T$$

$$C_{p,m} = \sum m_l C_{pl}$$

$$C_{p,l} = \frac{R}{M_l} (C_{1l} + C_{2l} T + C_{3l} T^2 + C_{4l} T^3 + C_{5l} T^4)$$

THE COMBUSTION IS MODELED AS A SOURCE TERM FOR THE MASS FRACTION OF FUEL, m_f

$$Sm_f = -\rho \frac{\epsilon}{K} \min \left[Am_f, \; A \frac{m_{O2}}{STOIC}, \; AB \frac{m_{pr}}{STOIC+1} \right]$$

A and B are reaction constants
ϵ/K may be thought of as an eddy lifetime

THE RATE OF COMBUSTION IS

$$R_f = -Sm_f$$

FUEL PREBURNER INJECTOR CONFIGURATION

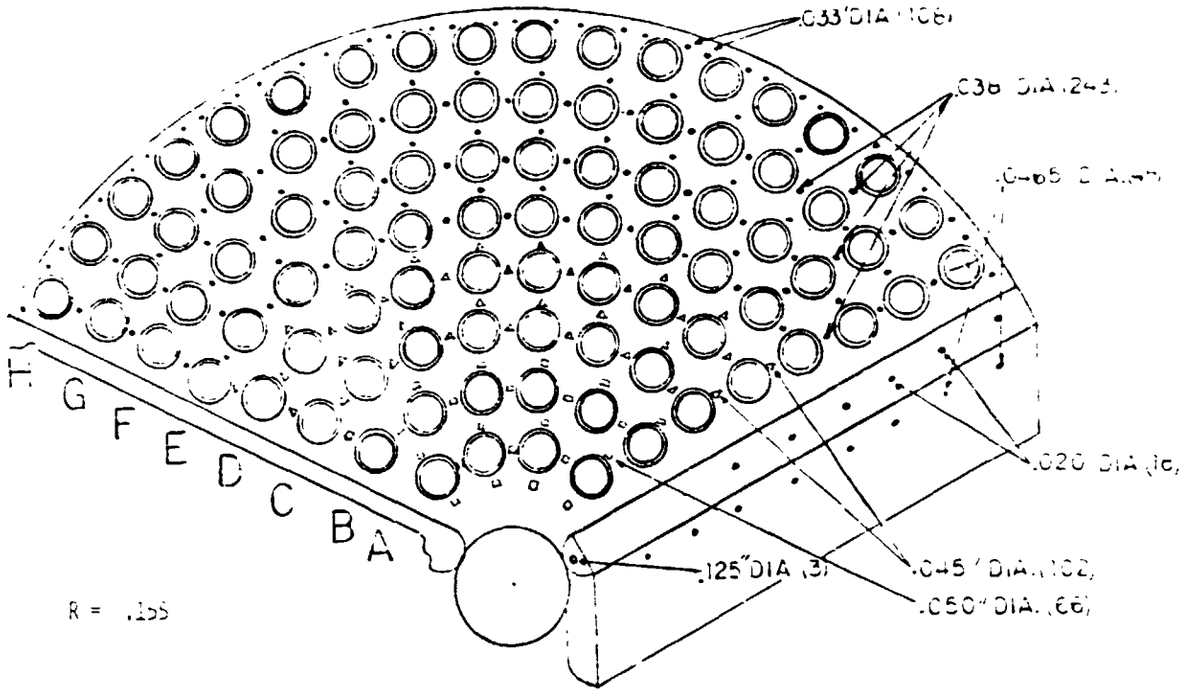

THE PREBURNER INJECTOR WAS DIVIDED INTO FIVE ZONES

ZONE	MASS FLOW (kg/s) O_2	H_2	VELOCITY (m/s)	TEMP (K)	EQUIVALENCE RATIO
IGNITER	.209		77.6	1000.0	9.2
A-B	4.70	4.81	23.9	162.8	8.18
C-D	8.46	7.92	24.7	162.5	7.49
EFG	19.75	17.44	23.3	162.4	7.07
H	7.52	8.27	25.6	162.9	8.79

T_{H_2}=165 K T_{O_2}=125 K

Zone H includes liner cooling

VELOCITY VECTOR DIAGRAM FOR BASELINE CALCULATION

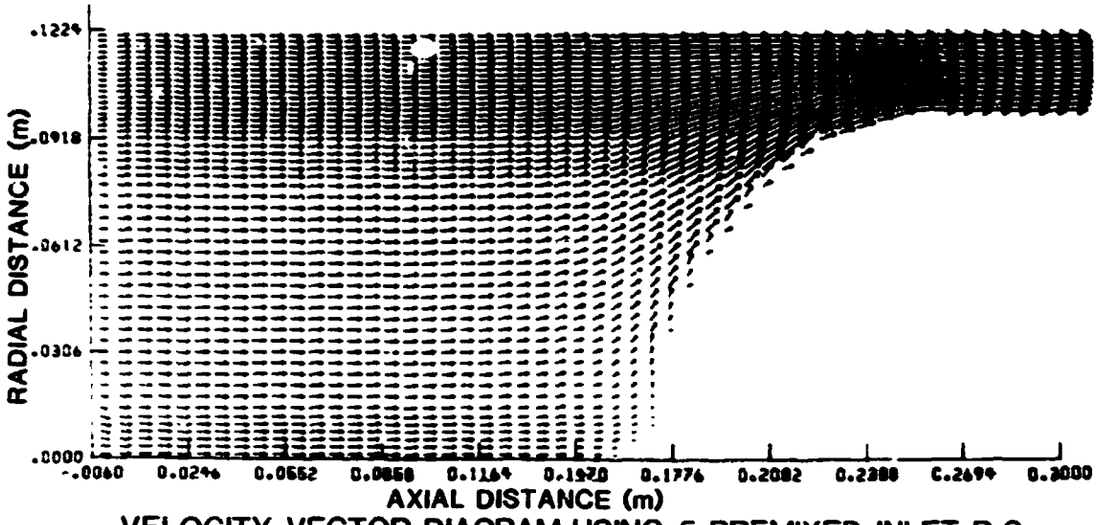

VELOCITY VECTOR DIAGRAM USING 5 PREMIXED INLET B.C.

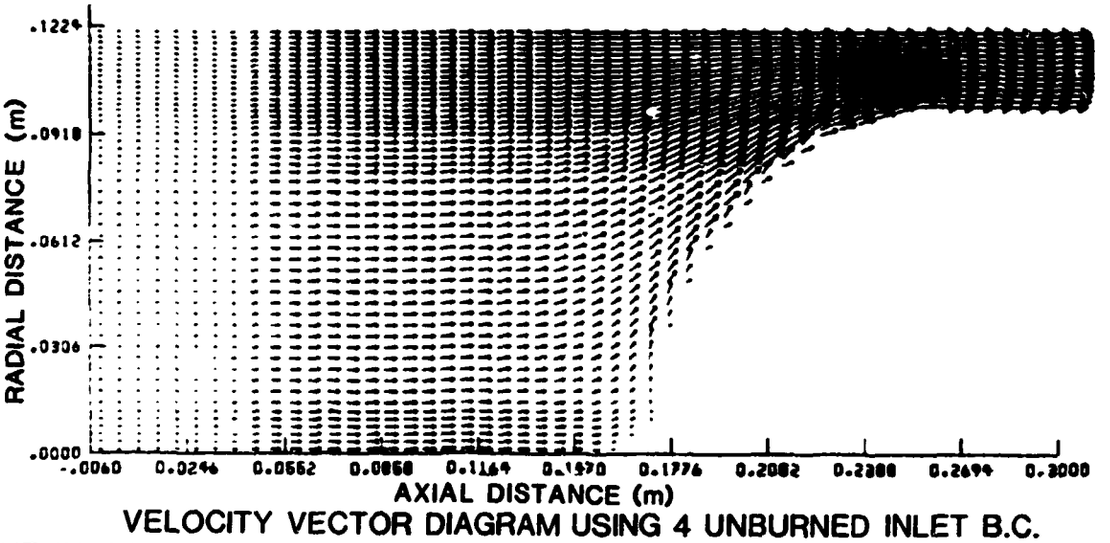

VELOCITY VECTOR DIAGRAM USING 4 UNBURNED INLET B.C.
THE INLET B.C. FOR ZONE A-B WAS ALSO USED FOR THE IGNITER ZONE

TURBINE INLET TEMPERATURE PROFILE AS A FUNCTION OF INLET B.C.

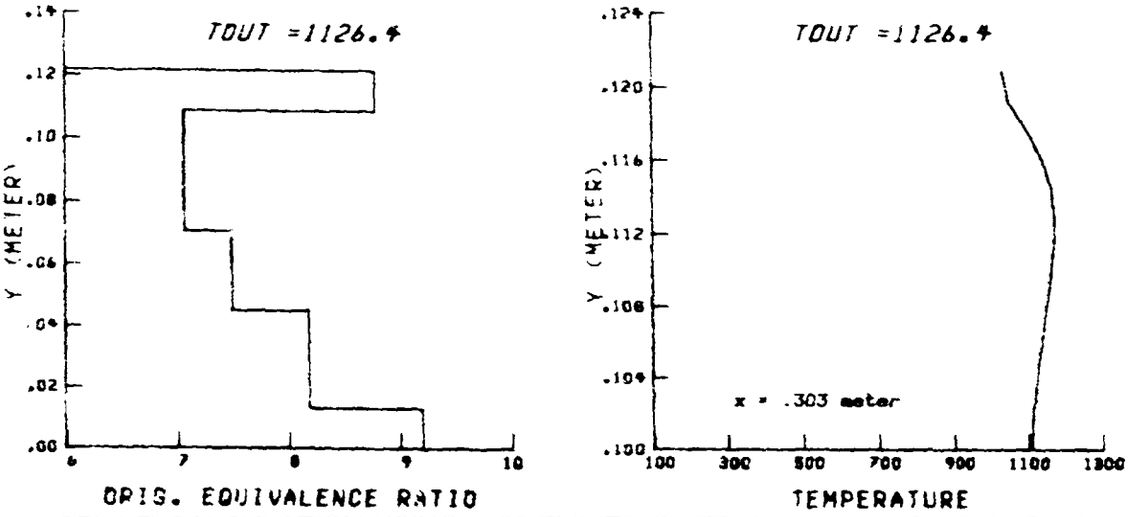

BASELINE CALCULATION USING 5 PREMIXED INLET B.C. CHANGING THE INLET TURBULENCE DIDN'T EFFECT THE TEMPERATURE PROFILE NOR DID MODELING OF THE INLET FLOW AS HOT BURNED GASES.

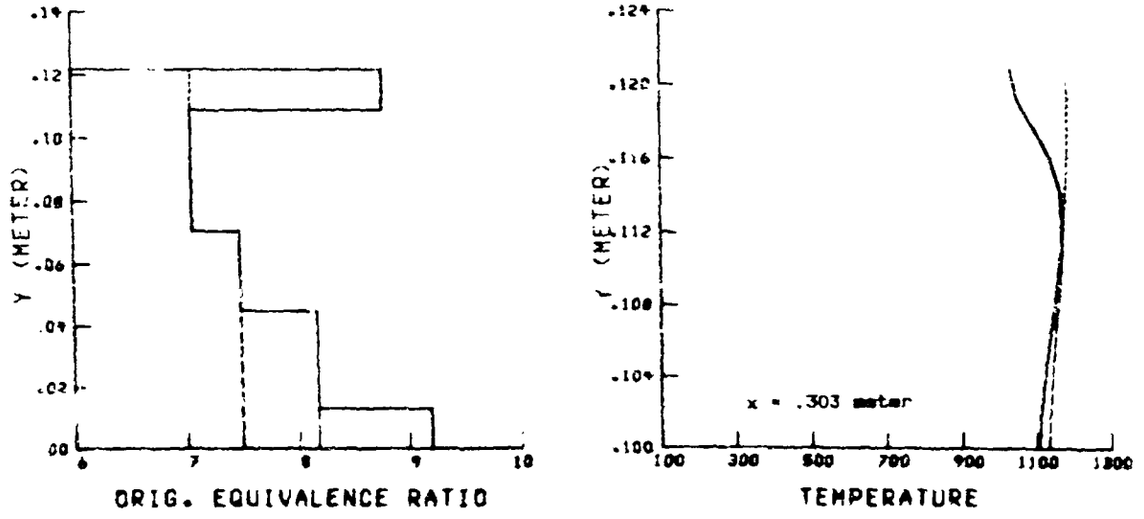

CHANGING THE INLET CONDITION FOR THE IGNITER TO THAT OF ZONE A-B DIDN'T CHANGE THE TEMPERATURE PROFILE NOTICEABLY, WHILE CHANGING B.C. FOR THE LARGER INLET ZONES DID CHANGE THE TEMPERATURE PROFILE

INLET TURBINE INLET TEMPERATURE PROFILE AS A FUNCTION OF INLET B.C.

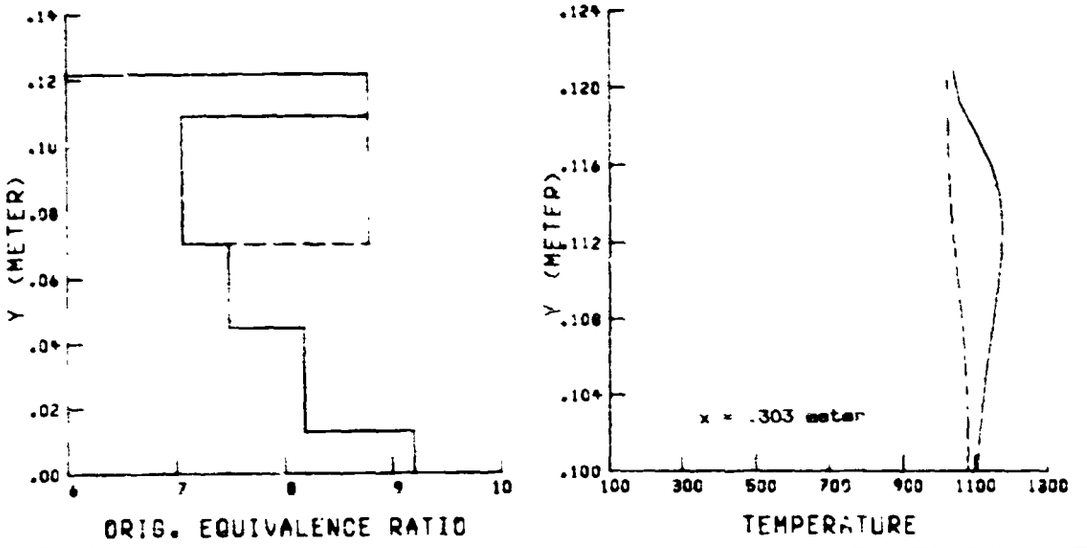

CHANGING THE INLET B.C. FOR ZONE E-F-G TO THAT OF ZONE H EFFECTED THE TEMPERATURE PROFILE THE MOST. ZONE E-F-G IS THE INLET FOR ALMOST 50% OF THE TOTAL FLOW.

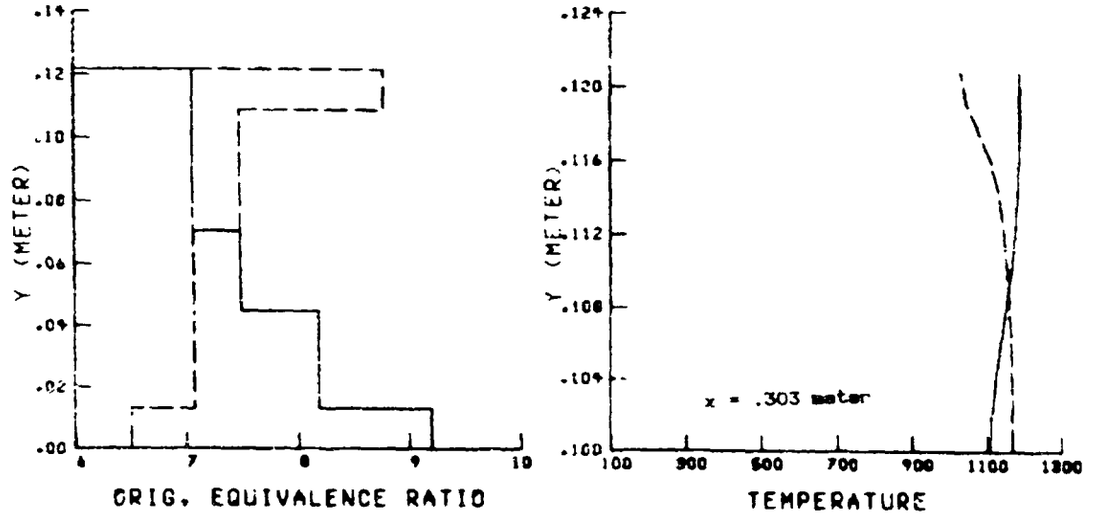

TEMPERATURE PROFILES RESULTING FROM A SET OF INCREASING OR DECREASING EQUIVALENCE RATIOS. THE INLET B.C. WERE CHANGED SO THAT THE OVERALL MASS FLOW WAS SIMILAR

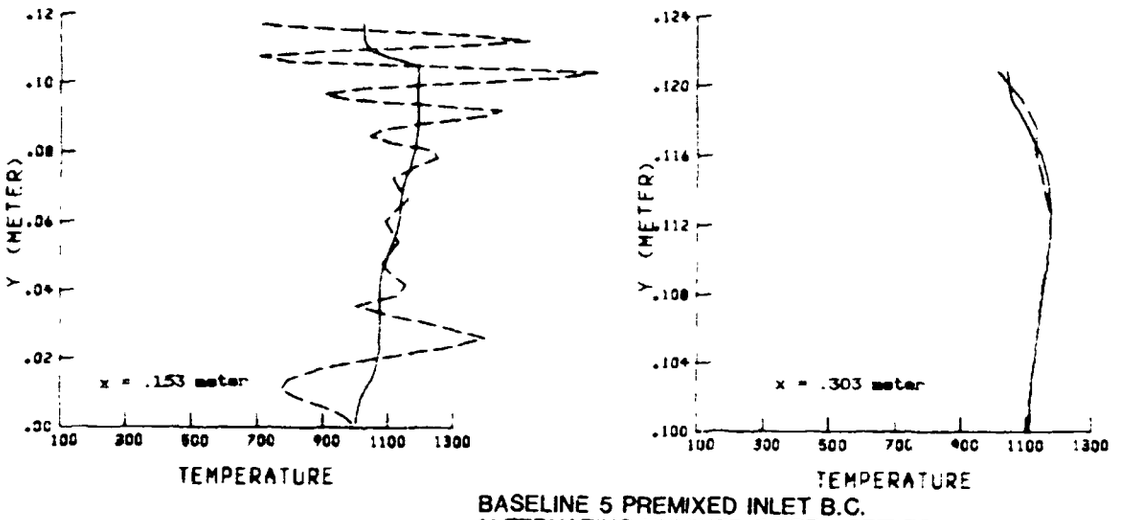

BASELINE 5 PREMIXED INLET B.C.
ALTERNATING UNMIXED INLET NOZZLES

THE TURBINE INLET TEMPERATURE PROFILE RESULTING FROM A LARGE NUMBER OF ALTERNATING PURE HYDROGEN OR OXYGEN INLET NOZZLES WAS ONLY EFFECTED AT THE TOP, EVEN THOUGH INTERMEDIATE TEMPERATURES DID VARY CONSIDERABLY

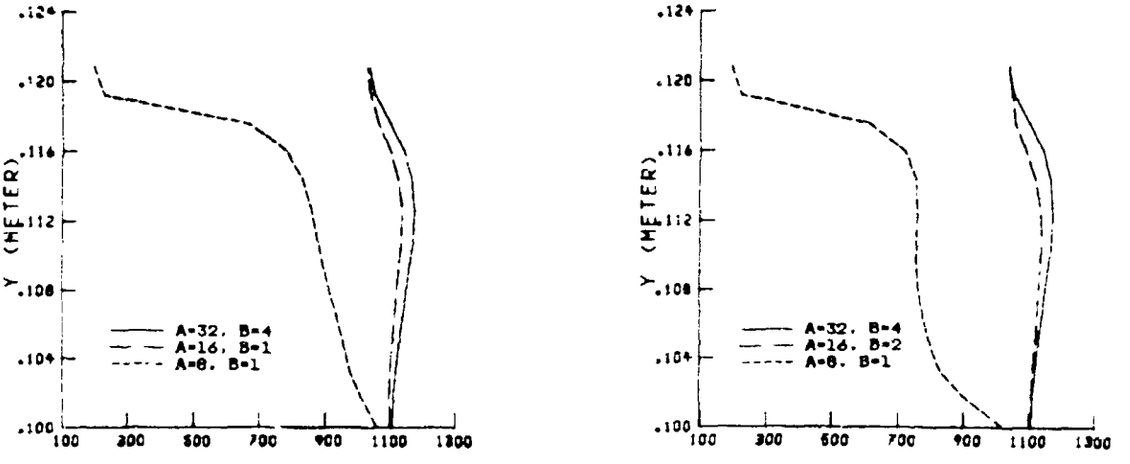

BASELINE INLET B.C.

IGNITER B.C. SAME AS ZONE A-B

USING LOWER REACTION CONSTANTS IN THE EDDY BREAKUP COMBUSTION MODEL RESULTED IN VARIOUS TEMPERATURE PROFILES

SSME TURBOPUMP TURBINE COMPUTATIONS*

Philip C.E. Jorgenson
Sverdrup Technology, Inc.
Middleburg Heights, Ohio 44130

A two-dimensional viscous code developed at the NASA Lewis Research Center is being used to predict the flow in the SSME high-pressure turbopump blade passages. The rotor viscous code (RVC) employs a four-step Runge-Kutta scheme to solve the two-dimensional, thin-layer Navier-Stokes equations. The Baldwin-Lomax eddy-viscosity model is used for these turbulent flow calculations. A viable method has been developed such that the relative exit conditions from an upstream blade row are used as the inlet conditions to the next blade row. The blade loading diagrams are compared with the meridional values obtained from an in-house quasi-three-dimensional inviscid code. Periodic boundary conditions are imposed on a body-fitted C-grid computed by using the GRAPE (GRids about Airfoils using Poisson's Equation) code. Total pressure, total temperature, and flow angle are specified at the inlet. The upstream-running Riemann invariant is extrapolated from the interior. Static pressure is specified at the exit such that mass flow is conserved from blade row to blade row, and the conservative variables are extrapolated from the interior. For viscous flows the no-slip condition is imposed at the wall. The normal momentum equation gives the pressure at the wall. The density at the wall is obtained from the wall total temperature.

To compute the flow for a given blade row, inlet conditions were based on the mass-averaged relative exit conditions from an upstream blade row. Inlet conditions to the first stator were taken from conditions given by Rocketdyne. Mass flow was then matched by varying the exit static pressure. This process was repeated for each of the blade rows. The calculations were done at midspan of each blade.

DISCUSSION

The results from the RVC were compared with those previously obtained by using an inviscid quasi-three-dimensional code at the mean span section of the blade. The comparisons were made for the engine balance flow conditions given by Rocketdyne for the SSME high-pressure fuel turbopump. Figures 1 and 2 show the computational grids used in computing the first stage. Figure 3 and 4 show the loading diagrams for the stator and rotor. Originally a separated region was computed on the pressure surface of the first-stage rotor (figs. 5 and 6). In the present calculation the flow has an adverse pressure gradient but does not quite separate (fig. 7). The original computation did not account for the effects of an upstream blade row; therefore the first-stage rotor had a lower inlet flow angle. The computational grids for the second stage are shown in figures 8 and 9. The RVC results of the second-stage stator compare quite well with the inviscid code results in figure 10. The difference in the loading diagram of the second-stage rotor was due to the different exit static pressure needed to match the mass flow of the turbine (fig. 11). Another calculation was made to match the exit static pressure of the inviscid code; however, this increased the mass flow by 6 percent (fig. 12). Figure 13 compares the

*Work performed under Lewis task number 82-24-01.

velocity diagrams of RVC and the inviscid quasi-three-dimensional code (at the mean section) for the SSME high-pressure fuel turbopump.

Originally only the two rotors were computed by using the inlet conditions given by the inviscid code. The current quasi-coupled results are believed to be more realistic.

Presently, work is being done on the SSME high-pressure oxidizer turbopump. The computational grid and loading diagrams for the first-stage stator computed by using the inviscid version of the RVC are presented in figures 14 and 15.

A two-dimensional Navier-Stokes code was used to predict the flow in the SSME high-pressure fuel turbopump. The relative upstream exit conditions were used as input to the successive blade rows, thus coupling the solutions. The results obtained by using the Runge-Kutta version of the RVC compared well with the results from the inviscid quasi-three-dimensional code. The RVC is good for understanding the physics of the flow. Work is continuing on the SSME high-pressure oxidizer turbopump.

COMPUTATIONAL GRIDS
FIRST STAGE

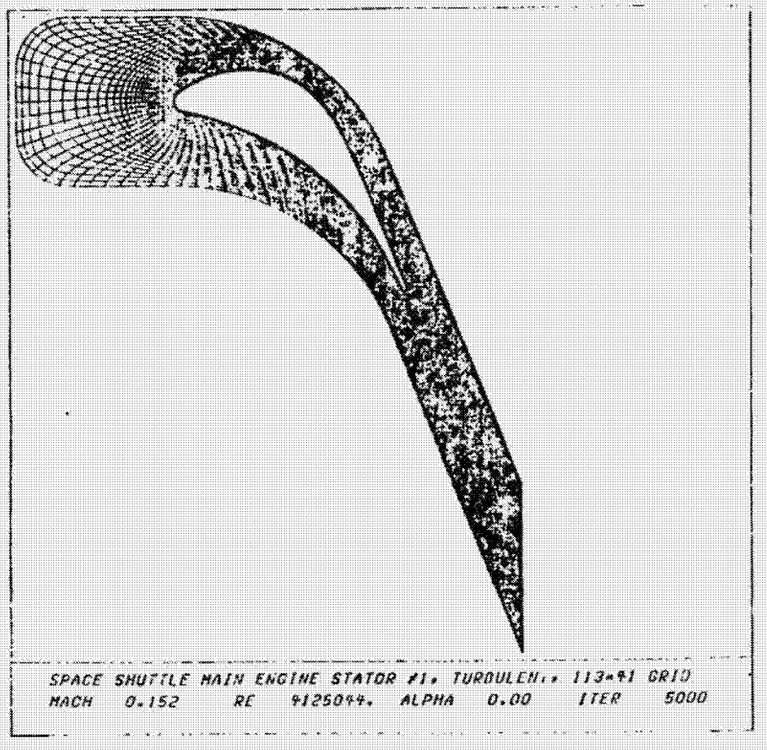

FIGURE 1.

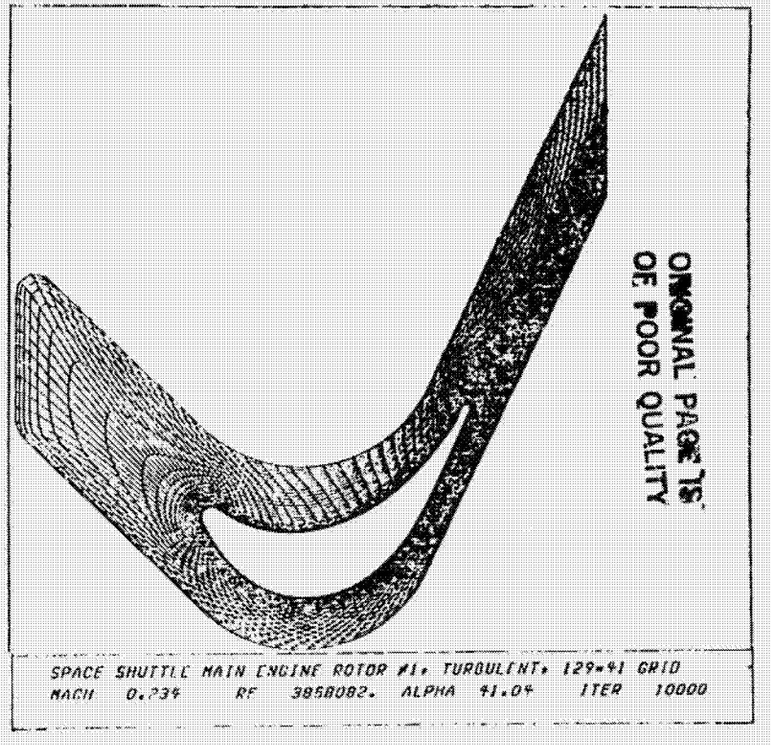

FIGURE 2.

△ RVC - COUPLED SOLUTION (PRESSURE)
□ RVC - COUPLED SOLUTION (SUCTION)
⊙ QUASI - 3D SOLUTION MEAN SECTION (PRESSURE)
▽ QUASI - 3D SOLUTION MEAN SECTION (SUCTION)

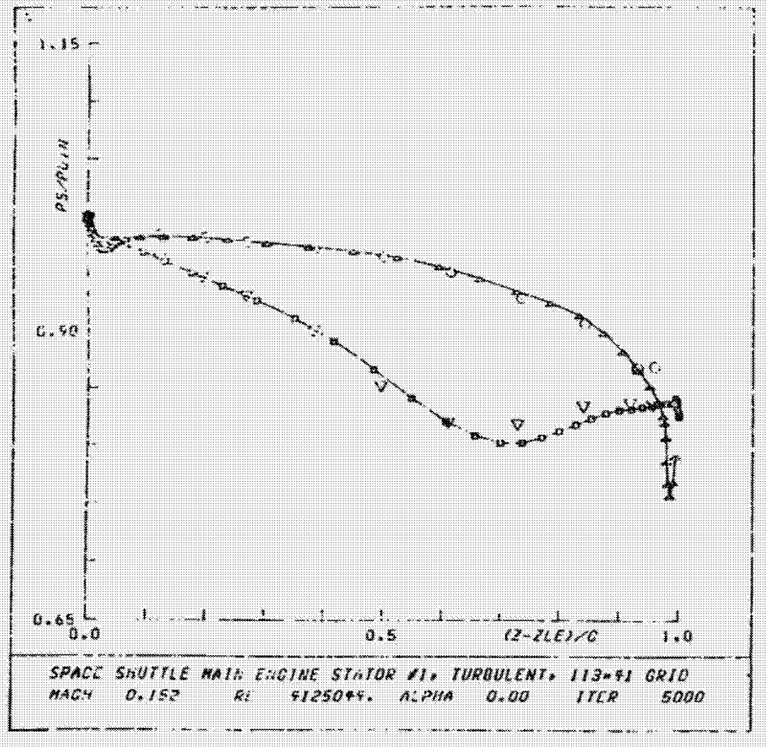

FIGURE 3.

RVC $\frac{\Delta P_b}{P_0} = .023$

QUASI - 3D $\frac{\Delta P_b}{P_0} = .0035$

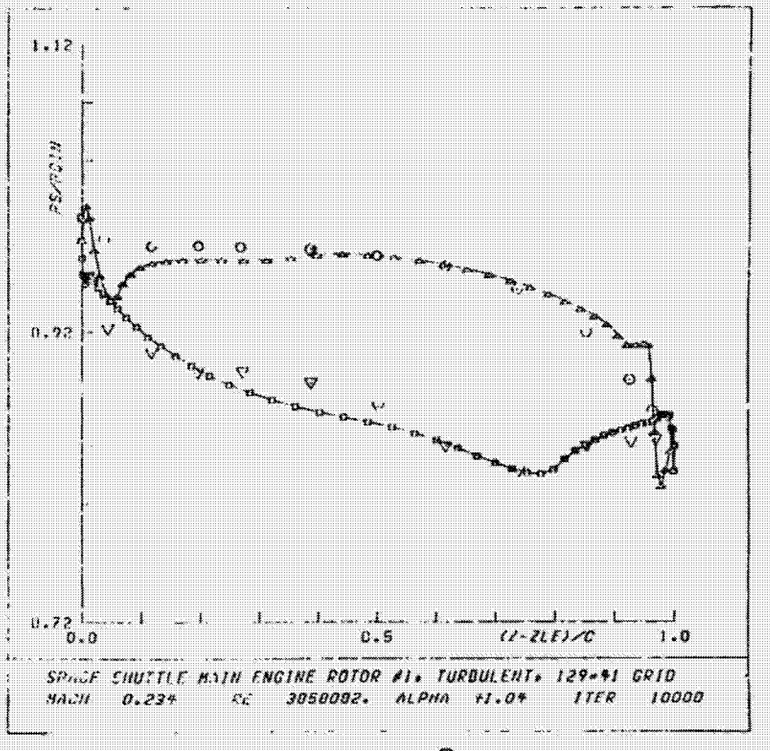

FIGURE 4.

RVC $\frac{\Delta P_b}{P_0} = .010$

QUASI-3D $\frac{\Delta P_b}{P_0} = .0043$

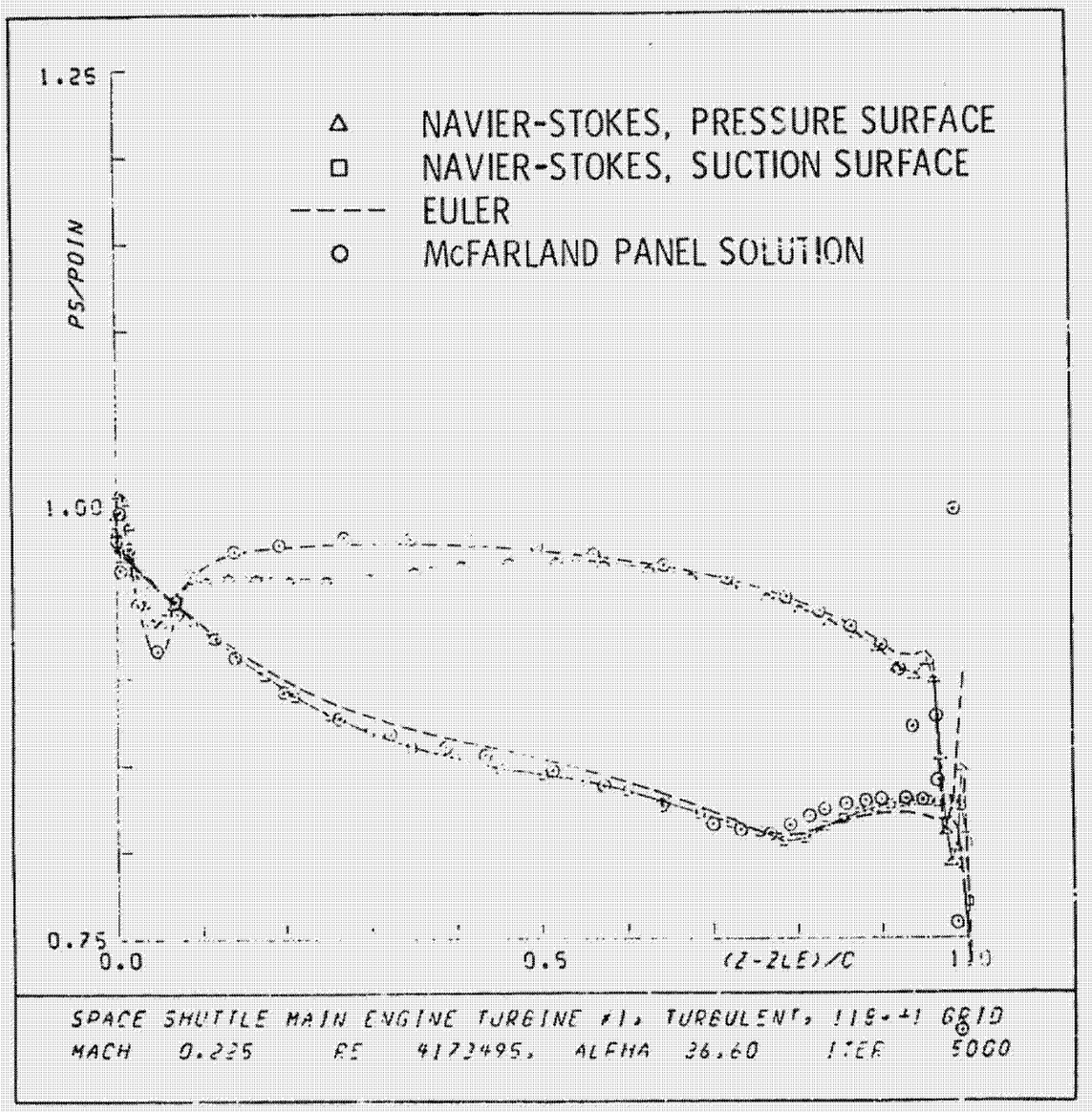

FIGURE 5.

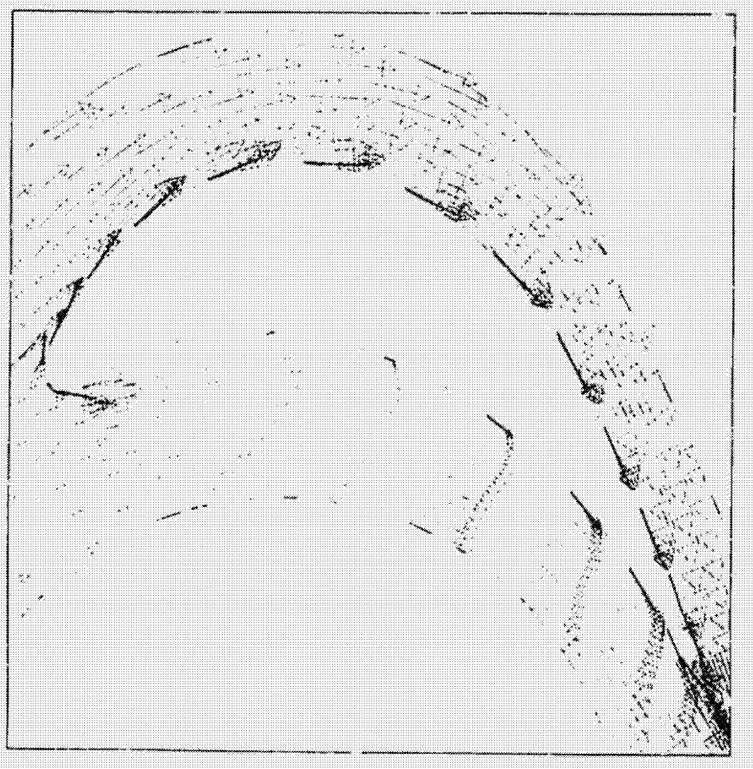

FIGURE 6.

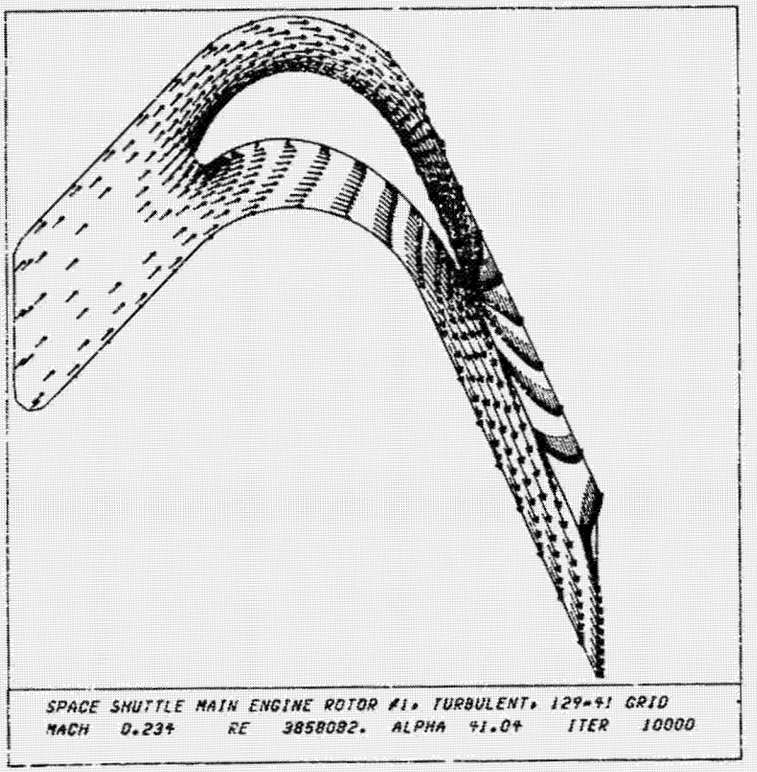

FIGURE 7.

COMPUTATIONAL GRIDS
SECOND STAGE

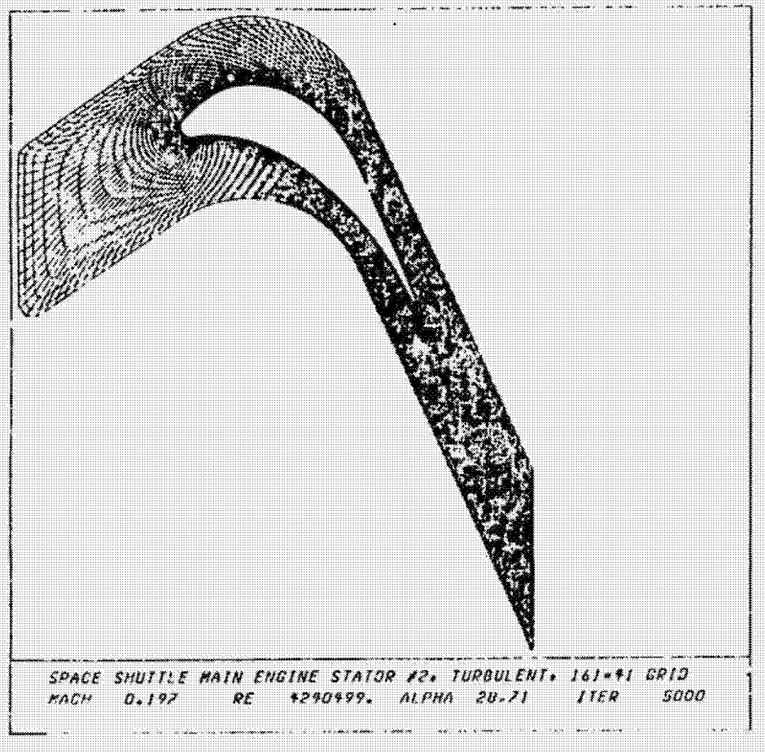

FIGURE 8.

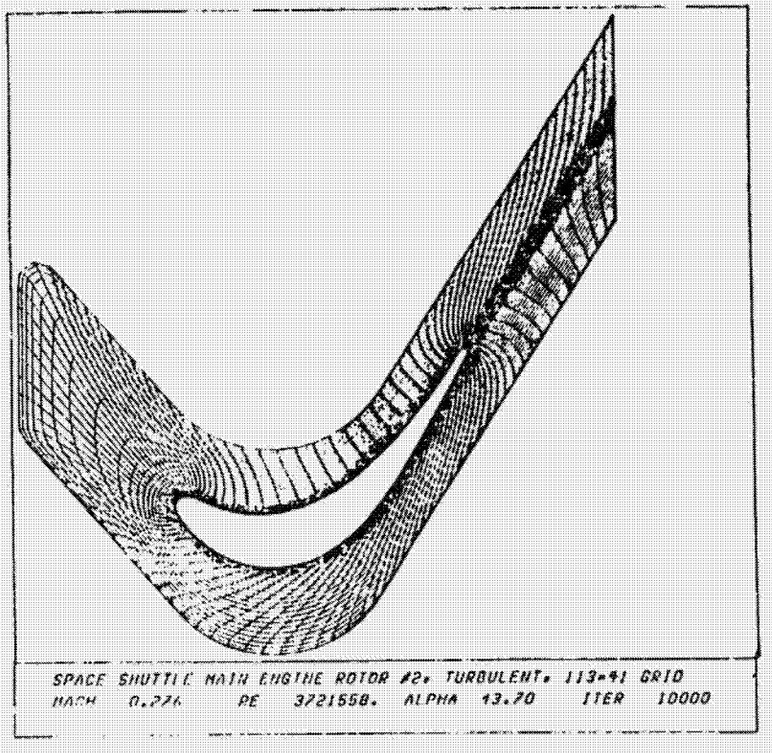

FIGURE 9.

△ RVC - COUPLED SOLUTION (PRESSURE)
□ RVC - COUPLED SOLUTION (SUCTION)
○ QUASI - 3D SOLUTION MEAN SECTION (PRESSURE)
▽ QUASI - 3D SOLUTION MEAN SECTION (SUCTION)

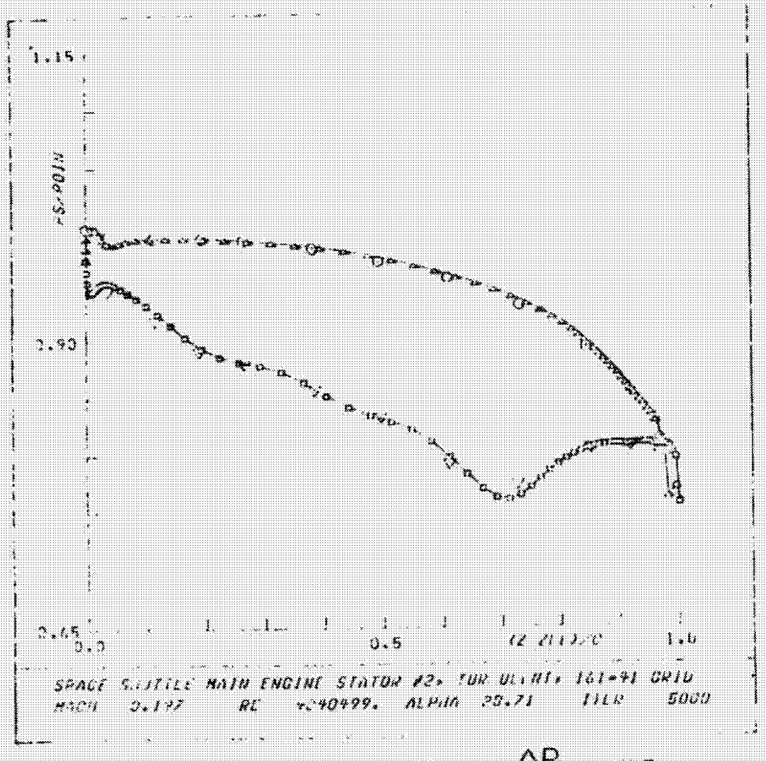

FIGURE 10.

RVC $\frac{\Delta P_o}{P_o} = .015$

QUASI - 3D $\frac{\Delta P_o}{P_o} = .0039$

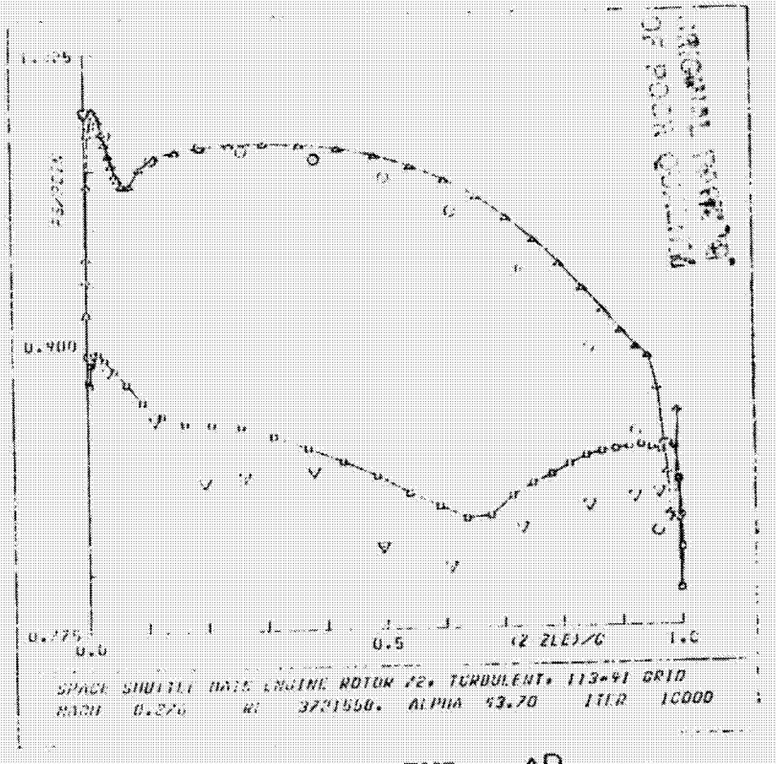

FIGURE 11.

RVC $\frac{\Delta P_o}{P_o} = .011$

QUASI-3D $\frac{\Delta P_o}{P_o} = .0040$

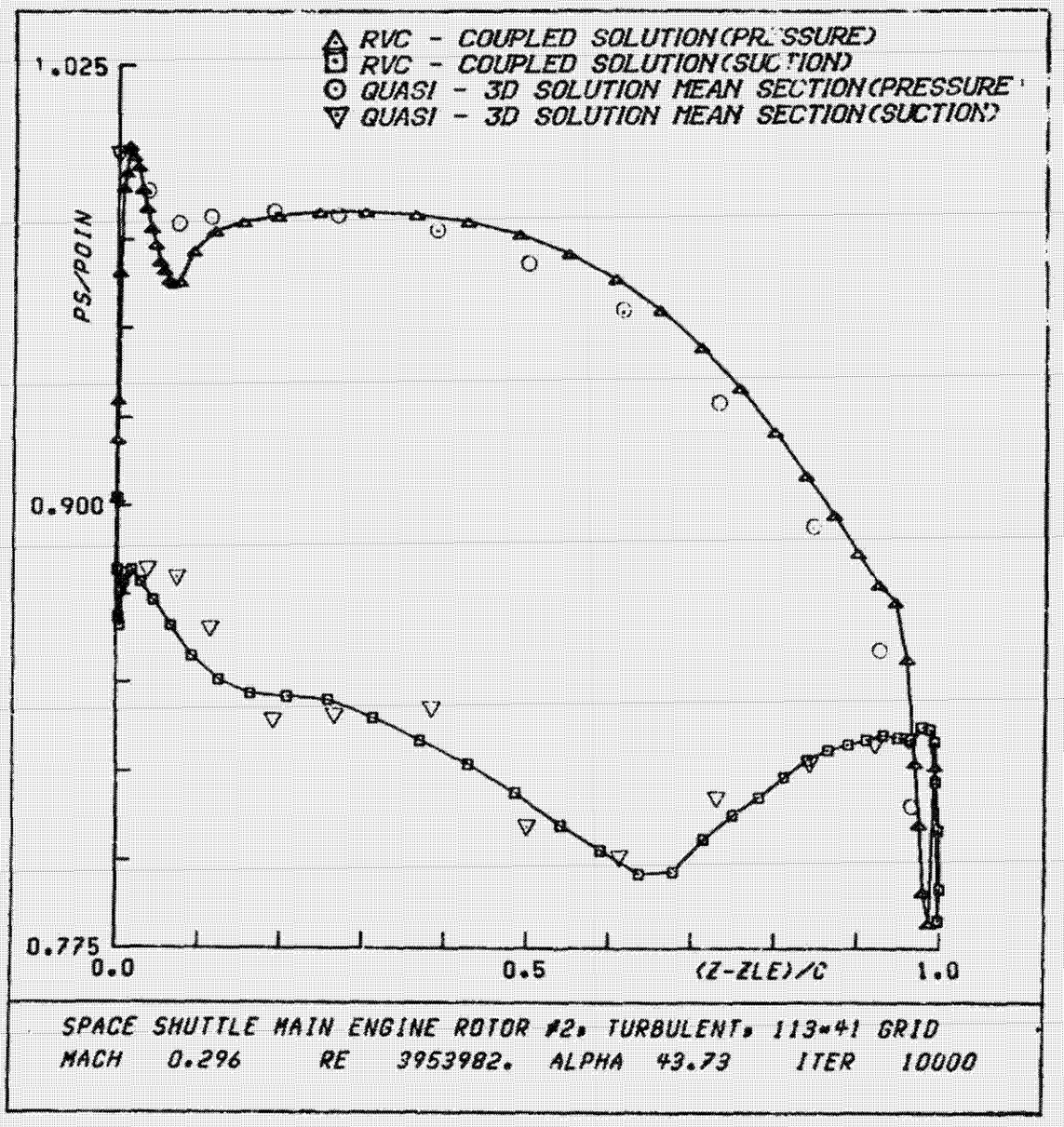
RVC - COUPLED SOLUTION(PRESSURE)
RVC - COUPLED SOLUTION(SUCTION)
QUASI - 3D SOLUTION MEAN SECTION(PRESSURE)
QUASI - 3D SOLUTION MEAN SECTION(SUCTION)
1.025
0.900
0.775
PS/POIN
0.0
0.5
1.0
(Z-ZLE)/C
SPACE SHUTTLE MAIN ENGINE ROTOR #2, TURBULENT, 113*41 GRID
MACH 0.296 RE 3953982. ALPHA 43.73 ITER 10000

FIGURE 12.

VELOCITY DIAGRAMS ENGINE BALANCE FLOW
PRIMED VALUES FROM QUASI - 3D

FIGURE 13.

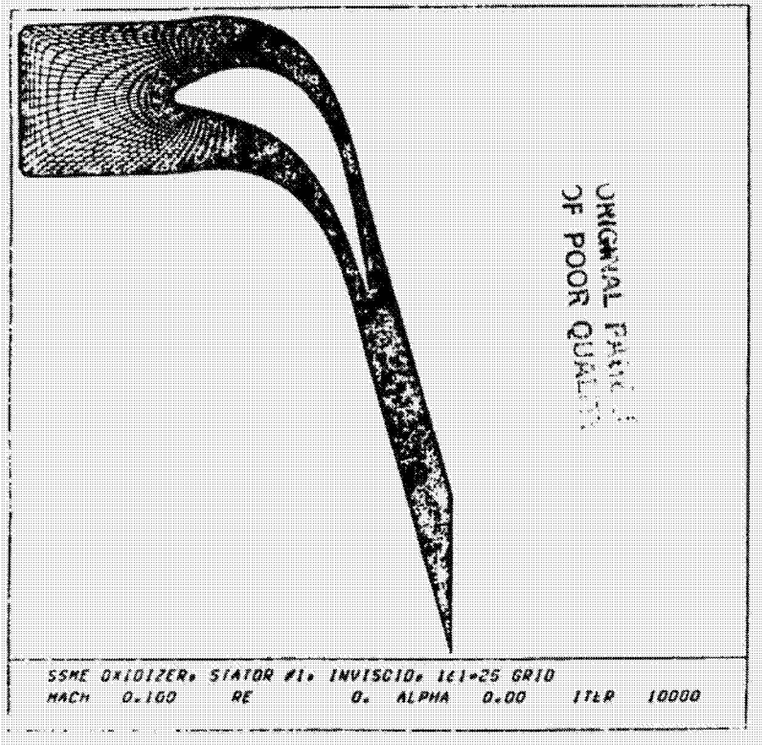

FIGURE 14.

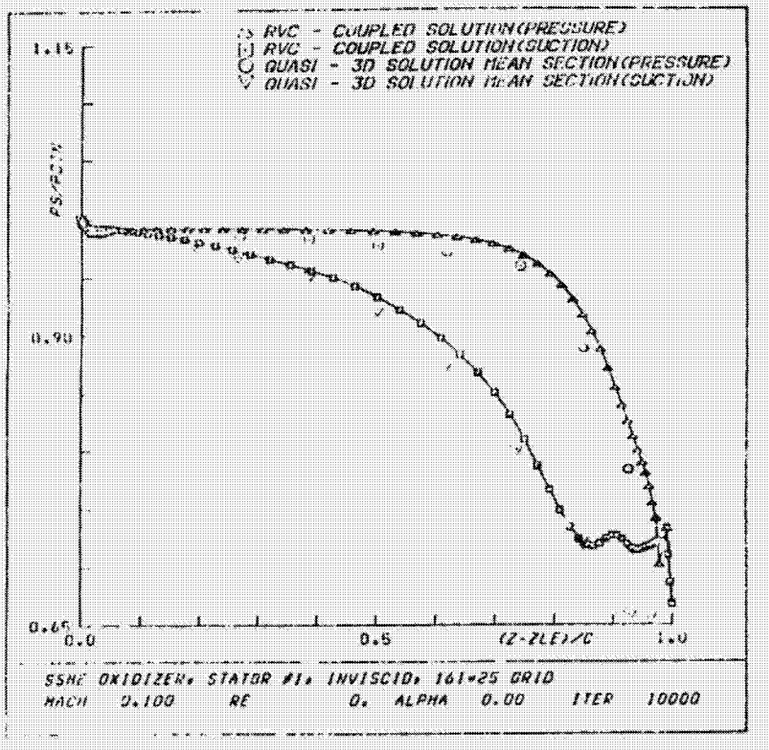

FIGURE 15.

SIMULATION OF MULTISTAGE TURBINE FLOWS*

M.L. Celestina and R.A. Mulac
Sverdrup Technology, Inc.
Middleburg Heights, Ohio 44130

John J. Adamczyk
National Aeronautics and Space Administration
Lewis Research Center
Cleveland, Ohio 44135

The long-term objective of the numerical simulation of turbine flows is to enhance our understanding of the flow phenomena within multistage turbomachinery components. The direct benefit of this activity is improved modeling capability, which in turn can be used to improve component efficiency and durability.

The flow field in multistage turbomachinery components (single stage being a limiting case) is extremely complex. The flow field is highly unsteady, with time scales ranging from a fraction of shaft speed to several times the highest blade passing frequency. The length scales of the flow are also diverse. They range from the circumference of the machine to a small fraction of a blade chord.

To assess the difficulty in analyzing the flow field within multistage turbomachinery components, a hierarchy of equations was formulated to serve as a base for analyzing these flows. The equation set that provides the most complete description is the Navier-Stokes equations. The simplest description is given by a set of equations that govern the quasi-one-dimensional flow. As one proceeds from the complete description, the number of unknowns to be solved for increases monotonically above the number of equations. The development of the additional set of equations needed to mathematically close the system of equations forms the closure problem associated with that level of description. For the Navier-Stokes equation there is no closure problem. For the quasi-one-dimensional equation set random flow fluctuations, unsteady (deterministic) fluctuations, nonaxisymmetric flow variations, and hub-to-shroud variations on the quasi-one-dimensional flow must be accounted for.

Given the capabilities of today's supercomputers (including N.A.S.) it seems reasonable to attempt to analyze the flow within multistage machinery by using a set of equations that describe the time-averaged flow field within a typical blade passage of a blade row. With respect to a given blade row the flow in a typical passage is steady and spatially periodic from passage to passage. There is one such description per blade row. The closure problem associated with this description requires accounting for the effects of random, unsteady (deterministic), and spatial fluctuations. The development of computer codes to solve the typical passage flow equations would enhance our ability to simulate the time-averaged, three-dimensional flow field within multistage components. These simulations should enhance our understanding of the flow physics associated with these devices. For example, a better insight should

*Work performed under Lewis task number 83-24-01.

be obtained into the mechanism by which low-momentum fluid is redistributed within a blade row and the effect of this redistribution on blade row performance and durability. These solutions should also yield a description of the unsteady, distorted flow field encountered by a blade row.

To date, a hierarchy of equations and their associated closure problems has been formulated for use in simulating flows in multistage turbomachinery. A computer code has been developed that is based on a Runge-Kutta integration scheme suggested by Jameson to solve the inviscid form of the equation governing the time-averaged flow in a typical blade passage. The inviscid closure problem associated with this equation set is being examined for counterrotating propellers, fans, and turbine stages. The preliminary results obtained for a counterrotating propeller configuration seem to suggest that rational inviscid closure models can be developed for this class of machines. Further work is planned in this area on the geometry supplied by General Electric for their unducted fan configuration.

Work will begin soon on including the viscous terms in the code. The closure problem associated with this equation set will be examined. It is also planned to develop a time-accurate code for solving the Reynolds-averaged Navier-Stokes equations by using the Runge-Kutta integration scheme. This code will be used to develop data bases for devising closure models for the average passage equation set.

TURBOMACHINERY MODELING EQUATIONS

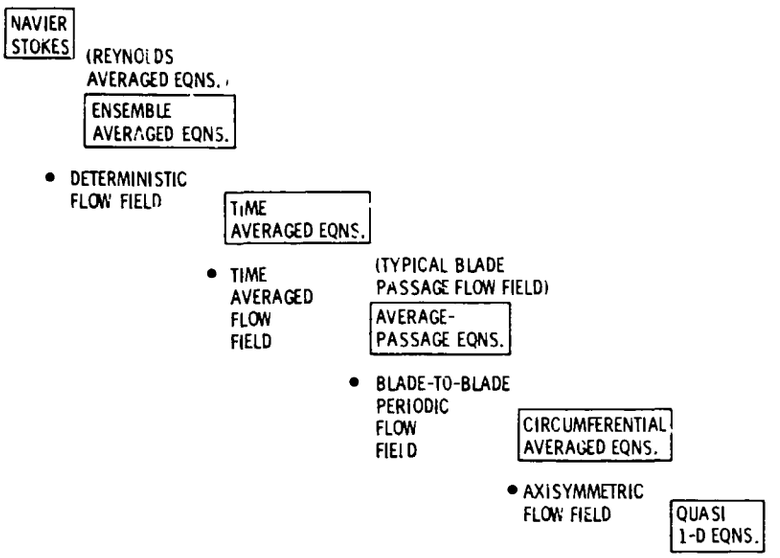

CD-85-15736

DIRECT SIMULATION OF UNSTEADY TURBOMACHINERY FLOWS

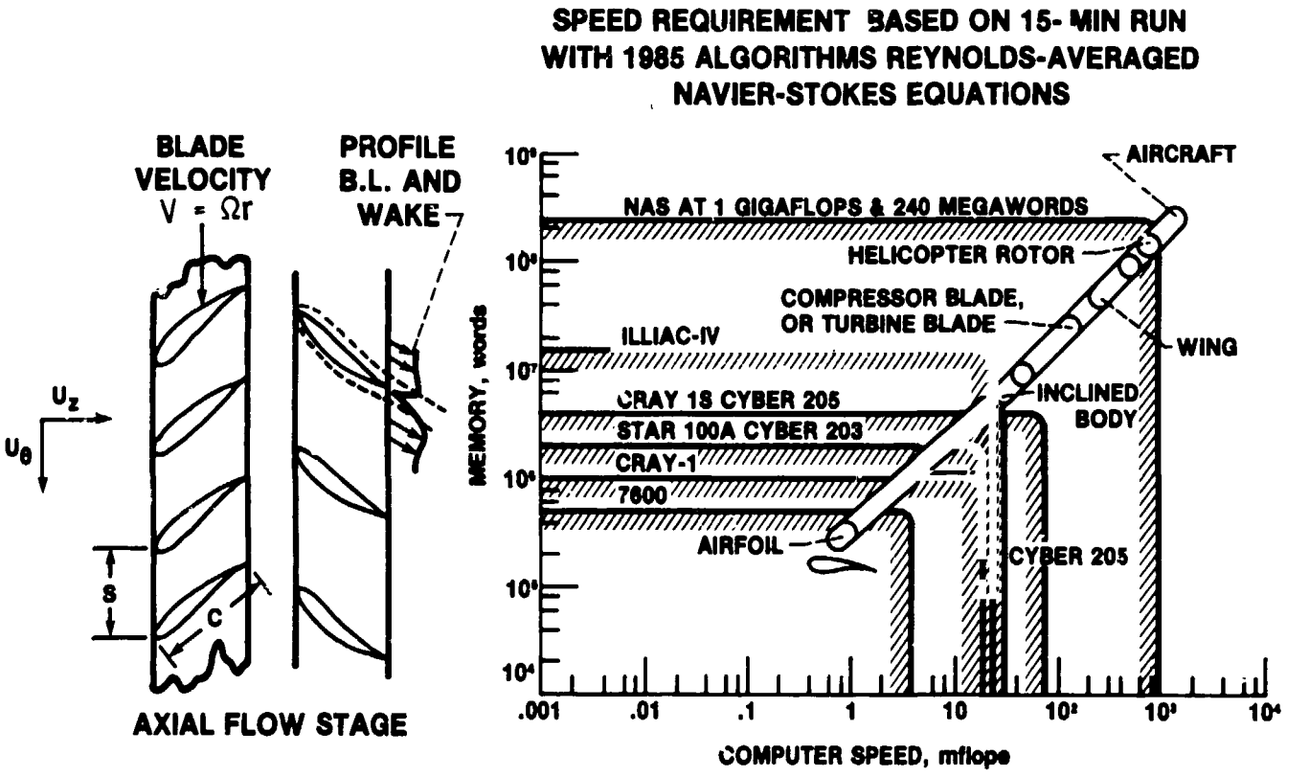

CD-85-15742

THREE–DIMENSIONAL CELL–CENTERED FINITE VOLUME EULER SOLVER

EULER EQUATIONS IN CYLINDRICAL COORDINATES

$$(\partial \lambda Q/\partial t)dV + \sum(\lambda F dA r + \lambda G dA\theta + \lambda H dAz) = S$$

FOR ROTATING SYSTEM

$$(\partial \lambda Q/\partial t)|abs = (\partial \lambda Q/\partial t)|rel - \Omega(\partial \lambda Q/\partial \theta)|rel$$

EULER EQUATIONS FOR ROTATING SYSTEMS

$$(\partial \lambda Q/\partial t)dV + \sum(\lambda F dA r + \lambda(G - r\Omega Q)dA\theta + \lambda H dAz) = S$$

JAMESON'S RUNGE–KUTTA INTEGRATION PROCEDURE

four stage scheme

second to fourth order accuracy

allows CFL > 1 ($CFL = 2\sqrt{2}$)

MODULAR CODE CONSTRUCTION

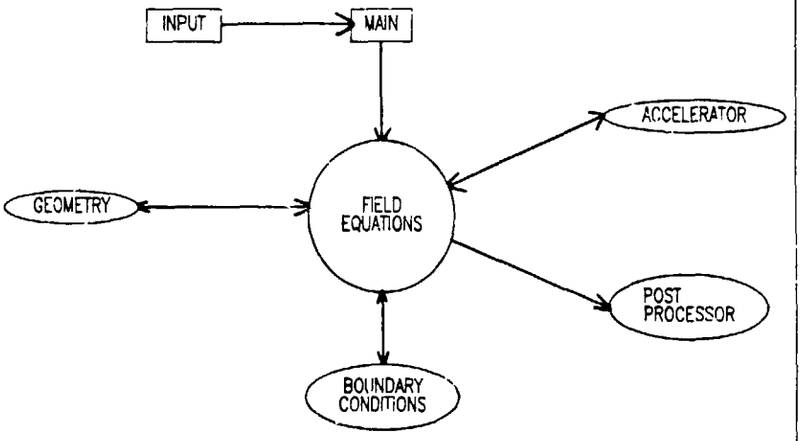

FIRST STATOR - SSME TURBOPUMP

CONVERGENCE HISTORY

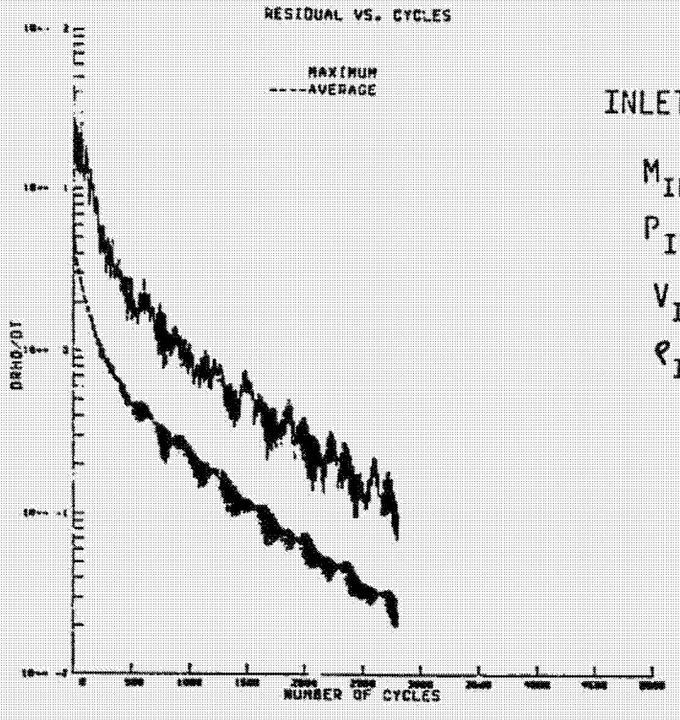

INLET CONDITIONS:

$M_{IN} = 0.1509$

$P_{IN} = 1.0$

$V_{IN} = W_{IN} = 0$

$\rho_{IN} = 1.0$

BLADE-TO-BLADE GEOMETRY

(70 x 21 x 21)

$\gamma = 1.347$

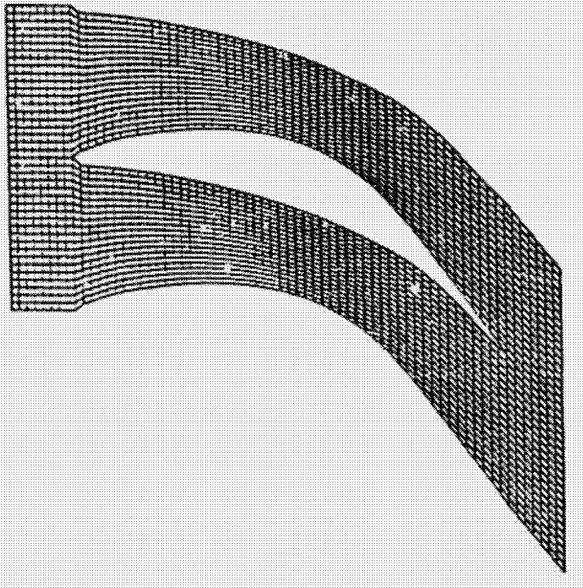

EXIT CONDITION:

$P_{EXIT} = 0.8542\ P_{IN}$

FIRST STATOR - SSME TURBOPUMP

PRESSURE CONTOURS

BLADE-TO-BLADE

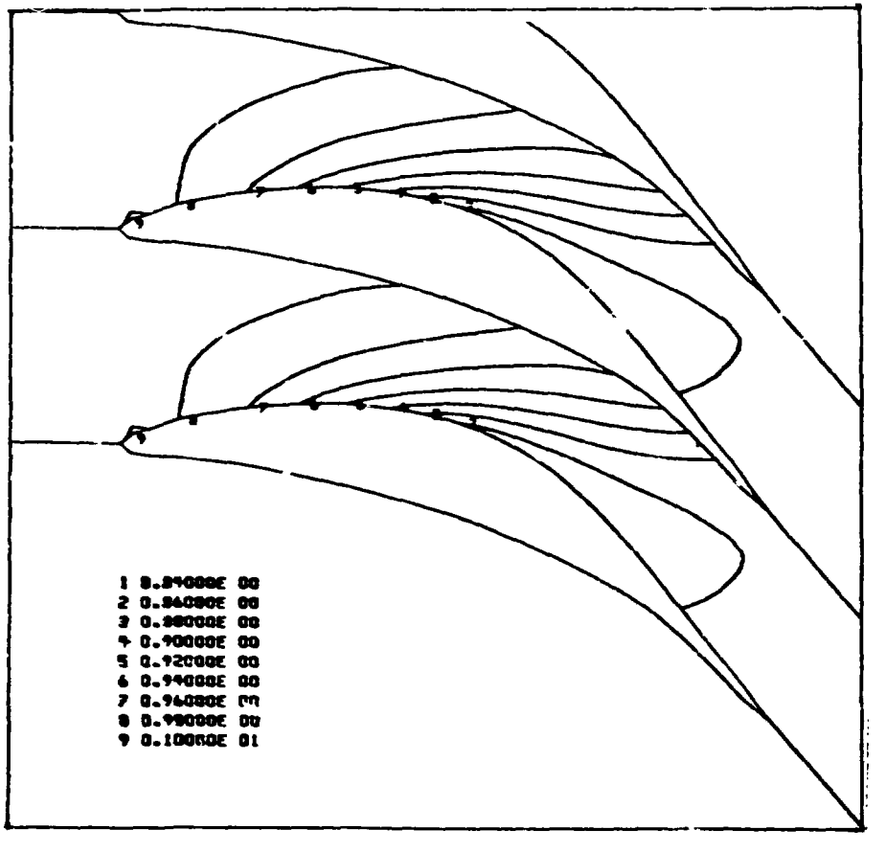

$\frac{P}{P_{O_{IN}}}$ vs. AXIAL DISTANCE

SHROUD

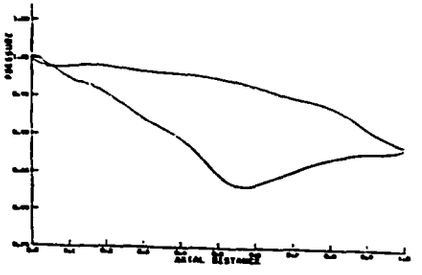

MEAN RADIAL STATION

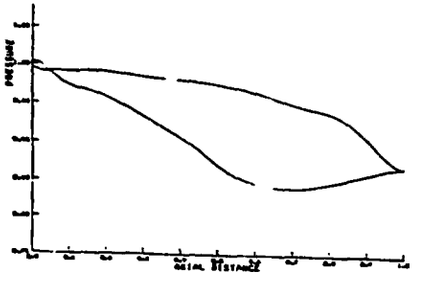

HUB

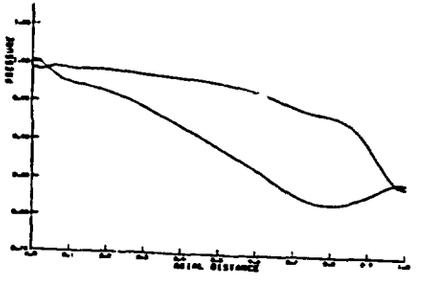

COUNTER-ROTATING PROPELLER

V AND W VECTOR FIELD AT CONST XI

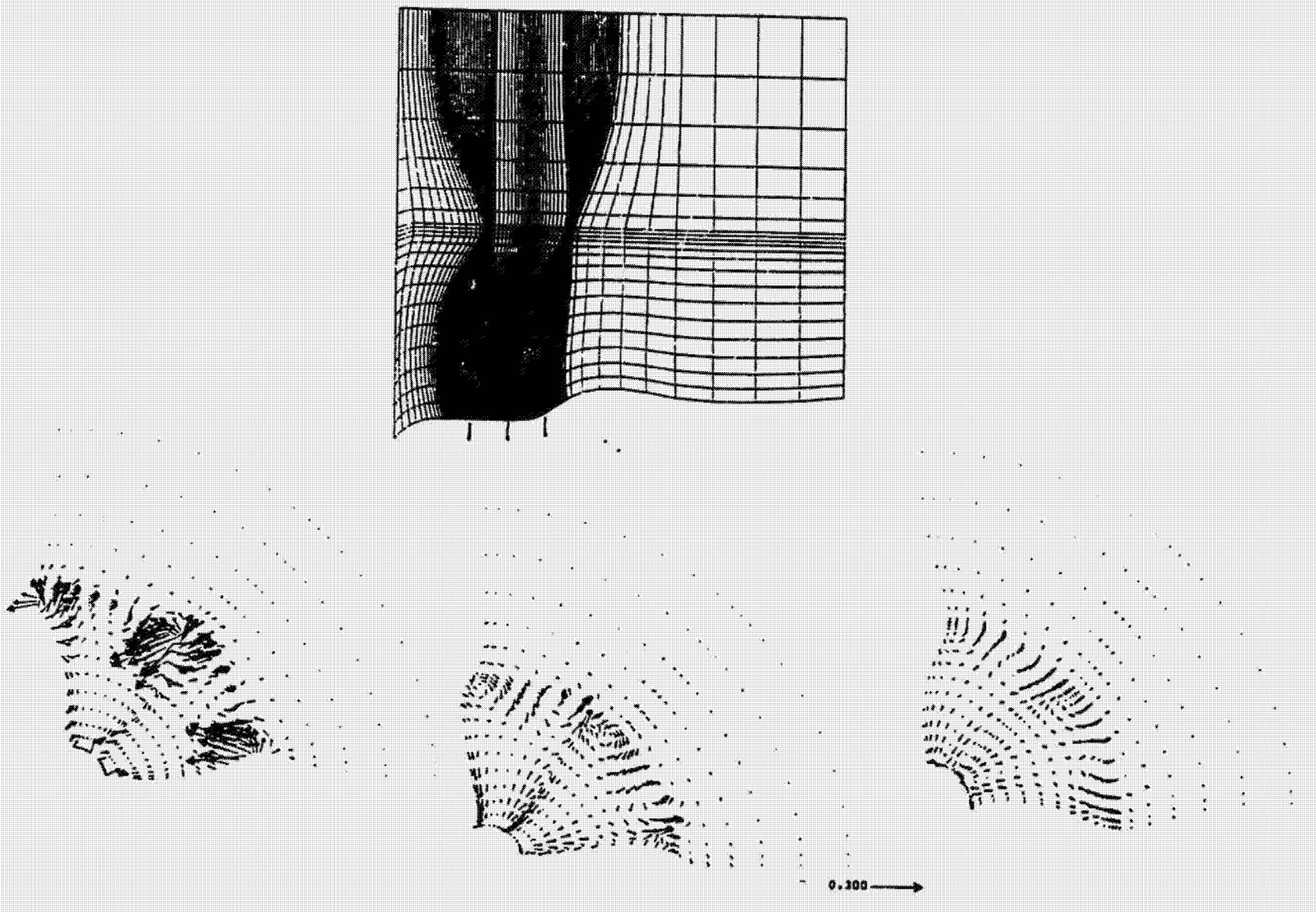

V AND W VECTOR FIELD AT CONST X I

CURRENT RESEARCH PLANS

WORK UNDER WAY

EXTENDING CODE TO PREDICT TIME AVERAGED FLOW FIELD THROUGH A STAGE

WORK TO BE INITIATED

1. INCLUDE VISCOUS TERMS
2. TIME DEPENDENT GRID (INVISCID CODE)
3. ROTOR STATOR INTERACTION
4. MULTIGRID ACCELERATION

UNSTEADY FLOW IN MULTISTAGE TURBINES

Surya P. Surampudi
Cleveland State University
Cleveland, Ohio 44115

In recent years there has been increasing interest in the development of distortion-tolerant engines. The solution to the problem of inlet distortion and forced vibration may require major engine redesign and retesting. The objective of the present research project is to develop an efficient model for the response of a multistage turbine to either a total pressure or total temperature distortion.

Each turbine blade row is modeled as an actuator disk. The actuator disk, which is defined as an artificial device producing sudden discontinuities in flow properties, is often used to describe the flow through turbine and compressor blade rows. The flow approaching the blade row is assumed to be subsonic and inviscid. The distortion occurs at upstream infinity and is in the form of total pressure or total temperature. Recently M. Celestina, R. Mulac, and J. Adamczyk (ref. 1) obtained a solution to unsteady Euler equations by using a finite volume method. With prescribed inlet and boundary conditions flow variables such as density, pressure, and velocities can be calculated at cell centers in the entire flow region. The inlet and exit of the blade row coincide with lines of constant ξ (fig. 1).

The annular duct code developed in reference 1 is used to obtain the flow variables at various cell centers for the region $0 < \xi < n$ and $n + 3 < \xi < m$. The characteristic equations for the region $n < \xi < n + 3$ are obtained from equations of continuity momentum and energy. These equations ((1) to (5)) are expressed in terms of flow variables such as density, velocity in three directions (u, v, w), and pressure p. Nondimensional time and space variables in axial (z), radial (r), and circumferential (φ) directions are given by τ, ξ, η, ζ. The characteristic equations are expressed in finite difference form by equations (7). A multistage Runge-Kutta method is used to integrate these equations. Equation (8) gives the details of the time-stepping scheme used in the analysis. After carrying out these integrations the relations between the flow variables (eqs. (9) to (13)) are obtained.

By making use of actuator disk theory for the flow across the blade row the following assumptions are used in the present analysis:

(1) Entropy loses are neglected.
(2) Hub-to-tip radius ratio is high.
(3) Total enthalpy is constant.

The exit angle is specified. From these assumptions the relations between flow variables at the inlet and exit of the blade row are derived. These relations are given by equations (14) to (18). Equations (9) to (18) form a set of nonlinear equations containing 10 unknown variables (ρ_1, u_1, v_1, p_1, w_1, ρ_2, u_2, v_2, w_2, and p_2). These equations can be further reduced to two nonlinear equations ((19) and (20)) containing two unknown variables, u_1, u_2. These two equations can be solved by using a Newton-Raphson method (ref. 3). The details of the Newton-Raphson method are given by equations (21) to (22).

A computer code based on this analysis is under development to obtain flow variables at the inlet and exit of the blade row. The preliminary results will be presented at the SSME durability conference.

REFERENCES

1. Celestina, M.L., Mulac, R.A., and Adamczyk, J.J.: Numerical Simulation of Multistage Turbomachinery Flows. In this preprint.

2. Horlock, J.H.: Actuator Disk Theory. McGraw-Hill International Company, London, 1978.

3. Brice, Carnahan; Luther, H.A.; and Wilkes, J.O.: Applied Numerical Methods. John Wiley & Sons, Inc., New York, 1969.

UNSTEADY HEAT TRANSFER DUE TO TIME-DEPENDENT FREE STREAM VELOCITY

Rama S.R. Gorla and Ali Ameri
Cleveland State University
Cleveland, Ohio 44115

There exists a need for a detailed study of the effects of the upstream unsteady flow on the heat transfer from a turbomachinery blade.

One of the most significant studies of laminar boundary layers under the influence of a purely time-dependent, free stream oscillation is done by Lighthill [1]. His analysis employed a linearization for small oscillation amplitudes. Lin [2] considered the effect of finite amplitude oscillation on a flow field. Mori and Tokuda [3] investigated the heat transfer from an oscillating cylinder. Recently, Gorla [4] examined the unsteady fluid dynamic characteristics of an axisymmetric stagnation point flow on a circular cylinder performing a harmonic motion in its own plane. He presented solutions for small and high values of the reduced frequency of oscillation.

The present work has been undertaken in order to study the unsteady combined convection from a horizontal circular cylinder to a transverse flow. A coordinate perturbation method is used to transform the governing set of partial differential equations into a system of ordinary differential equations. The free stream time-dependent velocity was assumed to be sinusoidal and the boundary layer response due to both low as well as high frequencies of oscillation will be studied. Currently numerical solutions are being obtained for the distribution of the unsteady Nusselt number and the friction factor.

METHOD OF SOLUTION

Assuming an incompressible flow with constant properties and negligible dissipation, the governing equations within the framework of the boundary layer approximation may be written as

$$\frac{\partial u}{\partial x} + \frac{\partial v}{\partial y} = 0 \tag{1}$$

$$\frac{\partial u}{\partial t} + u\frac{\partial u}{\partial x} + v\frac{\partial u}{\partial y} = \frac{\partial U_e}{\partial t} + U_e\frac{\partial U_e}{\partial x} + \nu\frac{\partial^2 u}{\partial y^2} + g\beta(T-T_\infty)\sin(\frac{x}{R}) \tag{2}$$

$$\frac{\partial T}{\partial t} + u\frac{\partial T}{\partial x} + v\frac{\partial T}{\partial y} = \alpha\frac{\partial^2 T}{\partial y^2} \tag{3}$$

In the above equations, x and y represent the distances along the streamwise direction and normal direction; u and v the velocity components in x and y directions; U_e (x,t) the external velocity; t the time; ν the kinematic viscosity of the fluid; α the diffusivity and T the temperature.

The boundary conditions are given by

$$y = 0: \; u = v = 0 \text{ and } T = T_w$$

$$y \to \infty: \; u = U_e(x,t) = U_o(x)\cdot(1 + \varepsilon\, e^{i\Omega t})$$

$$T \to T_\infty \qquad (4)$$

The solution strategy is to subject equations (1)-(3) to the linear perturbation analysis, expand the resultant zero and first-order equations in a series of x^* whose coefficients are function of η alone. Here, $x^*=(x/R)$ and $\eta=y\sqrt{2U_\infty/\nu R}$. The resultant ordinary differential equations are then to be solved numerically. Appropriate unsteady solutions will be developed for low frequency and high frequency of oscillations of the free stream velocity.

This work is currently in progress and it is hoped to report these results in the very near future.

REFERENCES

1. Lighthill, M. J. "The Response of Laminar Skin Friction and Heat Transfer to Fluctuations in the Stream Velocity," Proc. Royal Society, Series A, Vol. 224, 1954, pp. 1-23.
2. Lin, C. C. "Motion in the Boundary Layer with a Rapidly Oscillating External Flow," Proc. 9th Int. Congress of Applied Mechanics, Vol 4, 1957, pp. 155-167.
3. Mori, Y. and Tokuda, S. "The Effect of Oscillation on Instantaneous Local Heat Transfer in Forced Convection from a Cylinder," Proc. Third Int. Heat Transfer Conference, Vol. 3, 1966, pp. 49-56.
4. Gorla, R. S. R. "Unsteady Viscous Flow in the Vicinity of an Axisymmetric Stagnation Point on a Circular Cylinder," International Journal of Engineering Science, Vol. 17, 1979, pp. 87-93.

NEW FACILITY TO STUDY UNSTEADY WAKE EFFECTS ON TURBINE AIRFOIL HEAT TRANSFER

Robert J. Simoneau
National Aeronautics and Space Administration
Lewis Research Center
Cleveland, Ohio 44135

A significant portion of the SSME aerothermal loads program is directed at the heat transfer effects of the unsteady flows, particularly wakes, that occur naturally in turbomachinery. Although these phenomena occur in all turbomachines, we feel they will be more severe in the SSME turbines because of the high heat transfer associated with the very high Reynolds numbers over the SSME airfoils.

There has been a significant increase in both analytic and experimental research in turbomachinery unsteady flow phenomena in recent years. Computational and experimental measurement advances have made this research possible. Some very exciting results are beginning to emerge. The next 5 to 10 years should see a significant step upward. Most of the experimental work, however, will be conducted at Reynolds numbers typical of aircraft gas turbines, an order of magnitude below the SSME. At the NASA Lewis Research Center we are building a research facility to study fundamental unsteady wake effects on heat transfer. The facility will operate from SSME Reynolds numbers and span the gap down to aircraft turbine Reynolds numbers.

The experimental concept is shown in figure 1. The test section will be a single airfoil in an annular sector with walls contoured to match the airfoil. The airfoil will have a chord almost 1 foot long. The wake-forming disturbance generator will be a spoked wheel of small circular cylinders rotating on a mean diameter of 6 feet. A conceptual layout of the entire rig is shown in figure 2. The conceptual design phase is complete and the final design in under way. Construction should begin in the fall of 1985, and the rig should be ready for research in the summer of 1986.

The following is a brief overview of the expected simulation. Figure 3 is a schematic of wake behavior in a turbine stage. When a rotor blade passes through the stator wake, the suction surface sees the wake first. Since the wake absolute velocity is less than the mean, the velocity triangle shows that the wake relative velocity vector will be deflected around from the design stagnation point toward the suction surface (i.e . negative incidence). A careful examination shows exactly the same behavior for the rotor wake on the second stator. Thus, whether the wake is stationary or moving in space, the effect is the same. Figure 4 represents the simulation. As with the real case the bar wake in the simulation impinges on the suction surface first. The bar drag will also deflect the velocity vector toward negative incidence. The main similarity variables in this experiment are Reynolds number and Strouhal number, defined as follows:

$$Re = \frac{\rho(Vel)L}{\mu} \quad ; \qquad S = \frac{2\pi fL}{(Vel)}$$

Many characteristic velocities and dimensions could be used. We selected exit relative velocity and axial chord for the passage simulation and inlet relative velocity and diameter for the leading edge. The following table shows numbers for the SSME at full power engine balance conditions, for a NASA version of the Energy Efficient Engine (E^3), and for the bar wake simulation rig.

	SSME	E^3	Test rig
Passage conditions:			
Reynolds number	7.19×10^6	0.53×10^6	0.77×10^6 to 7.69×10^6
Strouhal number	3.81	2.70	3.81
Leading-edge conditions:			
Reynolds number	0.37×10^6	0.051×10^6	0.062×10^6 to 0.62×10^6
Strouhal number	0.59	1.13	1.83
Wakes per passage	1.6	1.3	1.8

The Strouhal numbers change very little from turbine to turbine while the Reynolds numbers vary by an order of magnitude. With the test rig the two parameters can be varied independently, and the full Reynolds number range can be spanned. Finally, in real machines there is always more than one but less than two wakes in the passage of one time. This too is simulated.

In a parallel program being conducted under basic research and technology, we have already begun to gather evidence that this approach will yield valuable results. Figure 5 shows a rig that is conceptually similar to, but smaller than, the new facility. It is a full annular passage approximately 1 foot in mean diameter. The test section, rather than an airfoil, is a heated cylinder with a splitter plate. Figure 6 shows typical instantaneous and ensemble-averaged wakes generated by such a spoked wheel. They look very similar to ones reported in the literature for turbomachinery. Early work in this facility indicates that on the average the wakes can be treated as an rms turbulence intensity to yield a heat transfer correlation (fig. 7). Although this may be useful for design, it does not tell the real story. To see the real effect of the wakes, a ceramic cylinder with thin-film sensors painted on the surface (fig. 8) was heated in a small radiation furnace and then suddenly injected into the flow stream behind the spoked rotor. The resulting instantaneous heat flux along the stagnation line of the cylinder (measured directly by the use of an analog circuit) is shown in figure 9. The data indicate a 25-percent spike in heat flux at the bar passing frequency. This early work suggests that the wake effects on heat transfer are real and measurable and could yield significant high-frequency temperature fluctuations at the surface of a turbine rotor blade. The value of this approach to studying the wake-generated unsteady flow effects has also been shown in some recent work at the University of Oxford in England.

In summary we feel the rig under design provides an excellent simulation of the important unsteady physics in the SSME turbines. The test section is large and accessible, which will allow detailed measurements to verify the complex analyses needed to describe the phenomena.

CONCEPT OF ROTOR WAKE SIMULATION HEAT TRANSFER EXPERIMENT

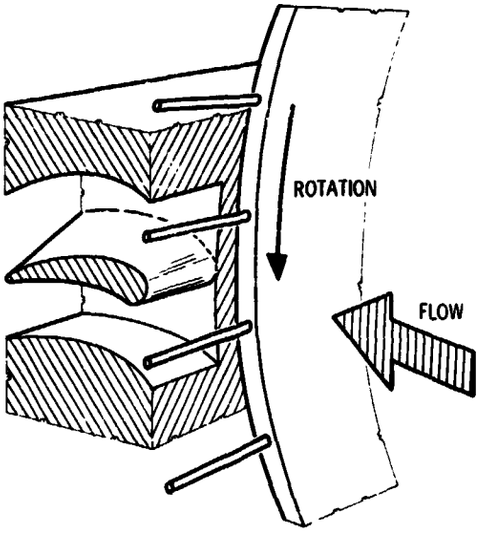

FIGURE 1

CONCEPTUAL ILLUSTRATION OF UNSTEADY HEAT TRANSFER TUNNEL

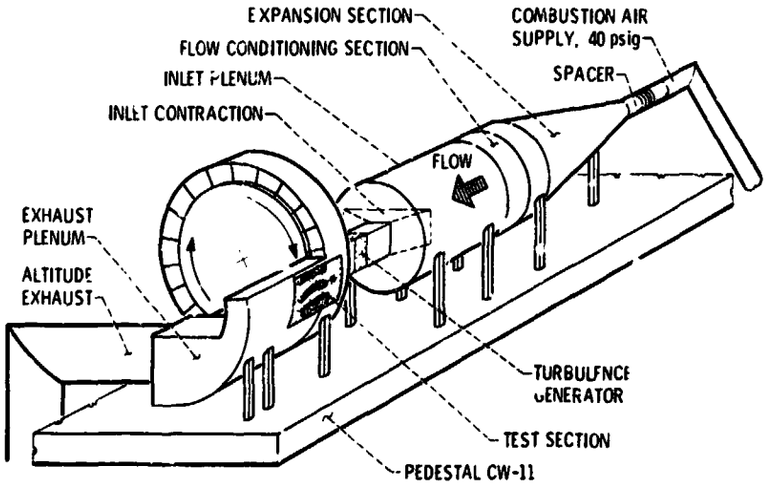

FIGURE 2

SCHEMATIC OF WAKE BEHAVIOR IN A TURBINE STAGE

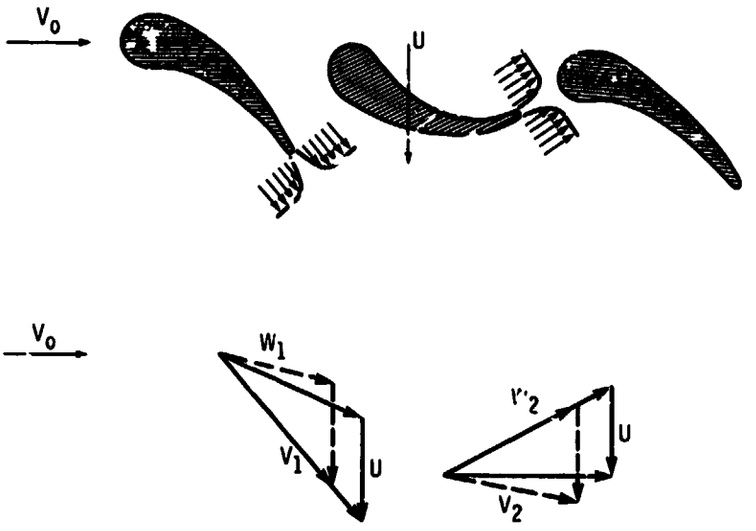

FIGURE 3

SIMULATION OF TURBINE WAKES USING A SPOKED WHEEL DISTURBANCE GENERATOR

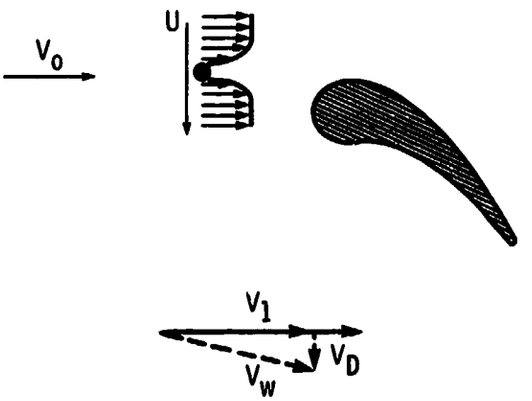

FIGURE 4

CONCEPTUAL SCHEMATIC OF ROTOR WAKE HEAT TRANSFER RIG

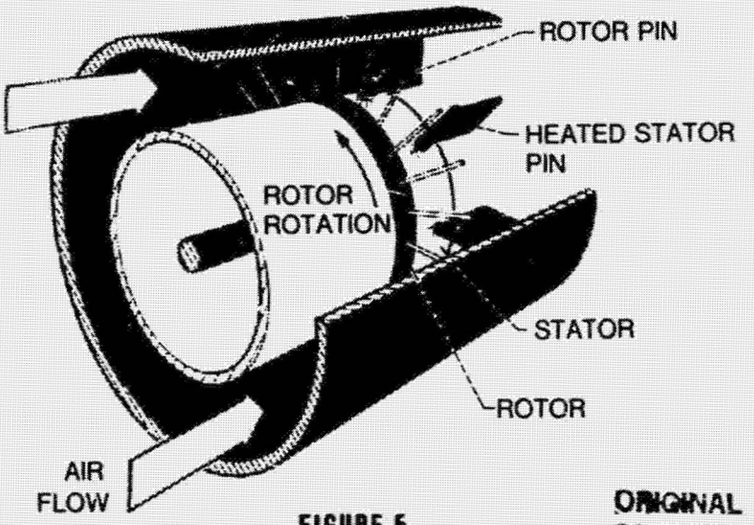

FIGURE 5

TYPICAL WAKES GENERATED BY
A SPOKED WHEEL DISTUBANCE GENERATOR

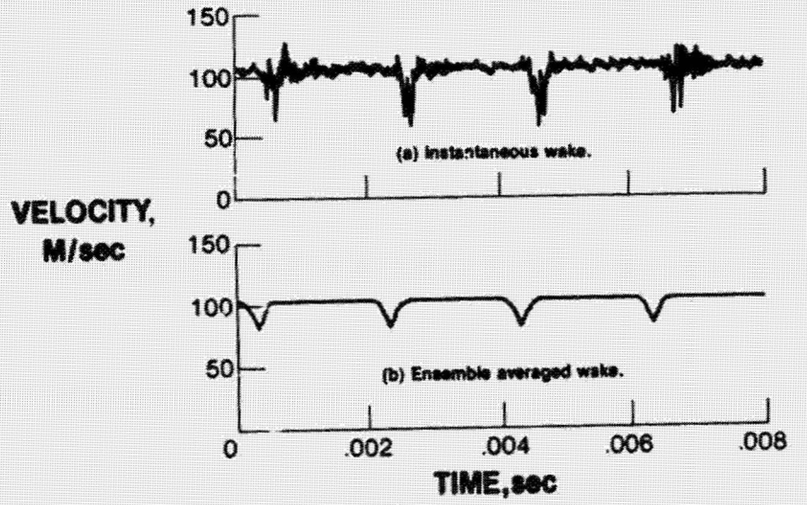

FIGURE 6

AVERAGE HEAT TRANSFER TO A CIRCULAR CYLINDER
IN SIMULATED ROTOR WAKES WITH ALL OF THE DISTURBANCES
TREATED AS TURBULANCE

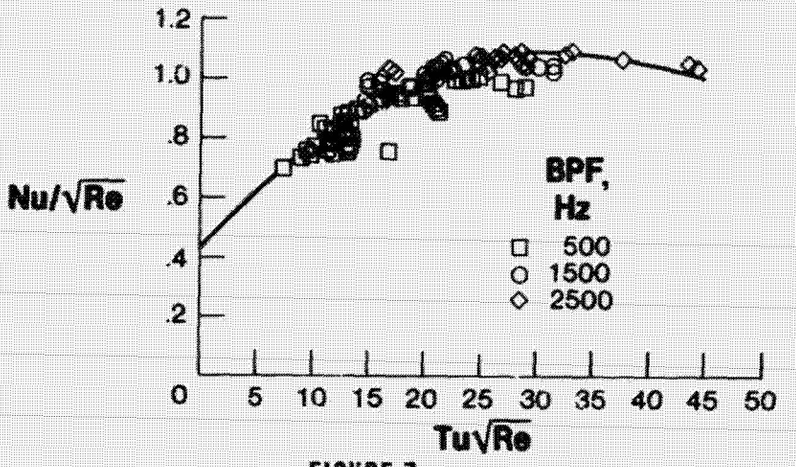

FIGURE 7

CIRCULAR CYLINDER WITH THIN FILM PLATINUM RESISTENCE
SENSORS ON THE SURFACE

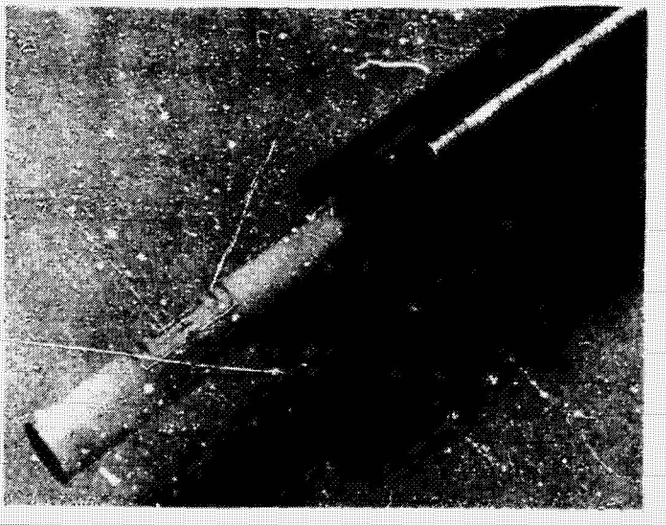

FIGURE 8

CS-85-0901

INSTANTANEOUS SURFACE HEAT FLUX ALONG THE STAGNATION LINE OF A CIRCULAR CYLINDER IN THE WAKE OF A SPOKED ROTOR (Re = 75 000; AND S = 0.19)

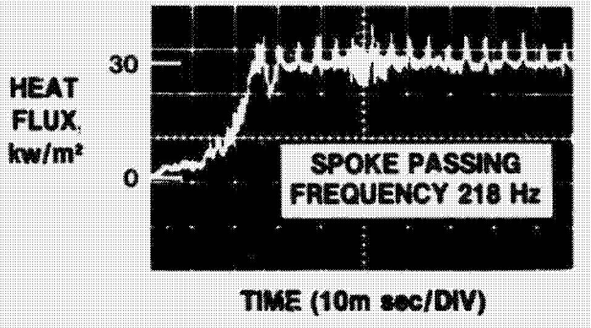

FIGURE 9

EXPERIMENTAL MEASUREMENTS AND ANALYSIS OF HEAT TRANSFER AND GAS DYNAMICS IN A ROTATING TURBINE STAGE

M.G. Dunn, W.J. Rae, and W.K. George
CALSPAN-UB Research Center
Buffalo, New York 14225

The life-cycle fatigue of a particular component of a high-pressure turbine stage is influenced by the local heat flux and the resulting metal temperature excursions experienced by this component during normal operation. Flow through a turbine stage is seldom uniform and is often influenced by nonuniform incoming gas streams that can result in locally high heat fluxes. In the case of the rotor blades passing through the nozzle guide vane wakes and passages, these local heat rates translate into local temperature fluctuations that will likely affect the fatigue life of the blade. In order to better understand the influence of the heat load on the component life, one would like to have both the local steady-state heat flux and the high-frequency component of the heat flux.

Relevant fundamental data of this type can be obtained by making use of a full-stage, rotating turbine model currently in use at CALSPAN. The turbine being used is the Garrett Turbine Engine Company TFE-731-2 HP stage, and both the nozzle guide vanes and the rotor blades are heavily instrumented with thin-film heat-flux gauges, as described later. The experimental technique is the short-duration, shock-tunnel approach, in which fast-response, thin-film thermometers are used to measure the surface temperature histories at prescribed locations on the turbine component parts. Heat-flux values are then inferred from the temperature histories by using standard data reduction procedures. Local variations in the stagnation temperature distribution incident on the rotor are created by injecting cold gas through the trailing-edge cooling slots of the nozzle guide vane. The injected gas (air) is at a known total temperature and a known weight flow rate.

INSTRUMENTATION

The major emphasis in this measurement program is on acquiring, analyzing, and predicting the rotor blade steady-state and time-resolved heat flux in the presence of variations in the incident total temperature distribution. Early in the program it was mutually agreed that the blades would be instrumented at the 10, 50, and 90 percent spanwise locations with the maximum gauge coverage at the 50 percent location. Two blade-contoured leading-edge inserts containing four gauges each were fabricated and installed in the midspan region. Five additional gauges were installed in the blade tips, and three additional gauges were installed on a fourth blade at the 50 percent spanwise location to aid in the analysis of the wake-cutting data. The pressure surface instrumentation, the suction surface instrumentation, the leading-edge inserts, and the final rotor assembly are shown in figures 1 to 4.

The purpose of this effort was to develop the data interpretation techniques necessary to interpret the high-frequency heat-flux data. The data acquisition system has been configured to acquire phase-locked, high-frequency heat-flux data. A previously developed (at CALSPAN) calculational technique

was integrated with the phase-locked system to enable the calculation of instantaneous heat-flux values during wake cutting. These techniques were then verified by piggybacking on the Air Force-sponsored Low Aspect Ratio Turbine (LART) measurement program.

The objective of the analytic phase of this research is to provide a theoretical/numerical complement to the experimental work. The data being gathered under this program are very basic and require continuing examination in the light of state-of-art analysis. Thus a key component in assembling the CUBRC program in turbomachinery has been the acquisition and exercising of the standard NASA flow-field analysis codes (refs. 1 to 3).

These codes were provided by the NASA Lewis Research Center* and were installed on the CDC Cyber 815 of the SUNY-Buffalo Computer Center. It was soon discovered that the storage requirements of the codes strained the limits available on this machine, and arrangements were then made to shift to a VAX 11/780 which had become available for research purposes. Since this is a virtual memory machine, no storage complications were encountered. However, a small amount of reprogramming was required in order to compensate for the way that ENTRY statements are handled by the VAX. These revisions were completed, and successful test runs were made by the end of the contract period.

Thus the program objective was completed: the basic NASA flow-field codes are now available for use in support of the experimental efforts at CALSPAN.

CONCLUSIONS

The measurement program described herein will be run in mid-May 1985. It is anticipated that at the time of the June 4-5 meeting, the measurements will have been performed. It is doubtful that any significant analysis of the data will have been completed at this time, but preliminary comments concerning the program will be presented.

REFERENCES

1. Katsanis, T.; and McNally, W.D.: Revised Fortran Program for Calculating Velocities and Streamlines on the Hub-Shroud Midchannel Stream Surface of an Axial-, Radial-, or Mixed-Flow Turbomachine or Annular Duct. Vol. I - User's Manual, NASA TN D-8430; Vol. II - Programmer's Manual, NASA TN D-8431, 1977.

2. Katsanis, T.: Fortran Program for Calculating Transonic Velocities on a Blade-to-Blade Stream Surface of a Turbomachine. NASA TP-1772, 1981.

3. McNally, W.D.: Fortran Program for Calculating Compressible Laminar and Turbulent Boundary Layers in Arbitrary Pressure Gradients. NASA TN D-5681, 1970.

---

*The authors are very indebted to K.C. Civinskas and R.E. Boyle for providing the codes and for many hours of assistance in making them operational.

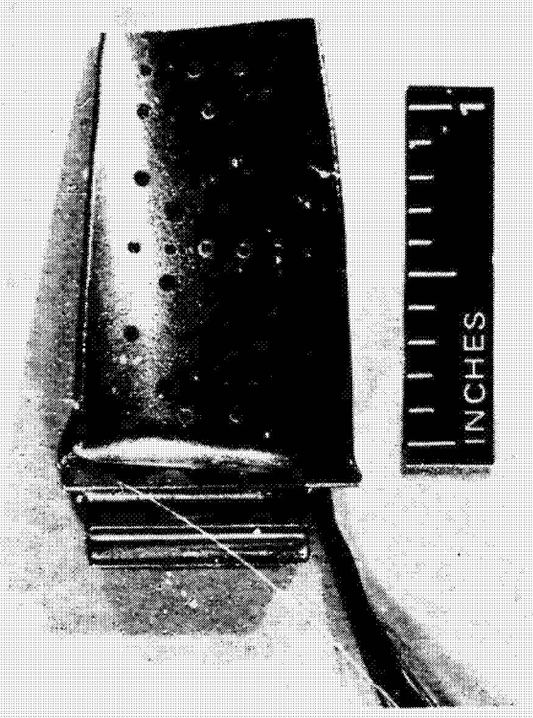

FIGURE 1 PRESSURE-SURFACE INSTRUMENTATION

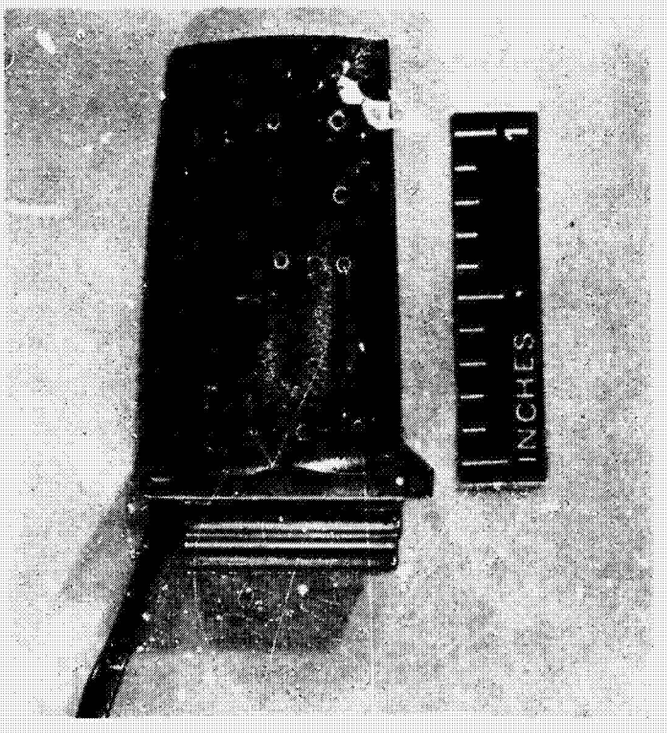

FIGURE 2 SUCTION-SURFACE INSTRUMENTATION

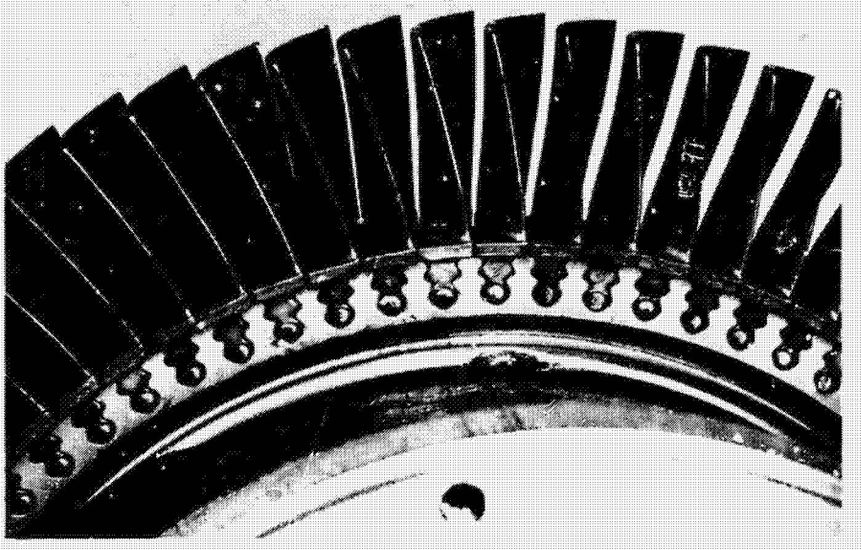

FIGURE 1 ROTOR ASSEMBLY WITH DISPRESENTATION

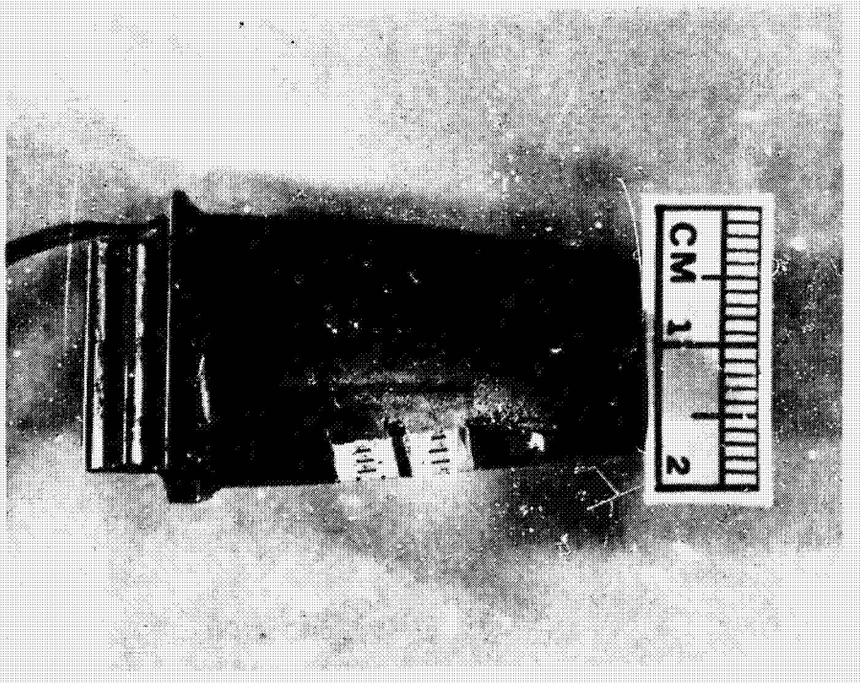

FIGURE 1 ROTOR ASSEMBLY WITH DISPRESENTATION

CALCULATION OF VISCOUS COMPRESSIBLE FLOWS IN SMALL GAS TURBINES

O.L. Anderson and G.D. Power
United Technologies Research Center
East Hartford, CT 06108

The NASA Lewis Research Center is conducting a program to develop improved technology for the Space Shuttle Main Engine (SSME). This program requires not only a component test program, but also the development of accurate and reliable analyses to support the program. Thus a computer analysis for the prediction of the flow of hot gases, composed of a variety of exhaust products, through rocket and gas turbine components would support this program and also would be suitable for a wide variety of other applications.

The Axisymmetric Diffuser Duct (ADD) code, developed by Anderson et al. (Ref. 1 and 2), has been shown to provide accurate and reliable viscous compressible flowpath calculations through small gas turbine components. It has been successfully applied to predict the flow in automotive gas turbine components (Ref. 2) such as that shown on Fig. 1, and swirling flow in a precombustion diffuser (Ref. 3). Vatsa et al., (Ref. 4) has extended the analysis to the prediction of supersonic underexpanded coflowing jet flows and Anderson et al., (Ref. 5) has extended the analysis to treat supersonic internal flow with shock waves and expansion waves. Subsequent operational use of the ADD code at NASA Lewis has identified a number of shortcomings in the code. The combined effects of low Reynolds number, large wall curvature, high swirl angles, and limitations in the turbulence models have taxed the capabilities of the code and produced stability and accuracy problems. The object of the present research program is to: 1) refine both the algebraic and two equation turbulence models presently in the code to include the effects of free stream turbulence and laminar/turbulent transition, 2) provide accurate predictions of the thermodynamic and transport properties of combustion product gases, and 3) improve the coordinate grid calculation for cases of long highly curved ducts. Following these code modifications, a matrix of test cases shall be calculated to: 1) identify numerical stability and computational accuracy problems occuring within the envelope of operation, 2) correct problems where possible, and 3) establish grid selection criteria to reduce operational problems.

DISCUSSION

Both the algebraic and two equation turbulence models in the ADD code, currently operational on the NASA Lewis Cray computer, have been modified to include the effects of free stream turbulence and laminar/turbulent transition. The effects of free stream turbulence have been included in the algebraic turbulence model by modifying the outer layer Clauser constant using an empirical correlation developed by Yuhas (Ref. 6). Calibration tests of the accuracy of this model are shown on Figs. 2 and 3 where the results are compared to the flat data of Blair (Ref. 7). Fig. 2 shows a skin friction plot versus Reynolds number based on momentum thickness. As can be seen on this plot, the calculated skin friction for 0.0% turbulence follows very closely the skin friction law of Coles (Ref 8) and is just slightly above the experimental data of Ref. 7. At the 5.0%

level the prediction is also slightly above the data, however the incremental change in skin friction has been predicted very accurately. Fig. 3 shows a comparison of the calculated velocity distributions with the experimental data of Ref. 7 for both the 0.0% and 5.0% turbulence levels in universal coordinates. Also shown on this plot is the law of the wall. Again, it can be seen that analysis shows excellent agreement with the experimental data in these calibration tests with the benchmark experiments of Blair (Ref. 7).

The two equation turbulence model developed by Chien (Ref. 9), which is currently in the ADD code, is under evaluation. This model only requires a proper specification of the initial conditions for the turbulent kinetic energy and dissipation since the physics contained in the equations account for both free stream turbulence and natural transition. In the boundary layer, the initial conditions are specified in the same manner as described by Wang (Ref. 10). Outside the boundary layer, the turbulent kinetic energy (turbulent intensity) and dissipation (dissipation length scale) are specified. Although turbulent kinetic energy is frequently measured and therefore usually known, the dissipation is not. Therefore, a brief analysis was conducted to provide estimates of the dissipation length scales for different levels of turbulence. Two types of analyses were employed. The first method estimated the free stream dissipation from the rate of decay of turbulent kinetic energy measured by Blair (Ref. 7). The second method estimated the dissipation from the turbulent kinetic energy spectrum, also measured by Blair, for different levels of free stream turbulence. A composite kinetic energy profile composed of both high frequency (dissipation length scale) and low frequency (integral length scale) correlations was fitted to the experimental data. Typical results of this latter procedure are shown on Fig. 4 which also shows the well known low frequency correlation of Von Karman. Based on these analyses, the dissipation length scale was found to be fairly consistant using both methods and was relatively constant for all levels of turbulence.

REFERENCES

1. Anderson, O. L.: Calculation of Internal Viscous Flows in Axisymmetric Ducts at Moderate to High Reynolds Numbers, Int. J. of Computers and Fluids, Vol. 8, No. 4, p 391-411, December, 1980.

2. Anderson, O. L., Hankins, G. B., and Edwards, D. E.: Extension to an Analysis of Turbulent Swirling Compressible Flow for Application to Axisymmetric Small LGas Turbine Ducts, NASA CR-165597, February, 1982.

3. Barber, T. J., Raghuraman, P., and Anderson, O. L.: Evaluation of an Analysis for Axisymmetric Internal Flows in Turbomachinery Ducts, Flow in Primary Non-Rotating Passages in Turbomachines, ASME Winter Annual Meeting, December, 1979.

4. Vatsa, V. N., Werle, M. J., and Anderson, O. L.: Solution of Slightly Underexpanded Two-Dimensional and Axisymmetric Coflowing Jets, AIAA J. Vol. 19, No. 3, March, 1981, p 303-311.

5. Anderson, O. L. and Power, G. D.: Investigation of Parabolic Computational Techniques for Internal High Speed Viscous flows, NASA Contract NAS11-/561, UTRC Report No. R84-956611, January, 1985.

6. Yuhas, L. J.: An Optimization Technique for the Development of a Two Dimensional Turbulent Boundary Layer, Thesis Lehigh University, September, 1981.

7. Balir, M. F.: Influence of Free Stream Turbulence on Turbulent Boundary Layer Heat Transfer and Mean Profile Development Part I and II, ASME J. of Heat Transfer, Vol. 105, February, 1983.

8. Coles, D.: The Law of the Wake in the Turbulent Boundary Layer, J. of Fluid Mechanics, Vol. 1 Part 2, July, 1956, p 191-226.

9. Chien, K-Y.: Predictions of Channel Flow and Boundary Flows with a Low-Reynolds-Number Two-Equation Model of Turbulence, AIAA 18th Aerospace Sciences Meeting, AIAA-80-0314, January, 1980.

10. Wang, J. H., Hartel, E. O.: Airfoil Heat Transfer Calculation Using a Low Reynolds Number Version of a Two Equation Turbulence Model, ASME J. of Eng. for Power, Vol. 107, January, 1985.

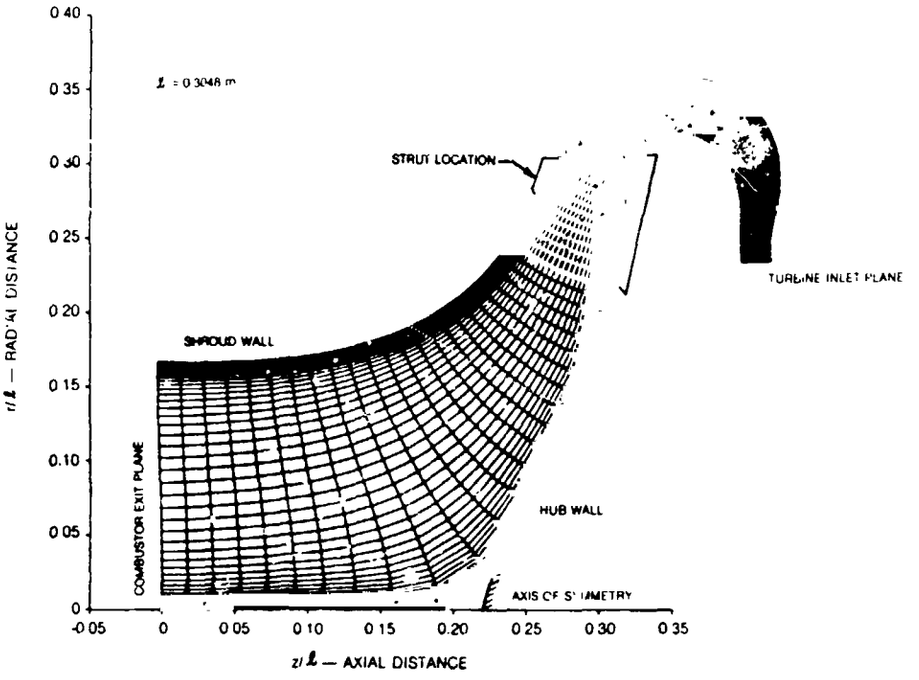

Figure 1 Computational Mesh for AGT101 Turbine Inlet Duct

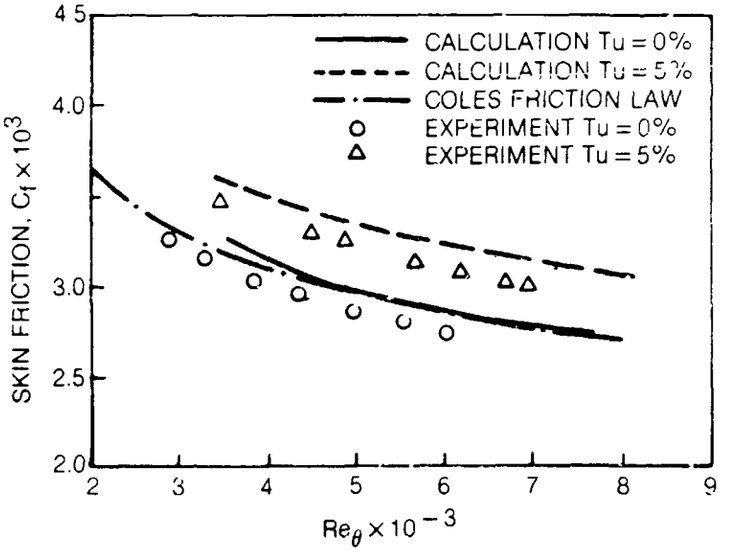

Figure 2 Skin Friction Coefficient versus Momentum Thickness Reynolds Number for Two Levels of Free-Stream Turbulence

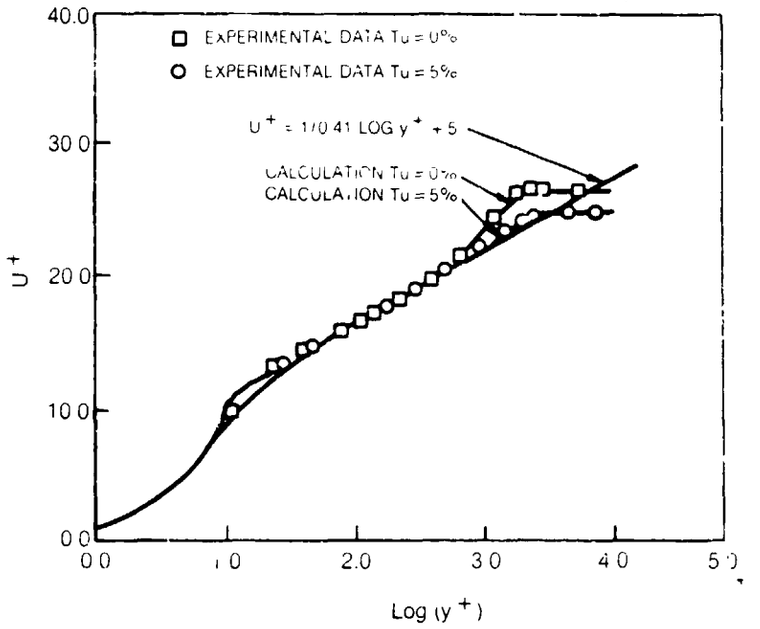

Figure 3 Universal Velocity Profiles for Tu = 0% and Tu = 5% at $Re_\theta = 6000$

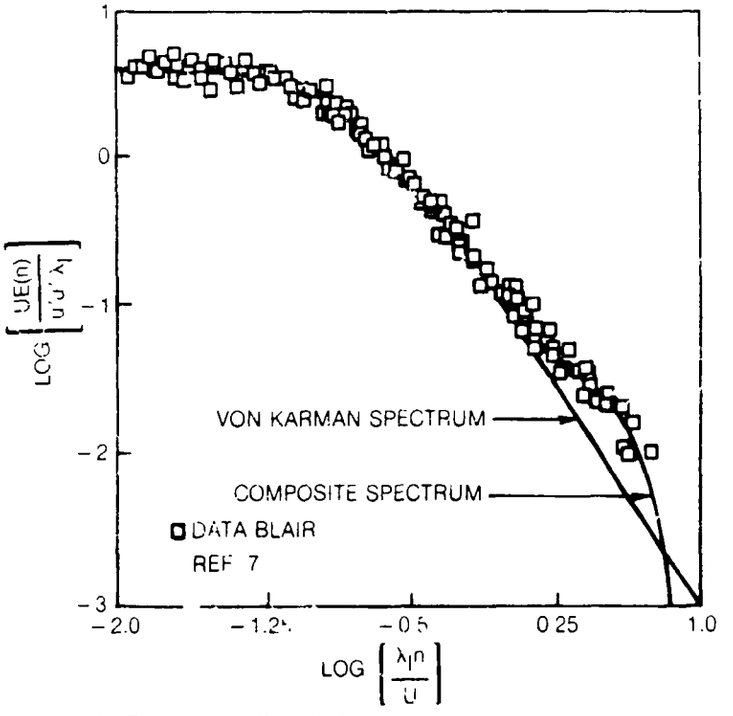

Figure 4 Turbulent Kinetic Energy Curve Fit — Tu = 6.0%

85-3-118-2

N85-27951

FLOW-INDUCED VIBRATION OF SSME MAIN INJECTOR LIQUID-OXYGEN POSTS

S.S. Chen, J.A. Jendrzejczyk, and M.W. Wambsganss
Argonne National Laboratory
Argonne, Illinois 60439

The liquid-oxygen (LOX) posts are exposed to hot hydrogen flowing over the tubes on its way to the combustion chamber. Fatigue cracking of some LOX posts was observed after test firing of the SSMEs. A current design modification consists of attaching impingement shields to the LOX posts in the outer row. This modification improved the vibration/fatigue problem of the LOX posts, but resulted in an increased pressure drop that ultimately shortened the life expectancy of other components.

A fundamental study of vibration of the LOX posts was initiated to understand the flow-induced vibration problem and to develop techniques to avoid detrimental vibrational effects with the overall objective of improving engine life. This paper summarizes this effort, including an assessment of the problem, scoping calculation and experiment, and a work plan for an integrated theoretical/experimental study of the problem.

RESULTS OF WORK

An assessment of the LOX post vibration problem has been performed to provide the basis for an integrated theoretical/experimental study. Different excitation mechanisms were considered and the results are summarized as follows:

1. Vortex Shedding: The synchronization of LOX post vibration with vortex shedding is not possible in either drag or lift direction because of several reasons: relatively large mass-damping parameter, swirlers (spoilers) on the LOX posts, high Reynolds number, relatively small pitch-to-diameter ratio, and highly turbulent flow.

2. Fluidelastic Instability: Based on a gap flow velocity of about 1670 ft/sec across the injector elements, the unshielded LOX posts are subjected to fluidelastic instability. Therefore, fluidelastic instability is identified as a potential mechanism that can contribute to LOX post damage in a short time.

3. Instability Due to Liquid Oxygen: The LOX posts will not become dynamically unstable due to the flow of liquid oxygen inside the LOX posts.

4. Acoustoelastic Resonance: The lowest acoustic frequency is potentially close to the lowest natural frequency of LOX posts. However, the significance of acoustic resonance depends on acoustic excitation, which may be associated with vortex shedding or turbulence. Vortex shedding is unlikely to become an important acoustic excitation. However, turbulence as well as other excitation sources have to be considered.

5. Turbulent Buffeting: The detailed turbulence characteristics are not known at this time. Turbulence burfeting is a potential excitation mechanism.

A scoping experiment was designed and performed for a tube array simulating a typical grouping of LOX posts. The experiments were performed in a water loop. The tube arrangement is to simulate post 77 in row 13 and its surrounding tubes. Figure 1 shows typical tube accelerations as a function of flow

velocity. The movements of the tubes depend strongly on flow velocity. At low flow velocities, the motion is small. As the flow velocity increases, tube aceleration increases. When the flow velocity exceeds a certain value, tube response increases rapidly; this threshold flow velocity is called the critical flow velocity. The critical flow velocity obtained in the water loop was used to evaluate the critical flow velocity of the unshielded LOX posts. It is found that the gap flow velocity of 1670 ft/sec is in the unstable region.

PERSPECTIVE/PLANS AND GOALS

The dynamic response of the LOX post can be represented by the following equation

$$[M_s + M_f]\{\ddot{Q}\} + [C_s + C_f]\{\dot{Q}\} + [K_s + K_f]\{Q\} = \{G\} \ , \qquad (1)$$

where Q is a generalized displacement; M_s, C_s, and K_s are the post mass, damping, and stiffness matrces, respectively; M_f, C_f, and K_f are the fluid added mass, fluid damping, and fluid stiffness matrices, respectively; G is the fluid excitation force. The key elements are C_f, K_f, and G.

At this time, there are no analytical or numerical methods available for calculating C_f and K_f for a general array of cylinders in crossflow. An analytical solution in conjunction with experimental data is being explored to provide some additional insight into the characteristics of the fluid forces. Another method is the numerical technique based on the computational fluid dynamics (CFD) method. The advantages and disadvantages of different numerical methods are being reviewed. A computer code will be developed to calculate C_f and K_f for the LOX post arrays.

Fluid excitation forces will be measured in a test section for a tube array simulating the LOX posts. Fluctuating fluid force components are to be measured in the drag and lift directions. Different grids will be used to simulate different upstream turbulence intensity. In addition, techniques will be developed to excite a tube in a tube array subjected to crossflow. At the same time the fluid force acting on the excited tube as well as the surrounding tubes will be measured as a function of tube motion. From these fluid forces, the required fluid force coefficients can be obtained.

CONCLUDING REMARKS

The LOX post array subjected to hot gas flow is a very complicated system. The detailed flow field is not known at this time, so a detailed evaluation of the LOX post vibration potential is not possible. The central issue in predicting the LOX post response is the fluid excitation force and motion-dependent fluid force. This remains a difficult issue. The work initiated by Lewis to develop techniques and to conduct tests to obtain the necessary fluid force is essential in the understanding of the vibration of the SSME LOX posts and in the development of techniques to avoid detrimental flow-induced vibration.

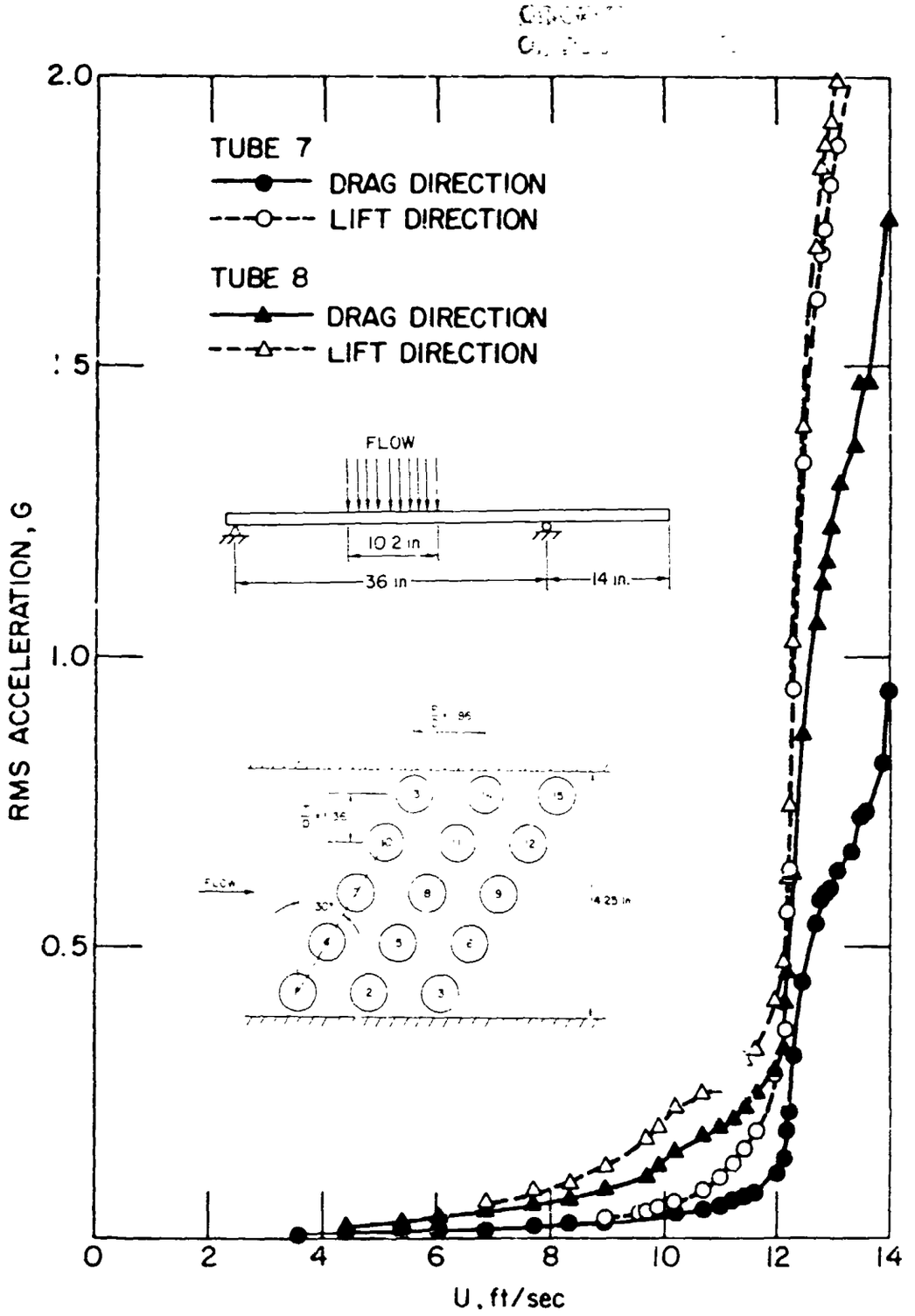

Fig. 1. Tube Acceleration as a Function of Flow Velocity

OVERVIEW OF STRUCTURAL RESPONSE: PROBABILISTIC STRUCTURAL ANALYSIS

Christos C. Chamis
National Aeronautics and Space Administration
Lewis Research Center
Cleveland, Ohio 44135

Advanced analysis methods are required to predict accurately the structural response (static, transient, cyclic, etc.) and accompanying local stresses in space propulsion system components operating in a fatigue environment consisting of complex thermal and mechanical load spectra. Advanced three-dimensional analysis methods must be formulated to accommodate the limited deterministic and probabilistic complex loading spectra as well as the anisotropic, thermoviscoplastic behavior of the material. Presently three-dimensional, deterministic, anisotropic, thermoviscoplastic analysis methods are not available and recourse is made to incremental, iterative analysis capabilities available in general-purpose structural analysis programs. Recognizing the importance and necessity of developing solutions for complex three-dimensional inelastic problems associated with aeronautical propulsion system components, Lewis is conducting intensive research under the HOST (Hot Section Technology) and Research and Technology (R&T) Base programs to develop the requisite deterministic analysis methodology for the solution of these problems. The deterministic, three-dimensional, inelastic analysis methodology developed under these HOST and R&T Base programs will be augmented to accommodate the complex probabilistic loading spectra, the thermoviscoplastic material behavior, and the material degradation associated with the corrosive and oxidative environments of space propulsion system structural components representative of the space shuttle main engine (SSME) such as turbine blades, transfer ducts, and liquid-oxygen posts.

The probabilistic approach to structural response consists of the following program elements: (1) composite load spectra, (2) probabilistic structural analysis methods development, (3) probabilistic finite element theory, (4) probabilistic structural analysis application, (5) structural tailoring of turbopump blades, (6) unified theory of dynamic creep buckling/ratcheting, (7) creep buckling/ratcheting analyzer, and (8) nonlinear COBSTRAN development. Research activities on all of these program elements (except the creep buckling/ratcheting analyzer) are under way. Program participants, program element description, and progress are the focus of this session.

SSME STRUCTURAL DURABILITY

STRUCTURAL RESPONSE

BACKGROUND:

- LOADING CONDITIONS ARE NOT DETERMINISTIC IN GENERAL
- MATERIAL THERMOMECHANICAL BEHAVIOR DIFFICULT TO CHARACTERIZE IN SSME SERVICE ENVIRONMENTS
- CONTINUING EVOLUTION OF NEW MATERIALS FOR USE IN SSME
- CONTINUING INCREASES IN PERFORMANCE REQUIREMENTS OF SSME

SSME STRUCTURAL DURABILITY

STRUCTURAL RESPONSE

RESULT:

- DETERMINISTIC METHODS ARE INADEQUATE TO DESCRIBE THE STRUCTURAL RESPONSE OF SSME CRITICAL COMPONENTS WHERE:
  - THE LOADING CONDITIONS ARE NOT DETERMINISTIC
  - THE MATERIAL THERMOMECHANICAL BEHAVIOR IS NOT FULLY CHARACTERIZED
  - THE DEMANDS FOR NEW MATERIAL AND INCREASED PERFORMANCE IS EVOLUTIONARY

SSME STRUCTURAL DURABILITY

STRUCTURAL RESPONSE

NEED/OBJECTIVE:

- o DEVELOPMENT OF PROBABILISTIC METHODS
  - o LOADING CONDITIONS DEFINITION
  - o MATERIAL BEHAVIOR DESCRIPTION
  - o STRUCTURAL ANALYSIS PREDICTION

FOR CRITICAL SSME STRUCTURAL COMPONENTS IN ATTENDANT SERVICE ENVIRONMENTS

SSME STRUCTURAL DURABILITY STRUCTURES RESEARCH ACTIVITIES

PROGRAM SCHEDULE

PROGRAM ELEMENT/ACTIVITY DESCRIPTION	TYPE	FY 84	85	86	87	88	89
COMPOSITE LOAD SPECTRA	CONTRACT						
PROBABILISTIC STRUCTURAL ANALYSIS METHODS	CONTRACT						
VARIATIONAL APPROACH TO PROBABILISTIC FINITE ELEMENTS	GRANT						
PROBABILISTIC STRUCTURAL ANALYSIS	IN-HOUSE						
STRUCTURAL ANALYSIS/TAILORING OF TURBOPUMP BLADES	IN-HOUSE						
UNIFIED THEORY OF DYNAMIC CREEP BUCKLING/RATCHETING	GRANT						
CREEP BUCKLING/RATCHETING ANALYZER	CONTRACT						
NONLINEAR COBSTRAN	IN-HOUSE						

STRUCTURES RESEARCH ACTIVITIES ON SSME STRUCTURAL DURABILITY

RESEARCH ACTIVITY	TYPE	BRIEF DESCRIPTION
COMPOSITE LOAD SPECTRA	CONTRACT	PROBABLISTIC METHODS TO DEFINE THE INDIVIDUAL AND COMBINED LOADS ON SSME COMPONENTS
PROBABILISTIC STRUCTURAL ANALYSIS METHODS	CONTRACT	PROBABILISTIC DETERMINATION OF GLOBAL/LOCAL NONLINEAR DISPLACEMENTS/STRESSES/STRAINS
VARIATIONAL APPROACH TO PROBABILISTIC FINITE ELEMENTS	GRANT	DEVELOPMENT OF ADVANCED PROBABILISTIC STRUCTURAL MECHANICS METHODS
PROBABILISTIC STRUCTURAL ANALYSIS	IN-HOUSE	APPLICATION OF EXISTING PROBABILISTIC METHODS TO STRUCTURAL ANALYSIS OF SSME TYPE COMPONENTS
STRUCTURAL ANALYSIS/TAILORING OF TURBOPUMP BLADES	IN-HOUSE	ADAPTATION OF STAEBL TO SSME TURBOPUMP BLADES
UNIFIED THEORY OF DYNAMIC CREEP BUCKLING/RATCHETING	GRANT	DERIVATION AND INTEGRATION OF MECHANISTIC MODELS OF VARIABLES INFLUENCING CREEP BUCKLING/RATCHETING
CREEP BUCKLING/RATCHETING ANALYZER	CONTRACT	DEVELOPMENT OF A COMPUTER CODE TAILORED FOR CREEP BUCKLING/RATCHETING
NONLINEAR COBSTRAN	IN-HOUSE	ADAPTATION OF COBSTRAN TO ACCOMMODATE THE THERMO-VISCOPLASTIC BEHAVIOR OF SSME TURBOPUMP BLADES

STRUCTURAL RESPONSE BENEFITS

- SHORT TERM:
  - MORE ACCURATE TIME-PHASING OF LOADS
  - IMPROVED ACCURACY OF PREDICTED STRESS/STRAIN
    - WITH ASSESSED PROBABILITY AND CONFIDENCE LEVEL
  - SPECIFIC GUIDELINES FOR DESIGN MODIFICATIONS TO INCREASE SERVICE LIFE
- LONG TERM:
  - PREDICTIVE METHODS TO DESIGN SSME CRITICAL COMPONENTS WITH SPECIFIED
    - STRUCTURAL DURABILITY
    - SERVICE LIFE
    - PROBABILITY
    - CONFIDENCE LEVEL

COMPOSITE LOADS SPECTRA FOR SELECT SPACE PROPULSION STRUCTURAL COMPONENTS*

J.F. Newell
Rockwell International
Canoga Park, California 91304

Rocket engine technology continues to demand higher performance with lighter weight components that have man-rated reliability requirements. These requirements have yielded higher operating pressures, temperatures, and transient effects as well as markedly increased mechanical vibration and flow-related loads. The difficulty in installation, cost, and potential for destroying an engine severely limited the required instrumentation and measurements to adequately define loads of key components such as turbine blades. Also, accurate analytical methodologies for defining internal flow-related loads are just emerging for problems typically found in rocket engines. The difficulty of obtaining measured data and verified analysis methodologies has led to the probabilistic load definition approach of this contract. Rocketdyne has the state-of-the-art methods for defining loads and analysing structural problems and has teamed with Battelle to utilize their expertise in the development of probabilistic models.

The objective of this program is to develop generic load models, with multiple levels of progressive sophistication to simulate the composite (combined) load spectra that are induced in space propulsion system components, representative of space shuttle main engines (SSME), such as transfer ducts, turbine blades, and liquid oxygen posts. These models will be developed through describing individual loading conditions using state-of-the-art probabilistic methods combined with deterministic coefficients related to key engine variables. The combinations of these loading conditions will use a similar approach to syntnesize the composite load spectra. The use of key variables, such as power level, flow, pump speed, or weight, allows for generic load definition for scaling and prediction of component loads.

The second approach in the option portion of the contract will consist of developing coupled models for composite load spectra simulation which combine the (mechanistic) models for thermal, dynamic, acoustic, high-pressure, and high rotational speed, etc. Probabilistic synthesis using statistically varying coefficients will be used to obtain the composite load spectra.

The unified theory required to combine the various individual load simulation models (hot-gas, dynamic, vibrations, instantaneous-position, centrifugal, etc.) into composite load spectra simulation models will be developed under this program. Results obtained from these models will be compared with available numerical results, with the loads induced by the individual load simulation models, and with available structural analysis results from independent analyses and tests. These theories developed under both approaches will be further validated with respect to level of sophistication and relative to predictive reliability and attendant level of confidence.

---

*Work performed under NASA contract NAS3-24382.

A computer code configured as an expert system will be developed that incorporates the various individual and composite load spectra models to construct the specific load model desired. The approach is to develop and deliver the computer code at four intervals in the contract. The first delivery will be an initial code for turbine blade loading. Each subsequent delivery will add sophistication to the component probabilistic load definition and the decision-making processes as well as installing a new set of loads for an additional component (e.g., liquid oxygen post). This allows for on-going evaluation and usage of the system by both Rocketdyne and NASA starting with the first code delivery.

The initial efforts for this program are proceeding with the probabilistic model theory. The surveys of individual loadings, combined loadings, probabilistic methods, and mission history profiles are in progress. The liquid oxygen post and turbine blade survey efforts have been completed. The survey of appropriate probabilistic methodologies applicable to the rocket engine has proceeded to testing and evaluating methodologies with typical SSME test data. This effort is summarized in a separate presentation.

The simulation of individual load models for turbine blades has been started so that the initial turbine blade code can be delivered by October. This includes both relating measured test data to the individual turbine blade load component-like pressure, temperature, or centrifugal loads and developing probabilistic coefficients from engine data.

The code development effort has just been started in parallel with the other tasks. Defining the overall approach and knowledge base requirements is the first task.

COMPOSITE LOAD SPECTRA FLOW CHART/TASK FEATURES SUMMARY

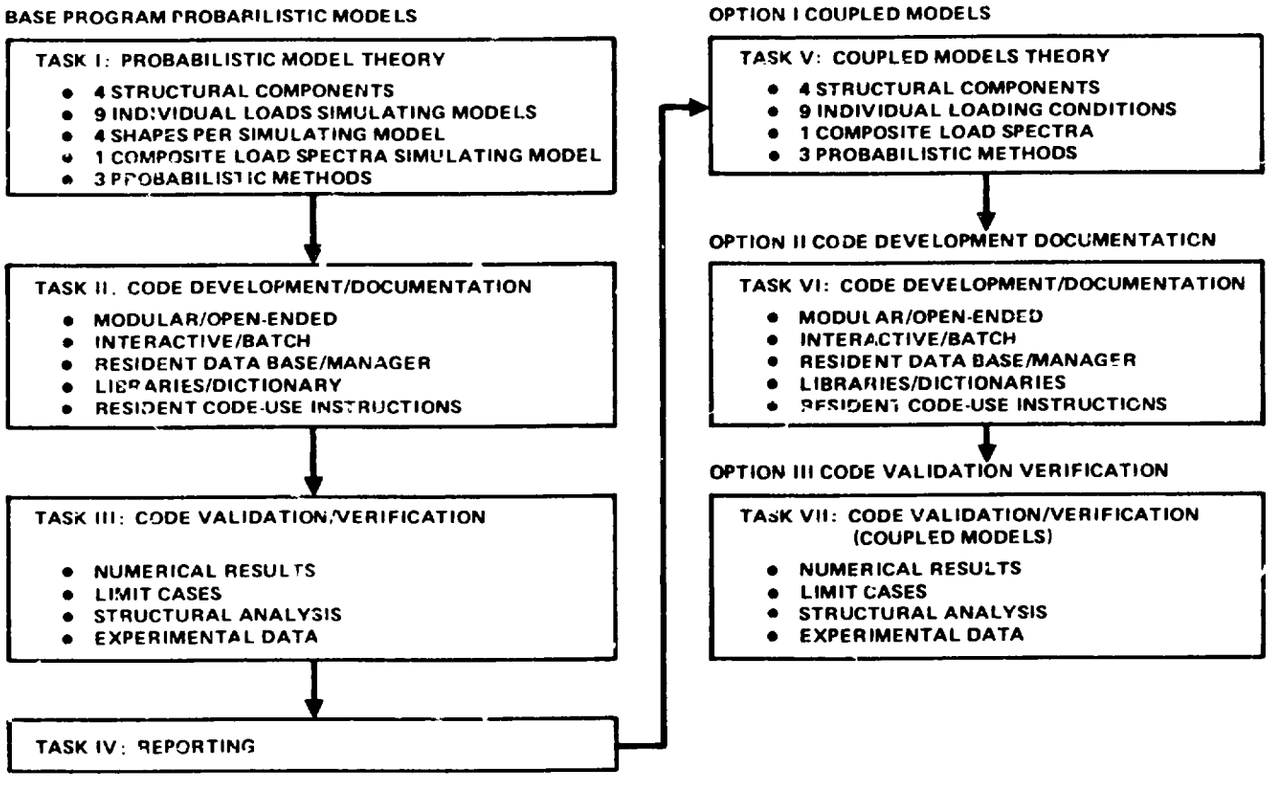

700-601

Rockwell International
Rocketdyne Division

FLIGHT MISSION DUTY CYCLES

SPACE SHUTTLE ASCENT ACCELERATION

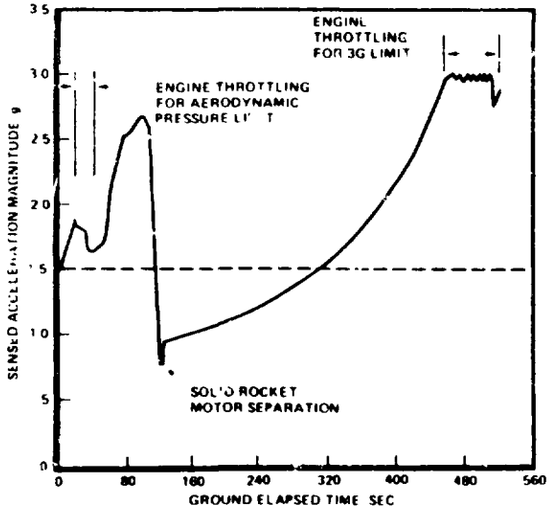

SSME PERFORMANCE DURING FOURTEEN LAUNCHES

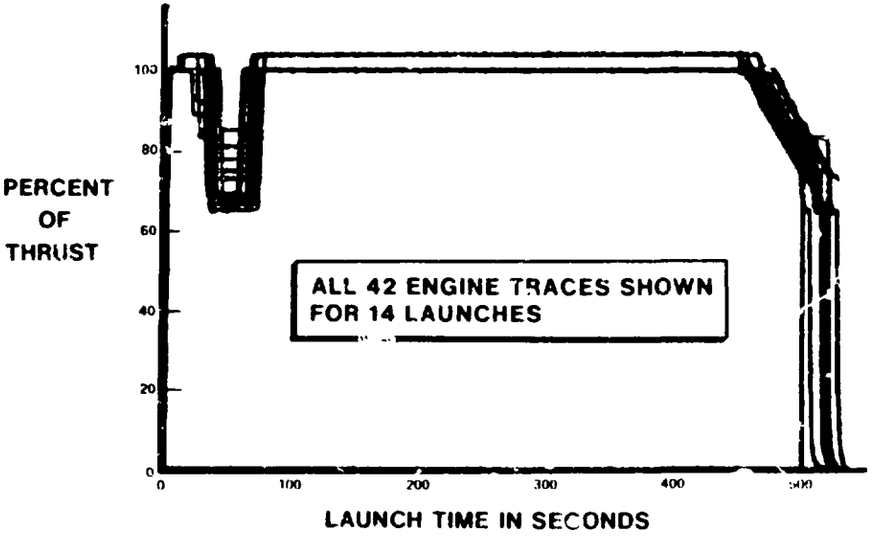

Rockwell International
Rocketdyne Division

GENERIC LOADS

- CONSIDER ALL POTENTIALLY SIGNIFICANT LOADS
- SSME SUBSET PRIMARILY USED
- LOADS APPLICABLE TO LO_2/LH_2 ENGINES
- LOADS RELATED TO COEFFICIENTS AND KEY PARAMETERS
- COMBINATION OF DETERMINISTIC AND PROBABALISTIC VARIABLES
- KEY PARAMETERS AFFECTING LOADS INCLUDE
  - ENGINE CONFIGURATION
  - THRUST
  - WEIGHT
  - INLET CONDITIONS
  - FLOW INTERRUPTIONS
  - PUMP TORQUE
  - PUMP SPEEDS
  - ETC
- COMPONENTS
  - LOX POST
  - TURBINE BLADE
  - TRANSFER DUCT
  - OTHER – MCC LINER, HPOTP DUCT, NOZZLE FEEDLINES

700 603

Rockwell International
Rocketdyne Division

SSME STANDARD INSTRUMENTATION AVAILABLE ON POWERHEAD

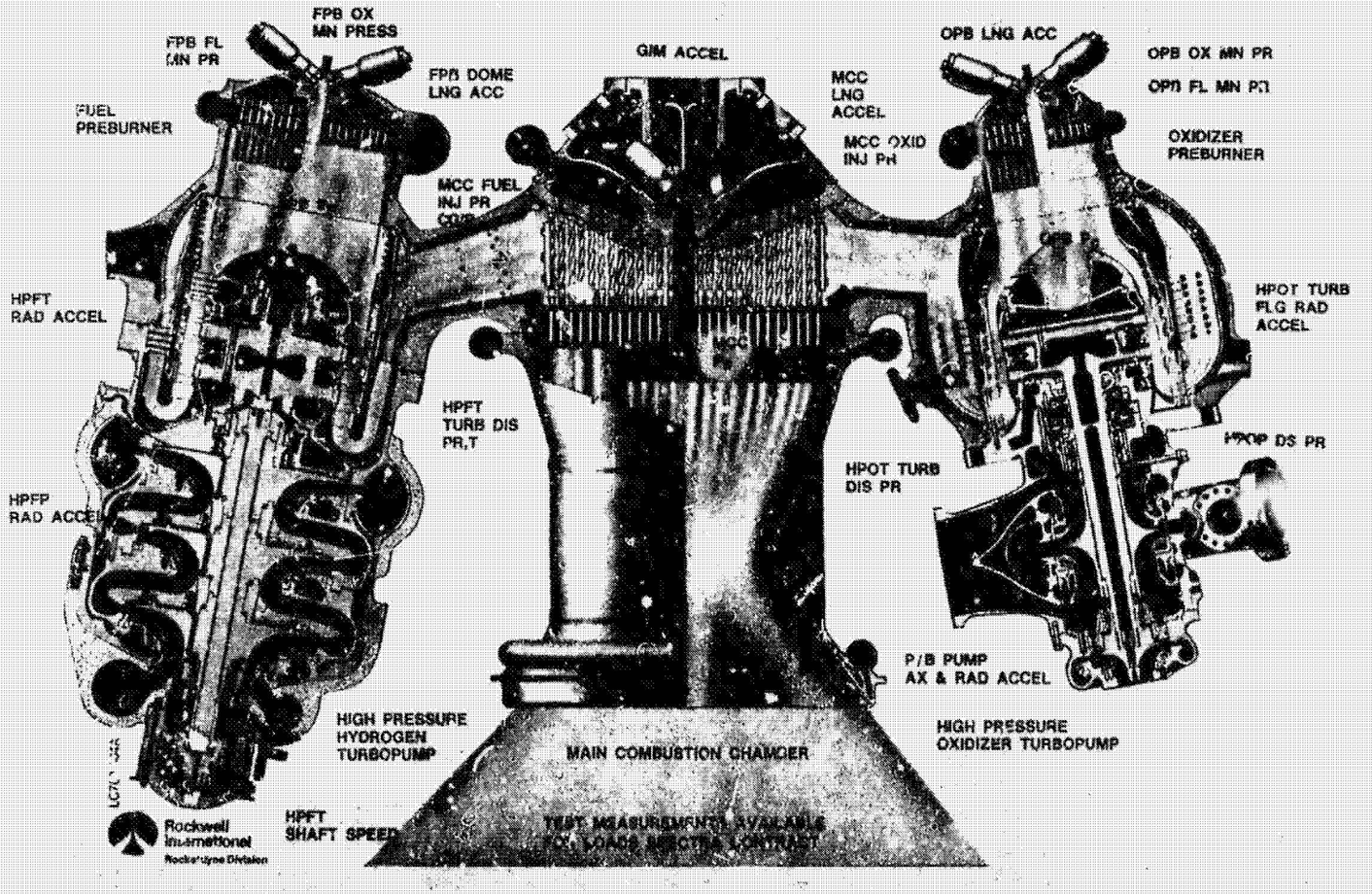

DATA ANALYSIS

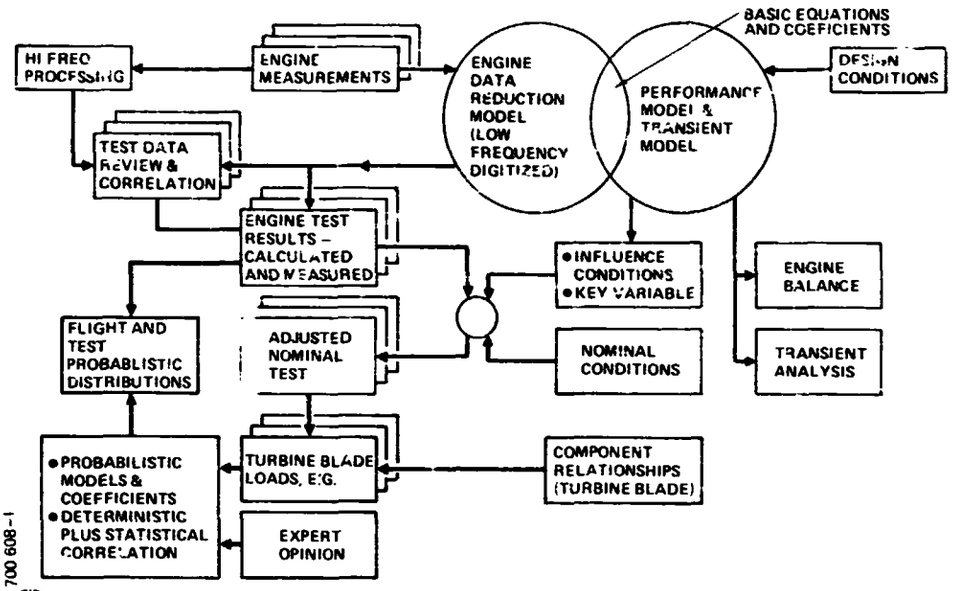

HPFTP TURBINE OPERATING CONDITIONS

COOLANT CIRCUIT

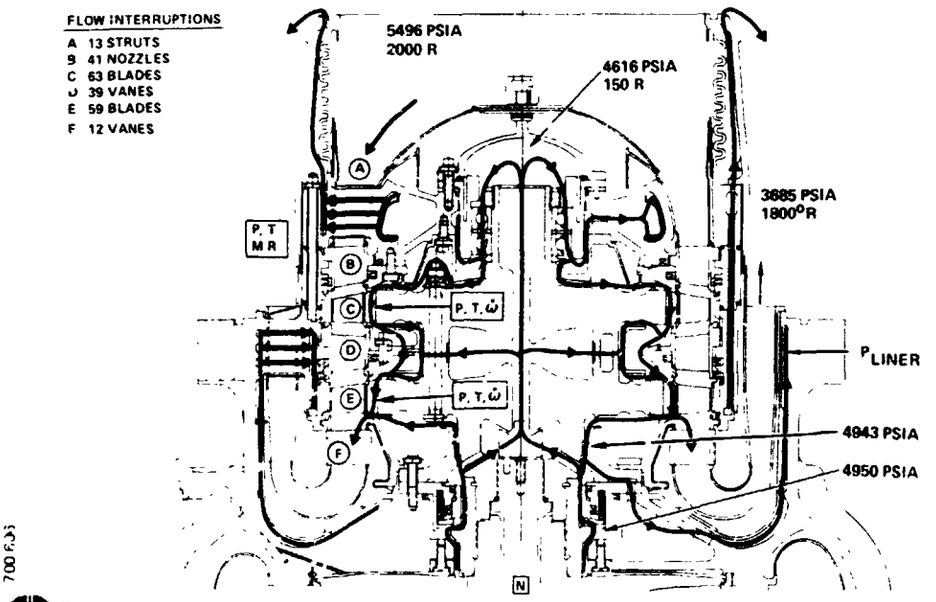

HIGH PRESSURE FUEL TURBINE TRANSIENT CHARACTERISTICS

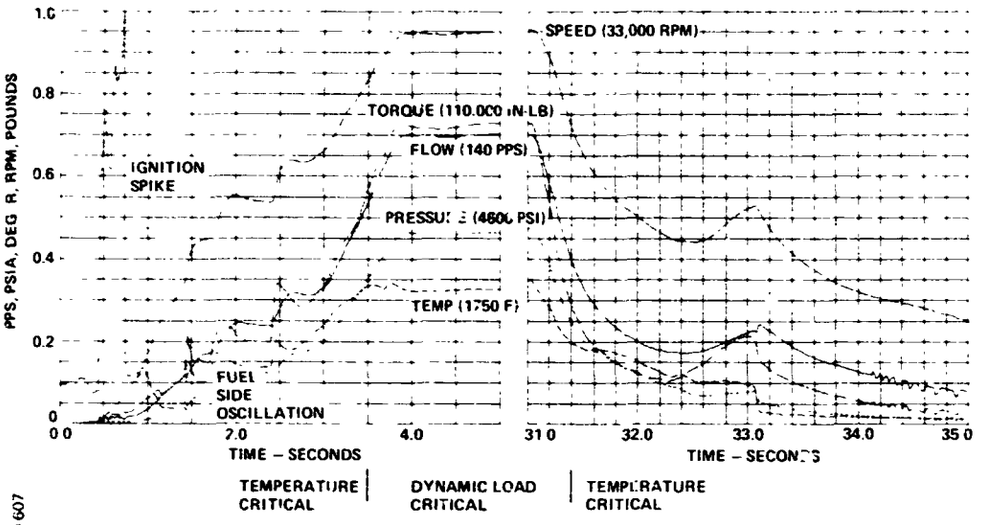

700 607

Rockwell International
Rocketdyne Division

TURBINE BLADE LOADS

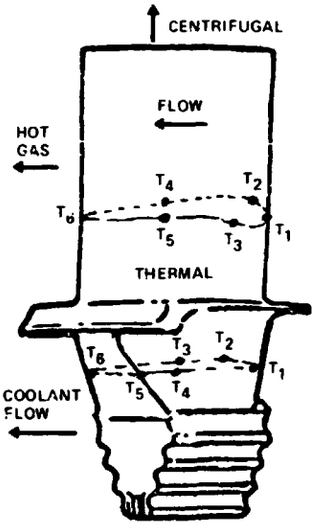

- AIRFOIL
  - CENTRIFUGAL
  - PRESSURE
  - BLADE TEMPERATURE
  - DYNAMIC ΔP
  - IMPINGEMENT LOADS
  - DAMPER/FRICTION
  - TIP RUBBING
- SHANK
  - PRESSURE
  - METAL TEMPERATURES
- EXPERT OPINION INPUT REQUIRED
  - LACK OF MEASURED DATA

KEY VARIABLES

	SPEED
	TURBINE ANALYSIS
	TURBINE/THERMAL ANALYSIS
	SPEED, INTERRUPTIONS
	UPSTREAM DEBRIS POTENTIAL
	GEOMETRY, WHIRLIGIG TEST
	DESIGN
	COOLANT FLOW AND THERMAL ANALYSIS

700 609

Rockwell International
Rocketdyne Division

LOAD SPECTRA CODE

- **INITIAL PLANNING STAGE**
- **DEFINING KNOWLEDGE BASE REQUIREMENTS**
  - INDIVIDUAL LOAD PROBABILISTIC FUNCTIONS
  - COMPOSITE LOAD SIMULATION TECHNIQUES
  - PROBABILISTIC METHODS AND SOLUTION ALGORITHMS
  - SSME BASELINE INFORMATION
    - KEY VARIABLES MISSION HISTORY PROFILES – GROUND TEST AND FLIGHT
    - ENGINE SYSTEM PACKAGING AND SIZING
    - ENGINE CYCLE AND COOLANT TECHNIQUES
    - COMPONENT CHARACTERISTICS
- **MEET OVERALL GOALS OF CONTRACT**
- **CODE SOPHISTICATION ENHANCED IN EACH DELIVERED MODULE**

70P 610

Rockwell International

INTERRELATIONSHIPS OF CONTRACT EFFORTS SSME AND PROBABILISTIC UTILIZATION

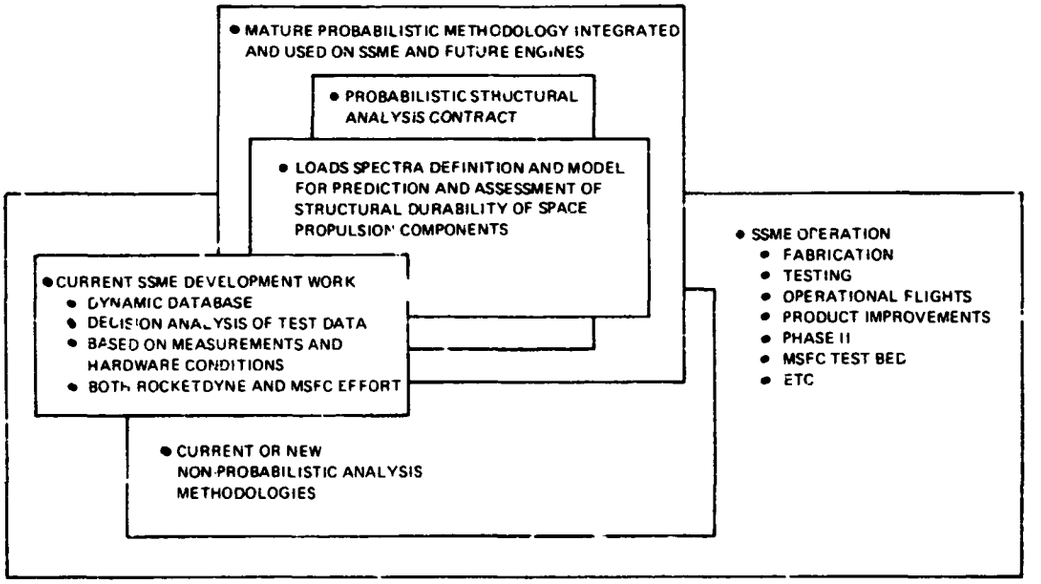

485-773

Rockwell International
Rocketdyne Division

COMPOSITE LOADS SPECTRA FOR SELECT SPACE PROPULSION STRUCTURAL COMPONENTS - PROBABILISTIC LOAD MODEL DEVELOPMENT*

Robert Kurth
Battelle Columbus Laboratory
Columbus, Ohio 43201

This effort is in support of the development of an expert system of computer codes to predict the loads on select structural components of a space propulsion engine. The development will be based primarily on the space shuttle main engine (SSME) test data base. Because of random variations of the many different sources of the loadings on the selected structural components and transients, a probabilistic approach to the problems has been adopted. The goal of this task is to characterize all of the individual sources of loads at critical structural locations, such as the turbine blades, the transfer ducts, and liquid oxygen posts, using state-of-the-art probabilistic methods with varying levels of sophistication.

The second phase of this work is the development of a composite load model based on a probabilistic synthesis of the individual load model previously developed. This model will be based on the stochastic combination of the load variables and not on the physical process for the combination of the individual loads to the composite load seen by the selected structural components.

The probabilistic load model effort has been started with an initial survey of available methods and an assessment of these methods using typical SSME data. The results of the first year of study will produce a model applicable to turbine blades in an engine represented by the SSME. The survey of appropriate statistical methods has been completed for this phase of the work and the assessment of these methods is in progress. The engine measurements related to turbine blade loads are under study primarily to support the first year code development effort.

*Work performed under NASA contract NAS3-24382.

SURVEY OF AVAILABLE METHODS

- LITERATURE SURVEY CONDUCTED
- MANY INVESTIGATIONS MADE BUT NUMBER OF DIFFERENT METHODS LIMITED
- MOST IMPORTANT METHODS INCLUDE
  - ANALYTIC
  - FIRST ORDER SECOND MOMENT
  - BARRIER CROSSING (FIRST PASSAGE)
  - DISCRETE SIMULATION

Rockwell International Rocketdyne Division

Battelle

ANALYTIC METHODS

- MATHEMATICALLY COMPLEX
- ONLY WORK FOR LIMITED SET OF DISTRIBUTIONS
- LIMITED APPLICATION TO SSME

Rockwell International Rocketdyne Division

Battelle

FIRST ORDER SECOND MOMENT METHODS

- IN USE PRIMARILY IN STRUCTURAL ANALYSIS
  - •RACKWITZ-FIESSLER
  - •CHEN-LIND
  - •WIRSCHING
- PROVIDE THE PROBABILITY OF A LIMIT STATE BEING EXCEEDED
- REQUIRES MANY APPLICATIONS TO DEFINE PROBABILISTIC NATURE OF LOADS
- COORDINATE TRANSFORMATIONS AND APPROXIMATIONS NEEDED TO HANDLE NON-NORMALLY DISTRIBUTED VARIABLES
- LIMITED USE FOR INDIVIDUAL LOADS BUT MAY BE USEFUL FOR COMPOSITE LOAD MODEL

Rockwell International Rocketdyne Division

Battelle

DISCRETE SIMULATION METHODS

- WILL BE NEEDED FOR THE EXPERT CODE DEVELOPMENT AT LEAST TO VERIFY THE CALCULATIONS
- MOST IMPORTANT METHODS ARE
  - •MONTE CARLO
  - •MARKOV CHAIN
  - •DISCRETE PROBABILITY DISTRIBUTION
  - •RASCAL

Rockwell International Rocketdyne Division

Battelle

BARRIER CROSSING METHODS

- PROVIDES AN EXPECTED NUMBER, OR RATE OF, CROSSINGS OF A GIVEN LEVEL, I.E., THE BARRIER
- CAN BE USED TO DETERMINE THE PROBABILITY OF ANY GIVEN LEVEL BEING EXCEEDED
- RELATIVELY STRAIGHTFORWARD TO APPLY

Rockwell International Rocketdyne Division

Battelle

CHARACTERIZATION OF CURRENT LOADS

- DESIRED RESULTS ARE
  - ESTIMATE OF THE MEAN
  - ESTIMATE OF CREDIBLE VARIATIONS
  - MOST SUITABLE PDF FORM
  - STATIONARITY TEST
  - CORRELATION EFFECTS, IF ANY
- FREQUENCY OF LOADS
  - DISTRIBUTIONAL FAMILY IS CHOSEN BY DISTRIBUTION SHAPE, I.E., SKEWNESS AND KURTOSIS
  - DISTRIBUTION PARAMETERS OBTAINED BY MOMENT MATCHING
    CHI SQUARE TEST USED TO CHECK

Rockwell International Rocketdyne Division

Battelle

PROBABILISTIC FUNCTION DEFINITION

- GOAL IS TO DEFINE THE LOAD LEVEL, L_1, AND ITS PROBABILITY OF OCCURRENCE, P_1
- THE LOAD LEVEL L_I IS DEFINED BY A FUNCTION WHICH IS A COMBINATION OF DETERMINISTIC AND PROBABILISTIC METHODS

  $L_I(T) = F_D(X_1, X_2, \ldots, X_N) \oplus F_P(Y_1, Y_2, \ldots, Y_M)$

  X_1 DETERMINISTIC INPUTS

  Y_1 PROBABILISTIC INPUTS

  F_D DETERMINISTIC FUNCTION

  $\oplus$ PROBABILISTIC FUNCTION

- SOME, OR ALL, OF THE X_1'S AND Y_1'S MAY BE THE SAME

Rockwell International Rocketdyne Division

Battelle

PROBABILISTIC FUNCTION DEFINITION

- THE FUNCTIONS F_D AND F_P ARE NOT NECESSARILY ANALYTIC, E.G. THEY MAY REPRESENT COMPUTER CODES
- THE COEFFICIENTS AND COMPLEXITY OF THE FUNCTION L_I (T) WILL BE DETERMINED BY THE ACCURACY REQUIRED BY THE ANALYST
- EXPERT OPINION IS CONTAINED IN THESE FORMULATIONS

Rockwell International Rocketdyne Division

Battelle

PROBABILISTIC FUNCTION DEFINITION

- THE PROBABILITY OF THE LOAD $L_1(T)$ OCCURRING IS GIVEN BY
  $P(L_1(T)) = P(Y_1)P(Y_2) \ldots P(Y_M)$
- THIS PROBABILITY CAN BE ONE
- IF Y_J IS DEPENDENT ON Y_K THEN CONDITIONAL PROBABILITY IS USED
- TO ADDRESS THE VARIATION ABOUT THE LOAD LEVEL $L_1(T)$ BARRIER CROSSING METHODS ARE USED

Rockwell International Rocketdyne Division

Battelle

PROBABILISTIC FUNCTION OUTPUT

- THE PROBABILISTIC FUNCTION OUTPUT IS AN ARRAY OF DISCRETE LOAD LEVELS WITH THEIR ASSOCIATED PROBABILITY OF OCCURRENCE

  $R = [(L_1, P_1), (L_2, P_2), \ldots (L_N, P_N)]$

- THE RELIABILITY (ACCURACY) OF THE OUTPUT CAN BE CONTROLLED BY INCREASING OR DECREASING N
- THE VECTOR OF ORDERED PAIRS R IS A DISCRETE REPRESENTATION OF THE DENSITY FUNCTION FOR THE LOAD AND CAN BE USED TO CALCULATE MEANS, VARIATIONS, AND SO FORTH

Rockwell International Rocketdyne Division

Battelle

STATUS OF PROBABILISTIC LOAD MODEL DEVELOPMENT

- SURVEY COMPLETED
- STATISTICAL ANALYSIS PACKAGE COMPLETED
- BARRIER CROSSING ANALYSIS METHOD COMPLETED
- TURBINE BLADE LOAD ANALYSIS STARTED
- JOINT DENSITY FUNCTIONS CALCULATED
- PROBABILISTIC FUNCTION DEVELOPMENT BEGUN AND TESTED FOR 65% AND 104% POWER LEVELS

Rocketdyne Division

Battelle

PROBABILISTIC STRUCTURAL ANALYSIS THEORY DEVELOPMENT*

O.H. Burnside
Southwest Research Institute
San Antonio, Texas 78284

The objective of the PSAM project is to develop analysis techniques and computer programs for predicting the probabilistic response of critical structural components for current and future space propulsion systems. This technology will play a central role in establishing increased system performance and durability.

Southwest Research Institute has assembled a project team from industry and the university community whose technical expertise and experience make them uniquely qualified for the PSAM effort. The participants on the team are: Southwest Research Institute - project management and solution strategies development; MARC Analysis Research Corporation - code development for probabilistic finite element methods; Rocketdyne Division, Rockwell International Corp. - Space Shuttle Main Engine (SSME) design and hardware experience; Prof. Paul Wirsching (University of Arizona) - probabilistic and reliability methods; Prof. Gautam Dasgupta (Columbia University) - stochastic finite elements; and Prof. Satya Atluri (Georgia Tech) - advanced material constitutive models.

The PSAM program was initiated in October 1984 and is a four-year effort. The first year's technical activity is concentrating on probabilistic finite element formulation strategy and code development. Work is also in progress at Rocketdyne to survey critical materials and SSME components such as turbine blades, liquid oxygen posts, and transfer ducts. This survey will provide information on the operating environment and failure modes encountered by space propulsion system components, as well as verification cases for the computer codes developed in PSAM.

The probabilistic finite element computer program NESSUS (Numerical Evaluation of Stochastic Structures Under Stress) is being developed by MARC Analysis Research. MARC's code development activities for NESSUS are presented elsewhere in these proceedings. The probabilistic FEM code development is scheduled for three years. The final probabilistic code will have, in the general case, the capability of performing nonlinear dynamic analysis of stochastic structures. Stochasticity can be found in the loads and in the structure due to material properties, geometry, and boundary conditions. The goal of the first-year effort is to develop a probabilistic FEM code for NASA-LeRC which has the capability to analyze linear elastic structures under static and dynamic loading. With this code, the dynamic response of components such as turbine blades can be computed. Nonlinear enhancements will be made in the final two years of the finite element task.

The remaining two technical tasks, Approximate Methods and Advanced Methods, will begin in the second year of the PSAM program. It is the goal of the Approximate Methods effort to increase problem solving efficiency relative to finite element methods by using energy methods to generate trial solutions which satisfy the structural boundary conditions. These approximate methods will be less computer intensive relative to the finite element approach because

---

*Work performed under NASA contract NAS3-24389.

of the reduced number of degrees of freedom and also the reduced number of random variables. The object of the Advanced Methods task is to seek new algorithms which can be applied to probabilistic structural analysis, rather than to refine existing ones. While selection of such methods has not been made, several candidates are under consideration. These include using weighted residual techniques for deriving the structural equations and the boundary element method applied in a probabilistic format, together with artificial intelligence/expert systems to aid the engineer in performing probabilistic analyses. The Advanced Methods task will be conducted over the final three years of the PSAM program.

Three approaches have been identified for computing the probabilistic structural response. These are fast probability integration (FPI) methods used in reliability analysis, methods of moments, and Monte Carlo simulation. Both FPI and moment methods are computationally efficient, but do involve certain approximations. Monte Carlo gives "exact" results, but requires a large number of realizations to obtain high accuracy. For large systems with many random variables, the Monte Carlo method does not appear practical because it is so computer intensive, especially if information about the tails of the distributions is desired. However, it is a valuable tool when applied to smaller systems for judging the accuracy of other methods.

In summary, the analysis methods and computer codes developed under PSAM are expected to provide the tools for both enhancing the reliability of space propulsion system designs and advancing the state of probabilistic structural mechanics.

PROBABILISTIC STRUCTURAL ANALYSIS METHODS (PSAM) FOR SELECT SPACE PROPULSION SYSTEM COMPONENTS

NASA-LeRC Contract No. NAS3-24389
SwRI Project No. 06-8339

- Program Objective -

Develop Analysis Techniques and Computer Programs for Predicting the Probabilistic Response of Critical Structural Components for Current and Future Space Propulsion Systems

PSAM PROJECT TEAM

Prime Contractor

- Southwest Research Institute
  San Antonio, Texas

Subcontractors

- MARC Analysis Research Corporation
  Palo Alto, California
- Rocketdyne Division, Rockwell International Corp.
  Canoga Park, California
- University of Arizona (Prof. Paul Wirsching)
  Tucson, Arizona
- Georgia Institute of Technology (Prof. Satya Atluri)
  Atlanta, Georgia
- Professor Gautam Dasgupta
  Columbia University
  New York, New York

PROBABILISTIC STRUCTURAL ANALYSIS METHODS
PROGRAM SCHEDULE

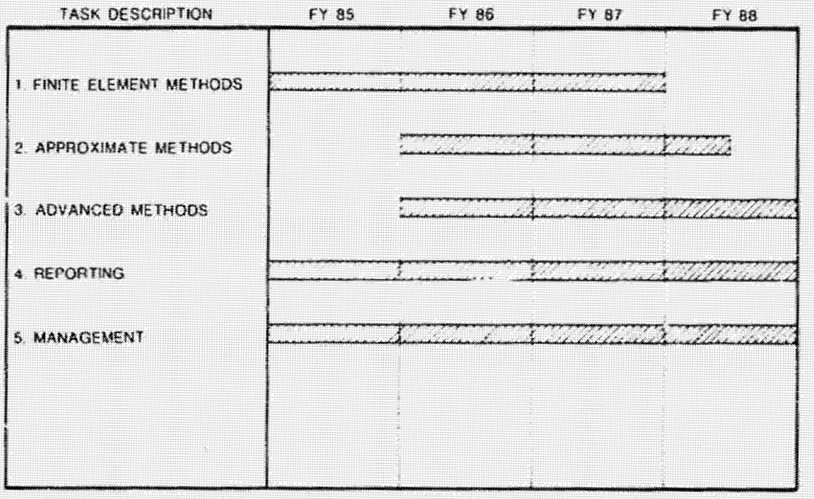

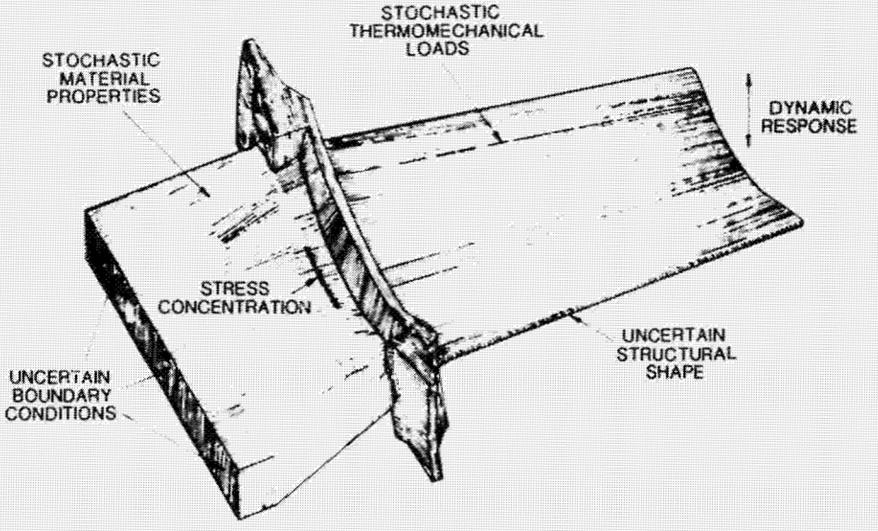

THE PROBABILISTIC
STRUCTURAL ANALYSIS PROBLEM

PROBABILISTIC LOADING CONDITIONS FOR PSAM

- Pressure
- Thermal
- Centrifugal
- Periodic
- Acoustic
- Impulsive

STRUCTURAL NONLINEARITIES IN PSAM

- Large Strains
- Large Displacements and Rotations
- Material Behavior
  (Plasticity and Thermoviscoplasticity)

CONCEPT OF PROBABILISTIC STRUCTURAL ANALYSIS

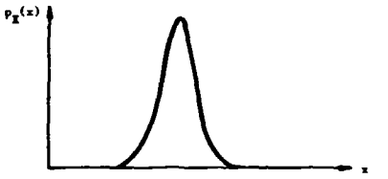

INPUT PDF
(Load, Material, Geometry, Boundary Conditions)

STRUCTURAL MODEL

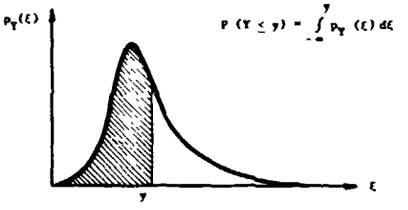

OUTPUT PDF
(Displacement, Strain, Stress)

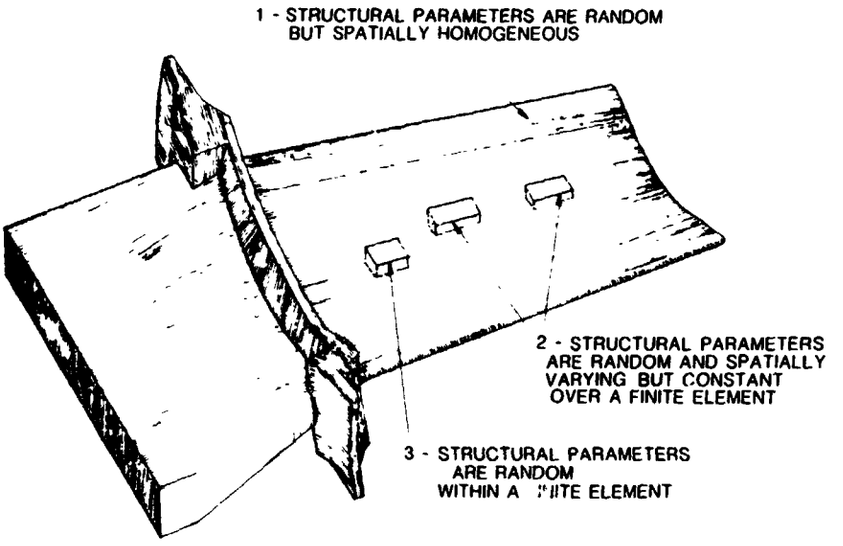

THREE LEVELS OF SOPHISTICATION FOR PROBABILISTIC FINITE ELEMENT ANALYSIS

STRATEGIES FOR COMPUTING THE
PROBABILISTIC STRUCTURAL RESPONSE

- Fast Probability Integration Techniques
- Method of Moments
- Monte Carlo Simulation

PSAM INTEGRATES EXISTING TECHNOLOGIES

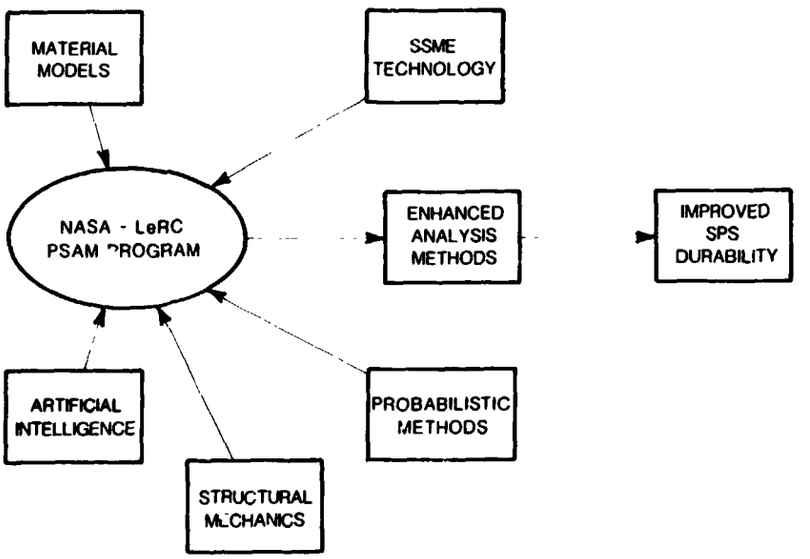

N85-27956

PROBABILISTIC FINITE ELEMENT DEVELOPMENT*

Jop Nagtegaal
MARC Analysis Research Corporation
Palo Alto, California 94306

The probabilistic finite element computer program NESSUS (Numerical Evaluation of Stochastic Structures Under Stress) is being developed by the MARC Analysis Research Corp. for the analysis of critical structural components for reusable space propulsion systems. This program has evolved from the HOST code, developed by MARC for Pratt & Whitney Aircraft Co. under NASA contract NAS3-23697, and which is now in use for the analysis of hot-section turbine components at Pratt & Whitney and the NASA Lewis Research Center.

The development of the NESSUS code is scheduled to take 3 years. First year efforts involve the formulation of the probabilistic analysis strategy and the development of a probabilistic linear analysis code. The ultimate goal of the 3-year program is the development of a finite element code capable of performing nonlinear dynamic analysis of structures having stochastic material properties, geometry, and boundary conditions and subjected to random loading.

Three levels of sophistication are envisioned for the stochastic description of the structural problem, namely:

Level 1: Homogeneous random variable for stiffness, mass, damping, and external loading
Level 2: Stochastic characterization of variables at the element level, with specified interelement correlations
Level 3: Stochastic interpolation of variables within a finite element

Two alternative probabilistic analysis methods will be developed, allowing for all three levels of modeling sophistication:

(1) A probability integration method, providing a direct estimate of the reliability of the structural configuration under study

(2) A simulation method, providing the means to verify the results obtained with method 1

Part of the formulation developed by Southwest Research Institute for the level 1 linear problem is currently available in a form that can be readily implemented in the NESSUS code. SwRI is continuing work on the formulation for the level 1 dynamic analysis, which should be available in the near future. Progress is being made in the formulation for the level 2 static problem. The major issue at this level remains the choice of an efficient algorithm for the evaluation of the derivatives of the stiffness, mass, and damping matrices with respect to each random variable present in the analysis. An approach to bypass this problem by efficiently extracting the static response of a perturbed

---

*Work performed under NASA contract NAS3-24389.

system without the need for explicit differentiation has been proposed by MARC. This method is based on a modified Newton-Raphson iteration scheme and could make use of some of the special numerical algorithms developed for the HOST program. MARC is presently testing this approach on a realistic problem while efforts are continued in the development of a similar formulation for the perturbed eigenvalue problem. The extension of this method into the nonlinear regime appears promising, especially in systems offering parallel computation capabilities.

NESSUS

NUMERICAL EVALUATION OF
STOCHASTIC STRUCTURES UNDER STRESS

- A COMPUTER CODE FOR THE PROBABILISTIC FINITE ELEMENT ANALYSIS OF CRITICAL COMPONENTS FOR SPACE PROPULSION SYSTEMS
- EVOLVED FROM THE HOST CODE DEVELOPED UNDER NASA CONTRACT NAS3-23697 FOR THE ANALYSIS OF HOT-SECTION TURBINE PARTS
- THREE YEAR DEVELOPMENT PROGRAM, RESULTING IN A CODE CAPABLE OF PERFORMING NONLINEAR STATIC AND DYNAMIC ANALYSIS OF A STRUCTURE WITH STOCHASTIC MATERIALS, GEOMETRY, BOUNDARY CONDITIONS AND LOADS.

NESSUS

FINITE ELEMENT LIBRARY

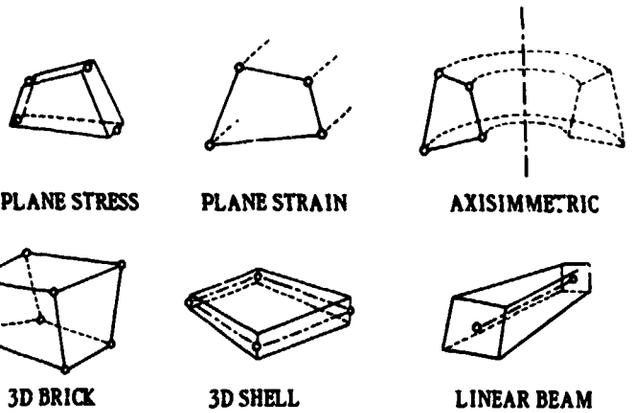

- o ALL ELEMENTS INTEGRATED NUMERICALLY
- o LINEAR LAGRANGIAN INTERPOLATING FUNCTIONS
- o SELECTIVELY REDUCED INTEGRATION

NESSUS

NONLINEAR ANALYSIS FEATURES

- o NONLINEAR PROBLEM MAY BE SOLVED WITH
  - (a) PURELY ITERATIVE METHODS
  - (b) INCREMENTAL-ITERATIVE METHODS
- o THREE TYPES OF INELASTIC CONSTITUTIVE MODELS

(i) SECANT ELASTICITY	Simplified Plasticity
(ii) VON MISES PLASTICITY	Radial Return, Associative Flow
(iii) CREEP-PLASTICITY	Walker's Model

- o USER SUBROUTINES FOR TEMPERATURE-DEPENDENT MATERIAL PROPERTIES, ANISOTROPY, CREEP, WORK-HARDENING, ETC.

NESSUS

DYNAMIC ANALYSIS FEATURES
for damped or undamped systems

1. EIGENVALUE EXTRACTION

   - o SUBSPACE ITERATION
   - o POWER SHIFTS

2. LINEAR DYNAMICS

   - o MODE SUPERPOSITION

     (i) FREE VIBRATION
     (ii) TRANSIENT FORCING FUNCTION *
     (iii) HARMONIC NODAL LOADING †
     (iv) HARMONIC BASE EXCITATION †

3. NONLINEAR TRANSIENT DYNAMICS

   - o NEWMARK-β

* Assumes linear load variation during each increment
† With phase defined independently at each node

NESSUS

PROBABILISTIC ANALYSIS FEATURES

- o THREE LEVELS OF SOPHISTICATION

  LEVEL 1: HOMOGENEOUS RANDOM VARIABLES
  LEVEL 2: STOCHASTIC VARIABLES AT THE ELEMENT LEVEL
  LEVEL 3: STOCHASTIC INTERPOLATION WITHIN ELEMENT

- o TWO ALTERNATIVE ANALYSIS STRATEGIES:

  A. PROBABILITY INTEGRATION
  B. SIMULATION (MONTE CARLO)

EFFICIENT SOLUTION OF THE PERTURBED STRUCTURE PROBLEM

A. CLASSICAL NONLINEAR FEM PROBLEM

- o EQUILIBRIUM

  $I(u) = P$

- o NEWTON ITERATION METHOD

  $K^* \, du^{(i+1)} = P - I(u^{(i)})$

  $u^{(i+1)} = u^{(i)} + du^{(i+1)}$ with $u^{(0)} = 0$

B. PERTURBED STRUCTURE PROBLEM

- o EQUILIBRIUM

  $I_{mod}(u) = P$

- o NEWTON-TYPE ITERATION

  $K_0 \, du_{mod}^{(i+1)} = P - I_{mod}(u_{mod}^{(i)})$

  $u_{mod}^{(i+1)} = u_{mod}^{(i)} + du_{mod}^{(i+1)}$ with $u_{mod}^{(0)} = u_0$

NUMERICAL EXAMPLE
Square Plate, Clamped Edges

1 in thickness

E = 30000 ksi
μ = 0.3
p = 10 psi

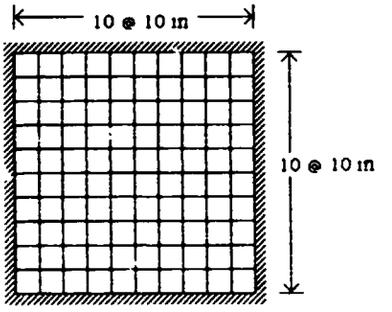

Reducing the thickness at 11 nodes along one clamped edge

	Center Deflection (in)		Residual on Displacement at Iteration		
	DIRECT	ITERATED	0	1	2
by 5%	-0.4615	-0.4614	0.038	0.001	n/a
by 10%	-0.4649	-0.4644	0.071	0.005	n/a
by 15%	-0.4669	-0.4672	0.099	0.010	n/a
by 20%	-0.4711	-0.4710	0.124	0.015	0.002
by 25%	-0.4740	-0.4736	0.144	0.021	0.003

with 1% tolerance on the displacement residuals

N85-27957

PROBABILISTIC FINITE ELEMENT - VARIATIONAL THEORY*

T. Belytschko and Wing Kam Liu
Northwestern University
Evanston, Illinois 60201

Traditionally, uncertainty analysis in structural mechanics has concentrated on problems of an almost totally stochastic nature. Within this setting, even a single degree of freedom system with nonlinearities poses a formidable challenge and has not been solved satisfactorily. However, in problems such as the nonlinear analysis of rocket engine components, concern lies more with deviations in loads from a deterministic path and in effects of uncertainties in material properties and boundary conditions. Thus the goal of this research is to provide techniques which are cost-effective and enable the engineer to evaluate the effect of uncertainties in complex finite element models.

It is important to be able to treat the effects of uncertainties in a reasonably economical manner; standard Monte Carlo procedures are simply too expensive. Furthermore, the methods should be designed so that they can be incorporated into widely used finite element programs in a natural and concise manner. Thus, the approach should be integrable with the elemental discretization and nodal assembly procedures that characterize finite element theory and software implementation.

For these reasons, embedding the probabilistic aspects in a variational formulation is a natural approach. In addition, a variational approach to probabilistic finite elements enables it to be incorporated within standard finite element methodologies. Therefore, once the procedures have been developed, they could easily be adapted to existing general purpose programs. Furthermore, the variational basis for these methods enables them to be adapted to a wide variety of structural elements and to provide a consistent basis for incorporating probabilistic features in many aspects of the structural problem: i.e., in the displacements, boundary conditions, body forces resulting from acceleration loads and any other features that cannot be clearly established. for example, the well known dilemma as to whether a shell is clamped or simply-supported at a boundary, could also be treated more rationally by using a probabilistic distribution for this boundary condition.

The tasks concluded in the first year's study include the following:

1. Theoretical Development of Probabilistic Variational Equations for Structural Dynamics. We have developed a methodology that can embed the probabilistic character of the constitutive properties and loads (i.e., material uncertainties and load uncertainties) with a finite element variational approach. The corresponding probabilistic character of the elemental nodal forces can then be assembled into a description of the probabilistic distribution of the nodal forces for the complete model and the appropriate mean response due to these uncertainties can be determined efficiently. The basic concept of this approach is to incorporate the probabilistic distributions, as reflected in the variance, of the material properties and the loading to obtain the corresponding variances in the

*Work performed under NASA grant NAG3-535.

elemental nodal forces of the finite element model. On the basis of the variance in the elemental nodal forces, the variance in the final solution will then be determined in the usual deterministic solution procedures.

2. The Development of Efficient Numerical Algorithms for Probabilistic Sensitivity Displacement and Stress Analysis. The second step of this approach to probabilistic analysis is to to construct an economical method of obtaining the probabilistic sensitivity element matrices which reflect the effects of randomness on response variables such as displacements, stresses, etc. The randomness is due to the preassigned probabilistic descriptions of the material properties and loads. While separate analyses for random distributions of all probabilistic response variables are an obvious possibility to achieving this aim, the computer cost would be formidable. It would require n analyses (n is the number of sample points) for each set of probabilistic variables. Obviously, more effective procedures must be devised. Relatively efficient solution procedures which have been developed here will be demonstrated with results for both a two-degrees of freedom spring-mass system and a ten-bar nonlinear system.

3. Integration of Methodologies into a Pilot Computer Code. The computer solutions obtained using this theory have been compared to the Monte Carlo methods and the Hermite-Gauss Quadrature integration schemes. The cost of the new method is substantially lower. We have demonstrated this with a ten-bar probabilistic nonlinear system where the random variables are the yield stresses. Exploitation of this characteristic in any probabilistic analysis may perhaps offer significant savings and we will further investigate this in the probabilistic finite element method.

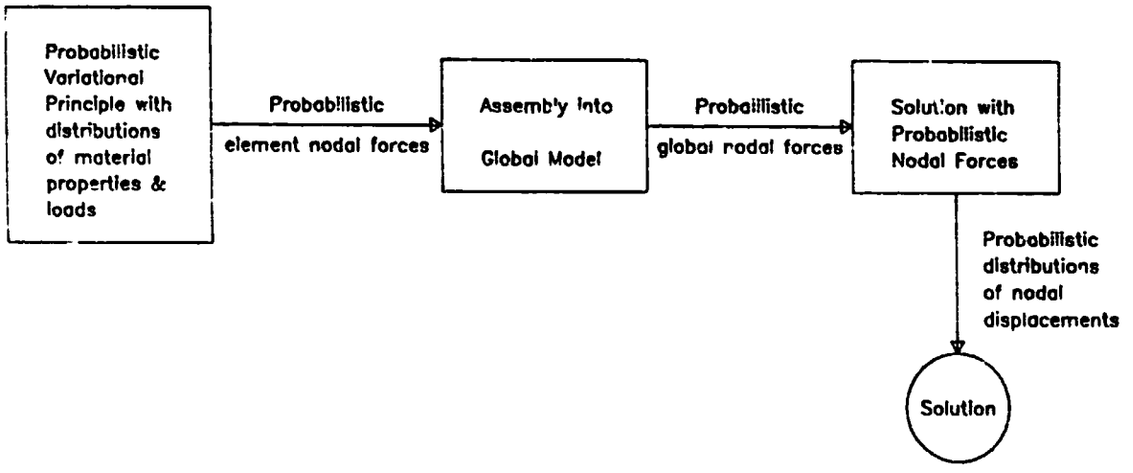

Schematic Illustration of the Probabilistic Finite Element Method (PFEM)

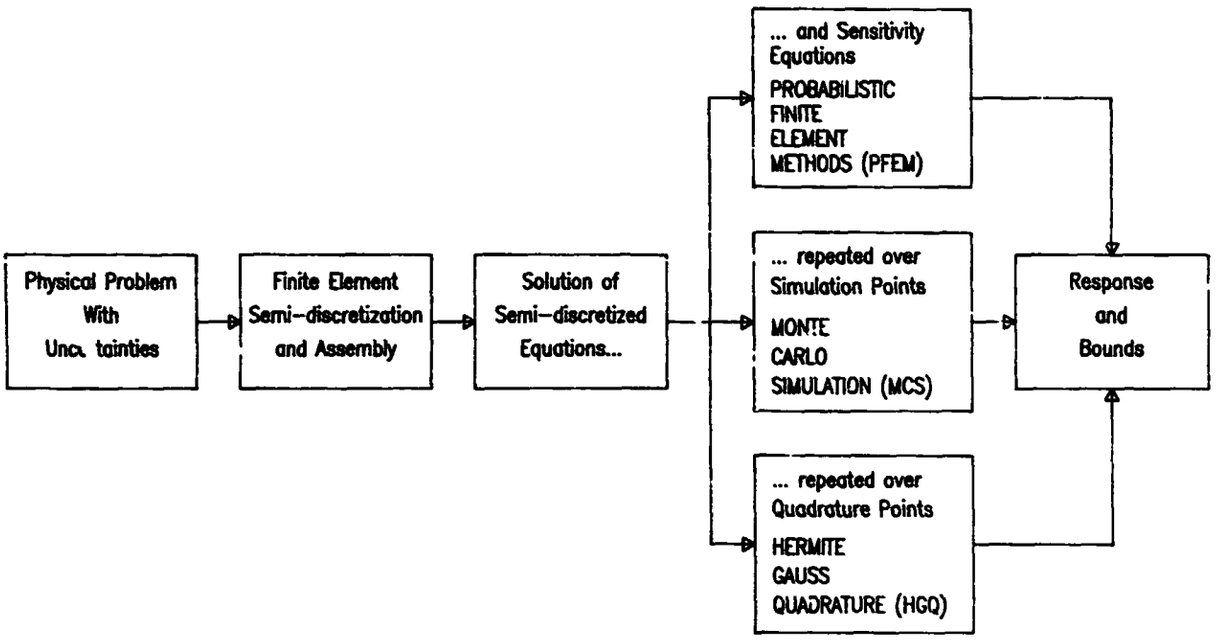

Schematic of Probabilistic Methods

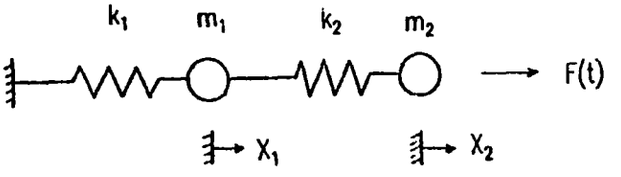

$F(t)=25.0 \times 10^6 \sin(2000t)$

$m_1=0.372 \qquad k_1=24.0 \times 10^6$

$m_2=0.248 \qquad k_2=12.0 \times 10^6$

A Two-Degree-of-Freedom Example.

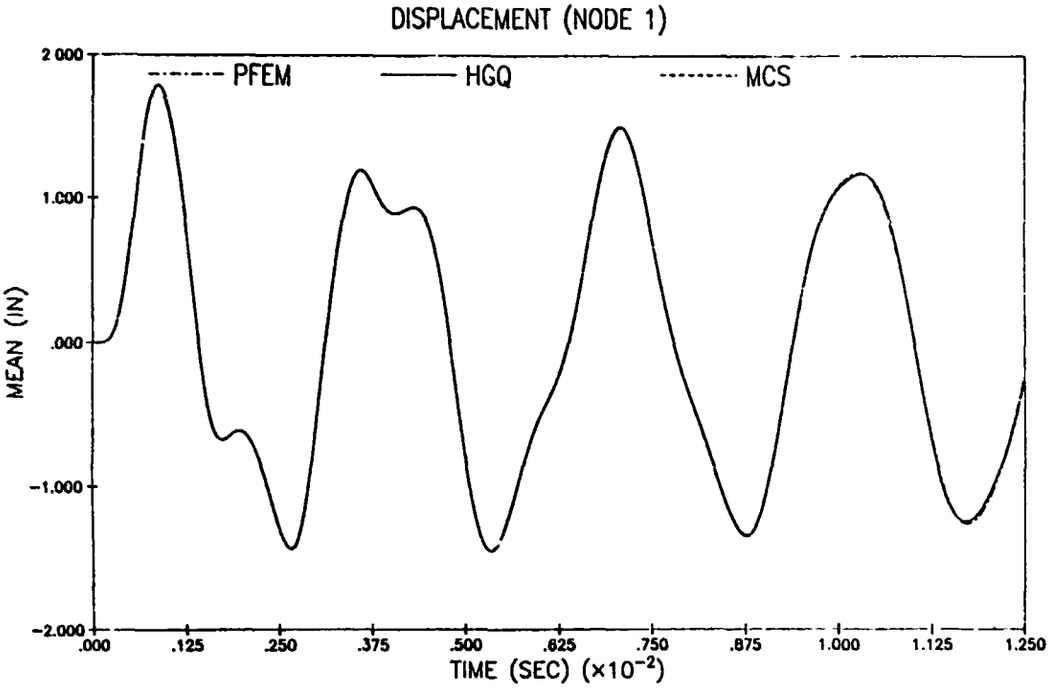

Comparison of the Mean Displacement at Node 1 Using:
(1) Probabilistic Finite Element Method (PFEM)
(2) Hermite Gauss Quadrature (HGQ)
(3) Monte Carlo Simulation (MCS)

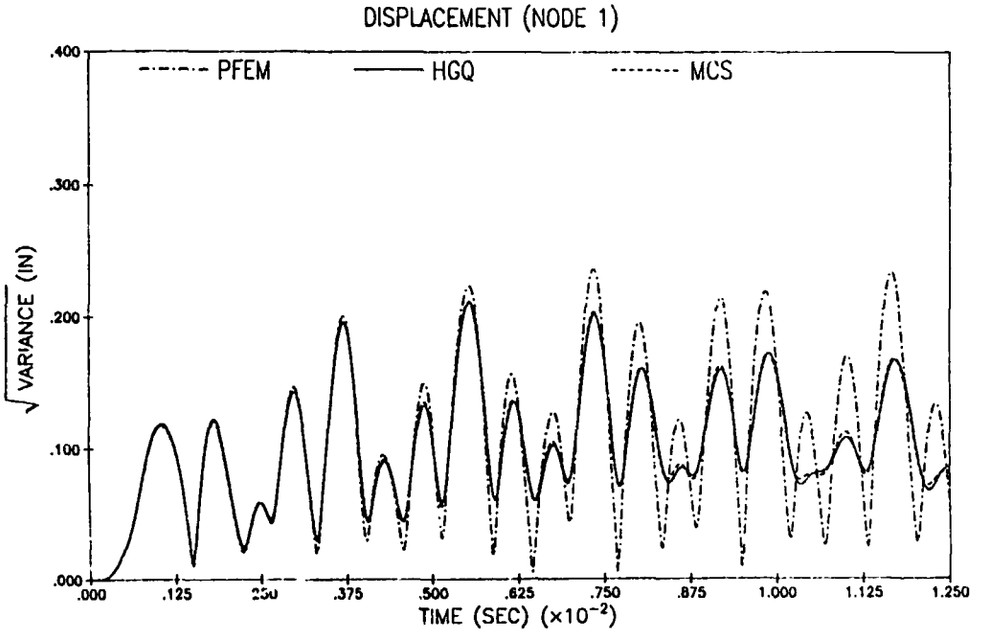

Comparison of the Variance of Displacement at Node 1 Using:
(1) Probabilistic Finite Element Method (PFEM)
(2) Hermite Gauss Quadrature (HGQ)
(3) Monte Carlo Simulation (MCS)

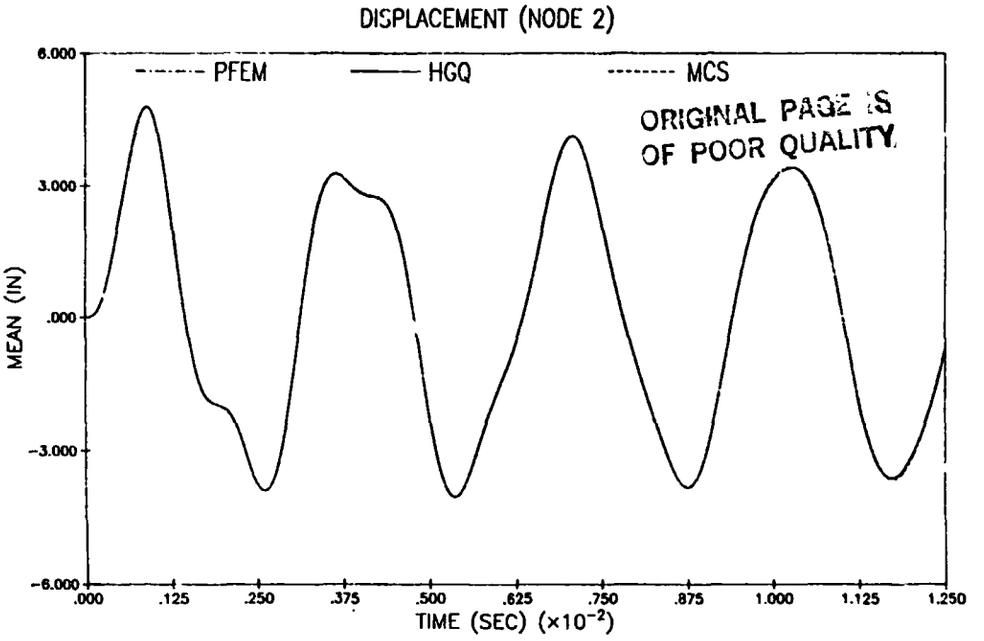

Comparison of the Mean Displacement at Node 2 using
(1) Probabilistic Finite Element Method (PFEM)
(2) Hermite Gauss Quadrature (HGQ)
(3) Monte Carlo Simulation (MCS)

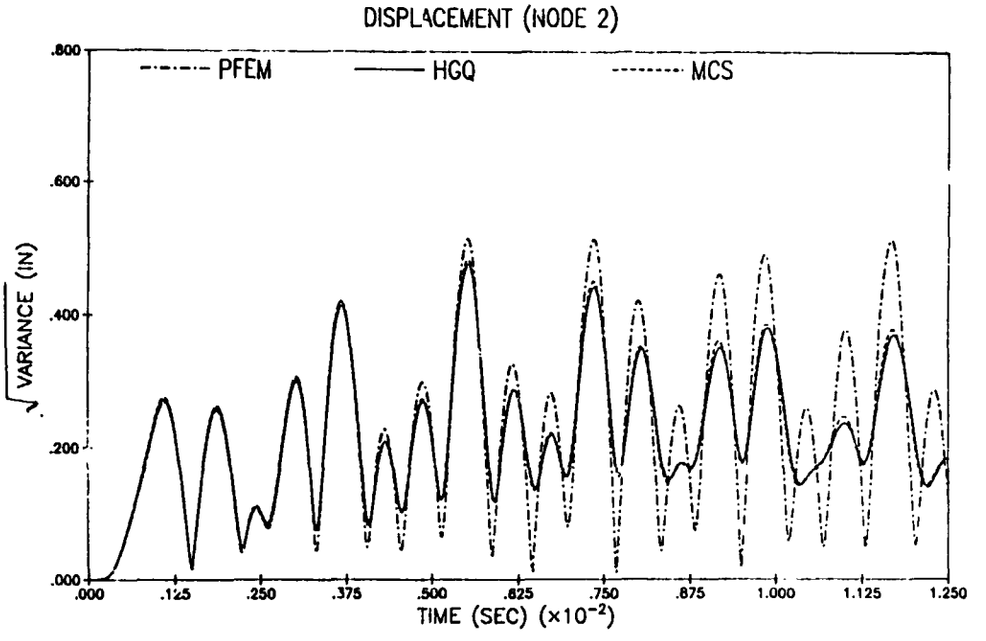

Comparison of the Variance of Displacement at Node 2 Using:
(1) Probabilistic Finite Element Method (PFEM)
(2) Hermite Gauss Quadrature (HGQ)
(3) Monte Carlo Simulation (MCS)

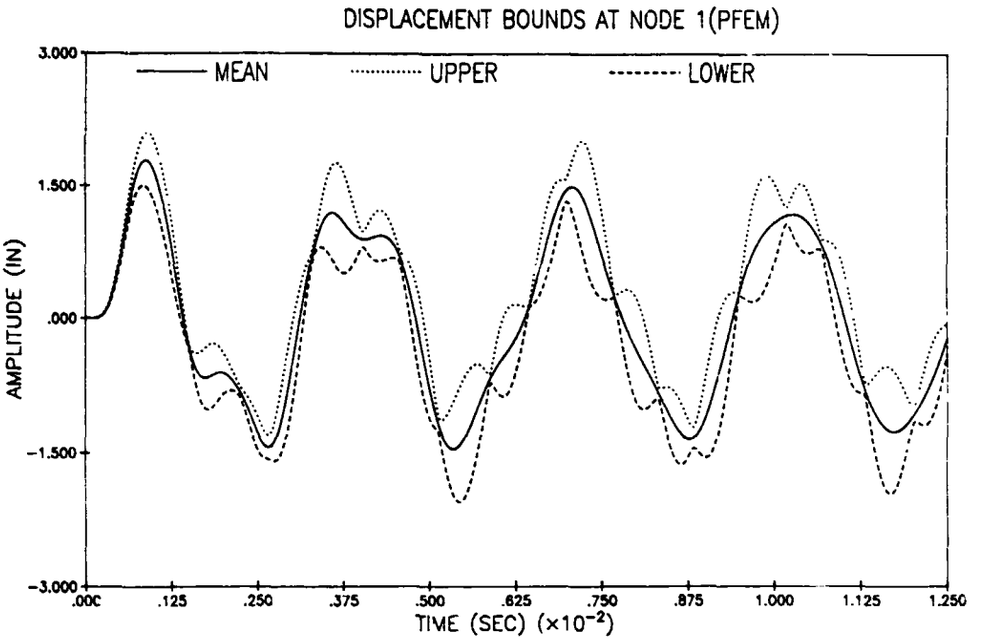

± 3 Sigma Bounds of the Displacement at Node 1
using Probabilistic Finite Element Methods (PFEM)

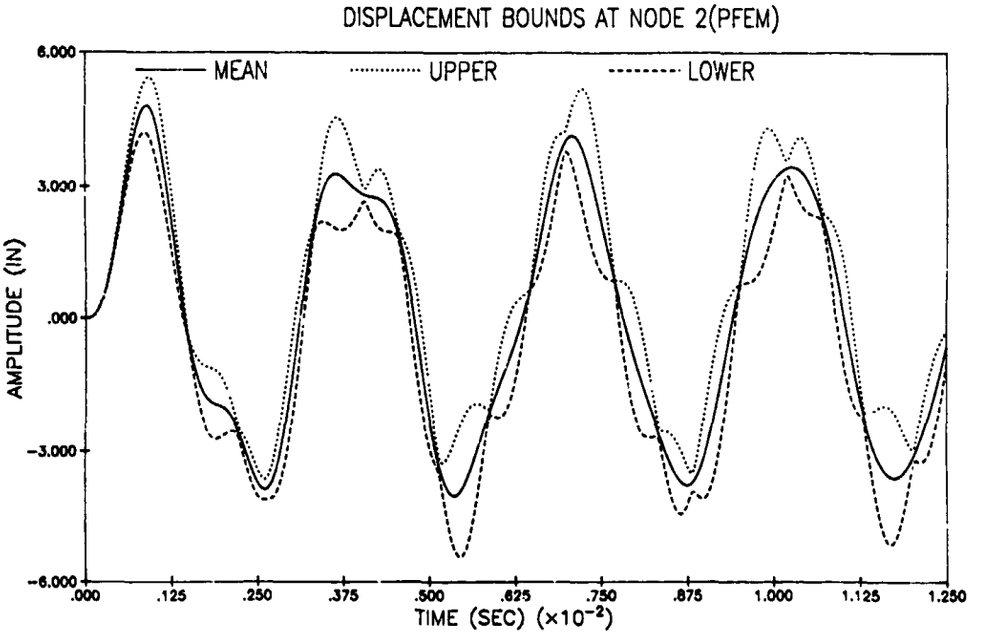

± 3 Sigma Bounds of the Displacement at Node 2
using Probabilistic Finite Element Methods (PFEM)

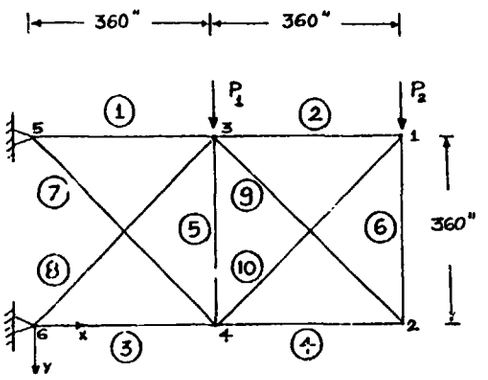

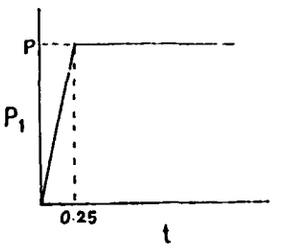

$E = 30.0 \times 10^6$

$E_T = 30.0 \times 10^4$

$A = 6.0$

$\rho = 0.30$

$\sigma_Y = 15000.0$

$P = 175.0 \times 10^3$

$P_2 = 0.0$

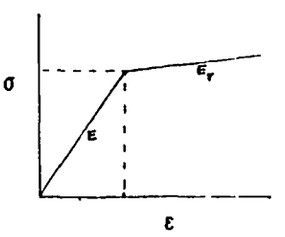

Problem Statement of a Ten-Bar Nonlinear Structure.

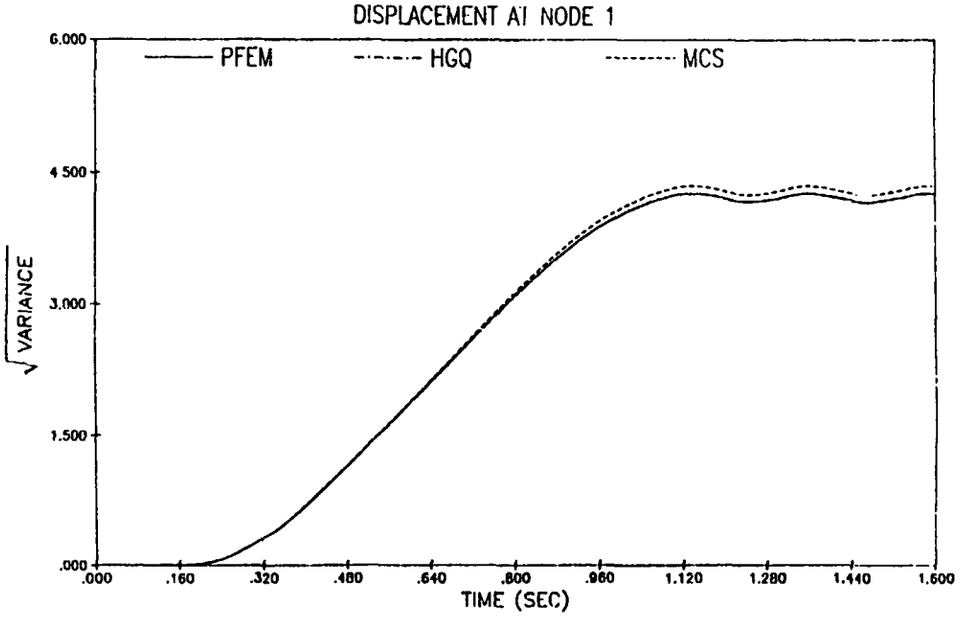

Comparison of the Variance of the y-displacement of Node 1 Using (1) Probabilistic Finite Element Method (PFEM); (2) Hermite Gauss Quadrature (HGQ); and (3) Monte Carlo Simulation (MCS).

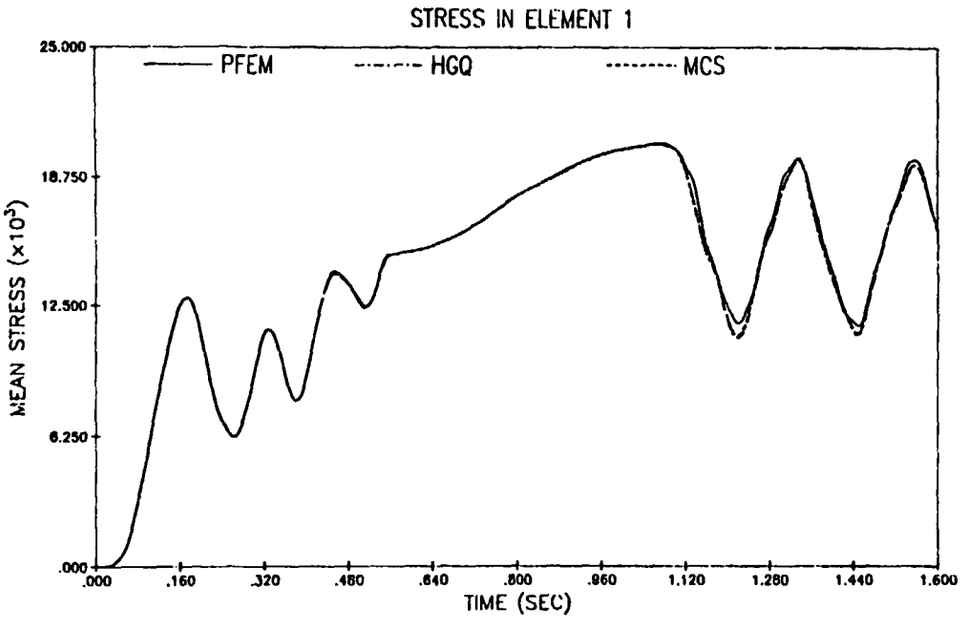

Comparison of the Mean Stress of Member 1 Using (1) Probabilistic Finite Method (PFEM), (2) Hermite Gauss Quadrature (HGQ); and (3) Monte Carlo Simulation (MCS).

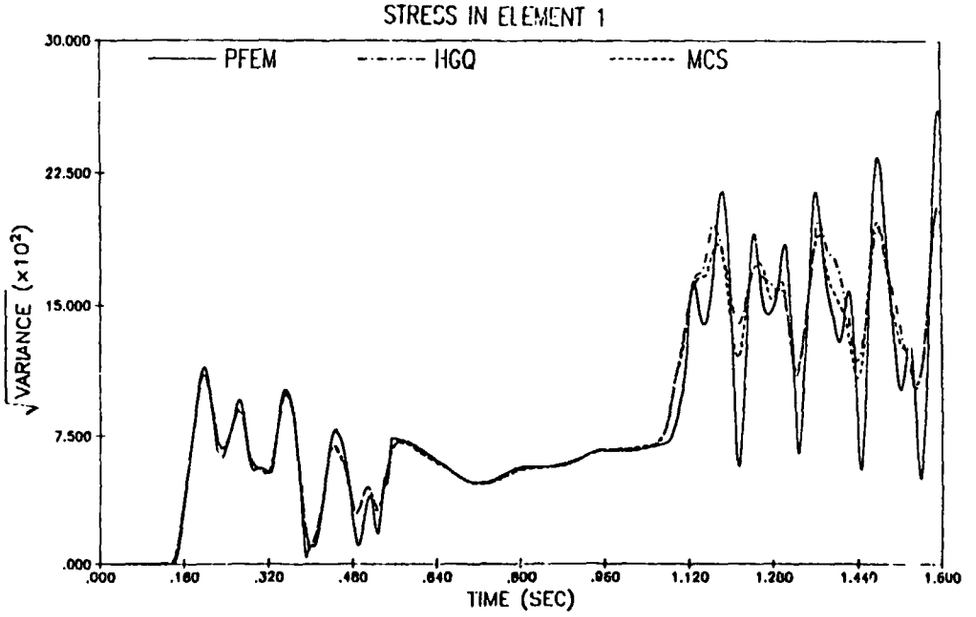

Comparison of the Variance of the Mean Stresses of Member 1 Using (1) Probabilistic Finite Element Method (PFEM); (2) Hermite Gauss Quadrature (HGQ); and (3) Monte Carlo Simulation (MCS).

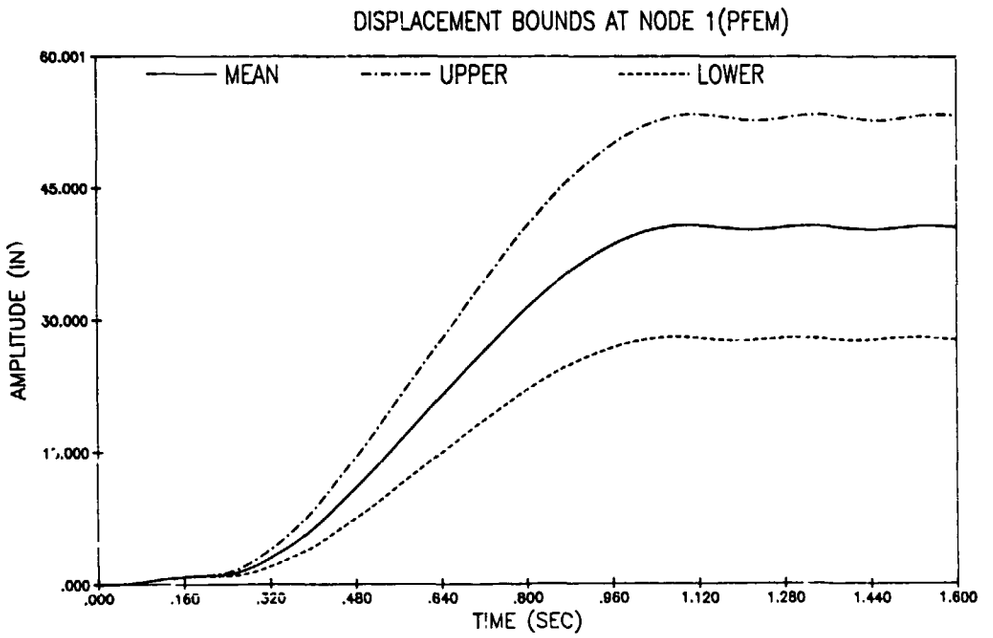

± 3 Sigma Bounds of the y-Displacement at Node 1
using Probabilistic Finite Element Methods (PFEM)

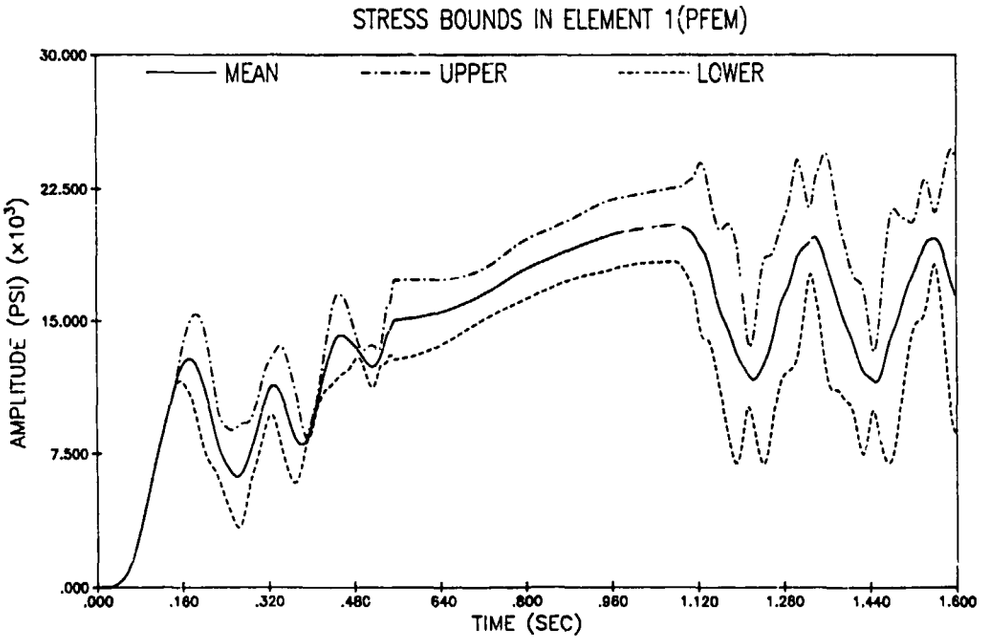

± 3 Sigma Bounds of the Stress in Member 1
using Probabilistic Finite Element Methods (PFEM)

PROBABILISTIC STRUCTURAL ANALYSIS OF SSME TURBOPUMP BLADES - PROBABILISTIC GEOMETRY EFFECTS*

Vinod K. Nagpal
Sverdrup Technology, Inc.
Middleburg Heights, Ohio 44130

A probabilistic study has been initiated at Lewis Research Center. The first objective of this study is to evaluate the precisions of the geometric and material properties tolerances on the structural response of turbopump blades. To complete this study, a number of important probabilistic variables have been identified which are conceived to affect the structural response of the blade. In addition, a methodology has been developed to statistically quantify the influence of these probabilistic variables in an optimized way.

The identified variables include random geometric and material properties perturbations, different loadings and a probabilistic combination of these loadings. Influences of these probabilistic variables are planned to be quantified by evaluating the blade structural response. The structural response includes natural frequencies, root (maximum) stress, stage weight and tip displacements.

Studies of the geometric perturbations have been conducted for a flat plate geometry as well as for an SSME blade geometry using a special purpose code which uses the finite element approach. The geometric perturbations which simulate the natural perturbations under operating conditions, are generated by randomly perturbing the x, y, and z coordinates of all the nodes of the finite element mesh. Analyses of both the geometries indicate that the variances of the perturbations about given mean values have significant influence on the response. However, for neither of the two geometries all three variances of perturbations along x, y, and z axes showed significant effect. Also, the two analyses indicated that the perturbation variances which influence the flat plate response significantly were different from those of the SSME blade geometry. Contrary to the influence of variances, the means of perturbations have insignificant influence on the response of either geometry.

Statistical models have been developed to predict the structural response for given perturbation means and variances for both geometries. Since means are not significant, statistical models based only on the significant variances have also been developed. In addition, probability distributions for the structural response have been developed. These distributions mostly appeared discrete. These distributions provide an assessment of variation in the structural response for a selected geometric perturbation. Also, these provide an estimate of the probability of getting a certain response for a given input.

---

*Work performed under NASA Lewis task number 84-52-03.

Statistical tests and methods were used to check the developed models. These tests indicated that the developed models are good fits. t-Tests were used to identify the significant variances of perturbations. F-tests, and plots and autocorrelations of residuals were used to check the goodness-of-fit tests.

The preliminary conclusions from the studies completed so far are that the means of geometric perturbations are insignificant. However, the variances of the perturbations have significant effect. Also an analysis indicates that the structural response varies by up to ten percent when a test run with the same mean and variance of a perturbation is replicated.

The studies of random perturbations in material properties, different loadings and their probabilistic combinations is underway.

PRESENT OBJECTIVE

CONDUCT PROBABILISTIC STRUCTURAL ANALYSIS OF
SSME BLADES USING PROBABILISTIC DESCRIPTION OF

GEOMETRY
MATERIAL PROPERTIES
LOADING CONDITIONS

PROBABILISTIC VARIABLES

- RANDOM GEOMETRIC PERTURBATIONS
- RANDOM MATERIAL PROPERTIES PERTURBATIONS
- LOADING

  DETERMINISTIC

  PROBABILISTIC

STRUCTURAL RESPONSE

- NATURAL FREQUENCIES
  - FIRST
  - SECOND
  - THIRD
- ROOT (MAXIMUM) STRESS
- STAGE WEIGHT
- TIP DISPLACEMENTS

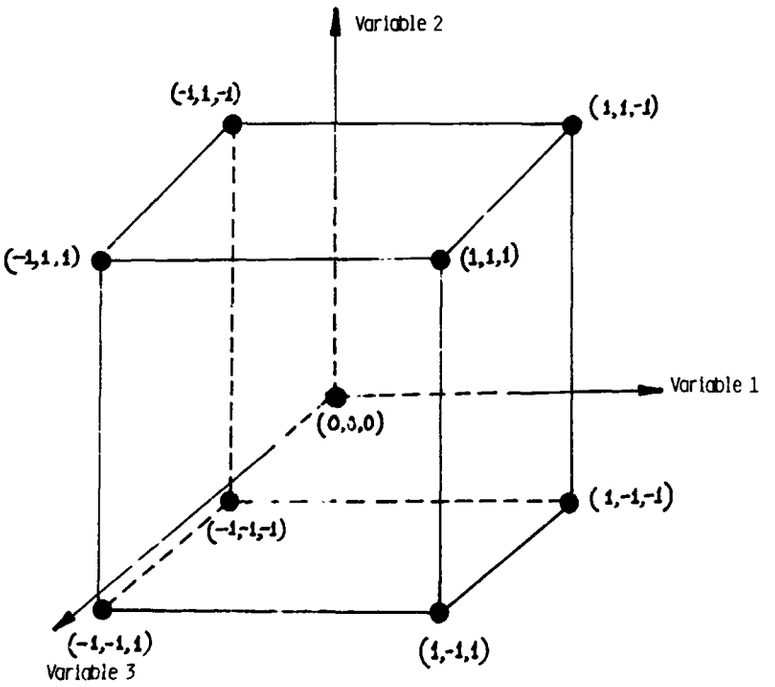

OPTIMIZED WAY OF STUDYING THREE VARIABLE EFFECTS

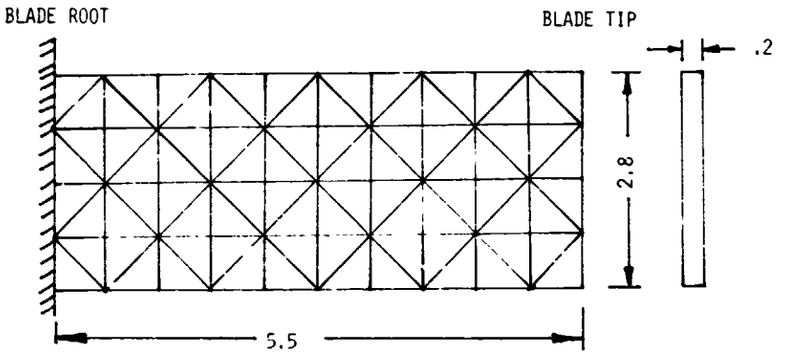

NUMBER OF ELEMENTS = 80
NUMBER OF NODES = 55

FINITE ELEMENT MESH FOR FLAT PLATE GEOMETRY

SUMMARY OF STATISTICAL MODELS
FOR SSME BLADE GEOMETRY

MODEL:

DEP. VAR. = CONSTANT + $COEFF_1\mu_1$ + $COEFF_2\mu_2$ + $COEFF_3\mu_3$ + $COEFF_4\sigma_1$ + $COEFF_5\sigma_2$ + $COEFF_6\sigma_3$

DEPENDENT VARIABLE	SYMBOL	CONSTANT	COEFFICIENTS OF						CALCULATE F-VALUE	TABLE F-VALUE 95%
			μ_1	μ_2	μ_3	σ_1	σ_2	σ_3		
FIRST FREQ.	F_1	6219.9	-2312.	-7437.	-974.	-8716.3	-496.	-8790.	23.01	
SECOND FREQ.	F_2	9923.3	-4517.	-5615.	492.	-11094	-6375.	-12612.	7.67	
THIRD FREQ.	F_3	15723.9	-5926.	5357.	-2671	-24816	-12360.	-36929.	27.34	2.26
ROOT STRESS	RS	57039.	1940.	257695.	71492.	117720.	123200.	236795.	2.83	
STAGE WEIGHT	WT	0.90731	1.3642	1.827	0.4323	5.4521	2.4369	5.6581	46.2	
TIP DISPL.	TD	-.0058	0.0279	0.288	0.144	-.0274	0.0572	-.0412	1.30	

SAMPLE OF DATA ACQUISITION ON GEOMETRIC PERTURBATION OF SSME BLADE

GEOMETRIC PERTURBATIONS						RESPONSE OF THE BLADE					
MEANS			STD. DEVIATION			NATURAL FREQUENCIES			ROOT STRESS	STAGE WEIGHT	DISPLACEMENTS
μ_x	μ_y	μ_z	σ_x	σ_y	σ_z	FIRST	SECOND	THIRD			
0.0	0.0	0.0	.02	0.0	.02	6396.7	8770.6	15882.	73776.	1.1435	.0007
						6139.7	8929.3	16118.	64004.	1.1383	.00053
						5901.6	8943.5	18173.	73786.	1.1466	- 00007
						5952.4	8649.2	15651.	80025.	1.1398	.00815
0.0	.02	0.0	.02	0.0	.02	6139.1	8804.5	16349.	61953.	1.1467	.00066
						6334.5	9286.9	16771.	64701.	1.1552	.00065
						6365.0	9190.1	16229.	70629.	1.1451	-.0001
						5980.9	8600.9	15894.	62124.	1.1762	-.00039
0.0	0.0	0.1	.02	0.0	.02	5834.9	9184.4	14240.	60456.	1.2360	.00306
						6202.7	8989.2	15530.	56356.	1.2338	.00211
						5775.1	9044.0	15113.	50943.	1.2054	.00248
						5671.1	8878.7	14580.	89466.	1.2103	.00328

DEFINITIONS

F - TEST

$$F = \frac{(\text{RESIDUAL SUM OF SQUARES})/\text{D.F.}}{(\text{REGRESSION SUM OF SQUARES})/\text{D.F.}}$$

T - TEST

$$t = \frac{\text{VALUE - MEAN}}{\text{ST. DEV.}}$$

PROBABILITY D'STRIBUTIONS FOR TEST RUN NO. 42

SAMPLE SIZE = 0

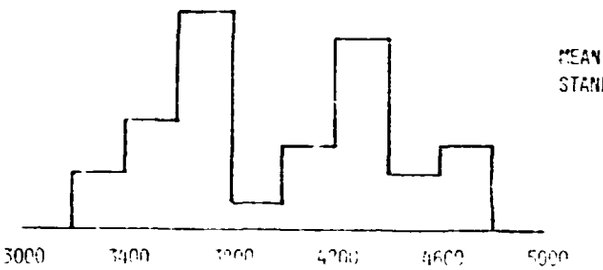

FIRST NATURAL FREQUENCY

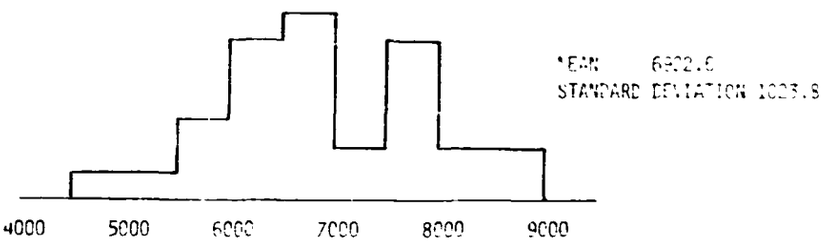

SECOND NATURAL FREQUENCY

Probability Distributions For Test Run No. 42

Sample Size 60

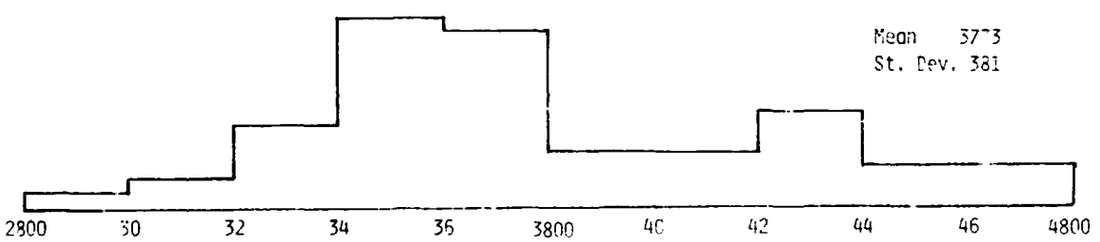

FIRST NATURAL FREQUENCY

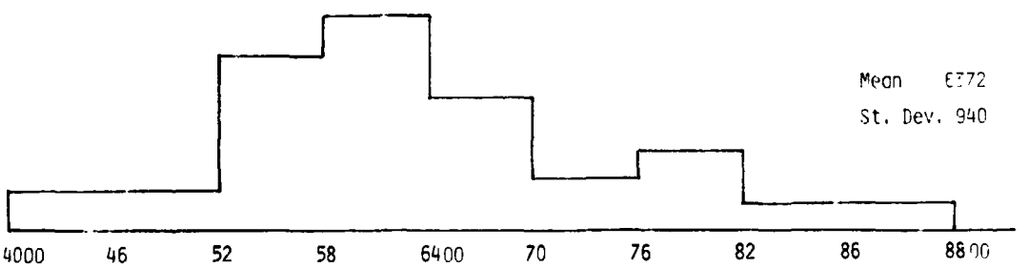

SECOND NATURAL FREQUENCY

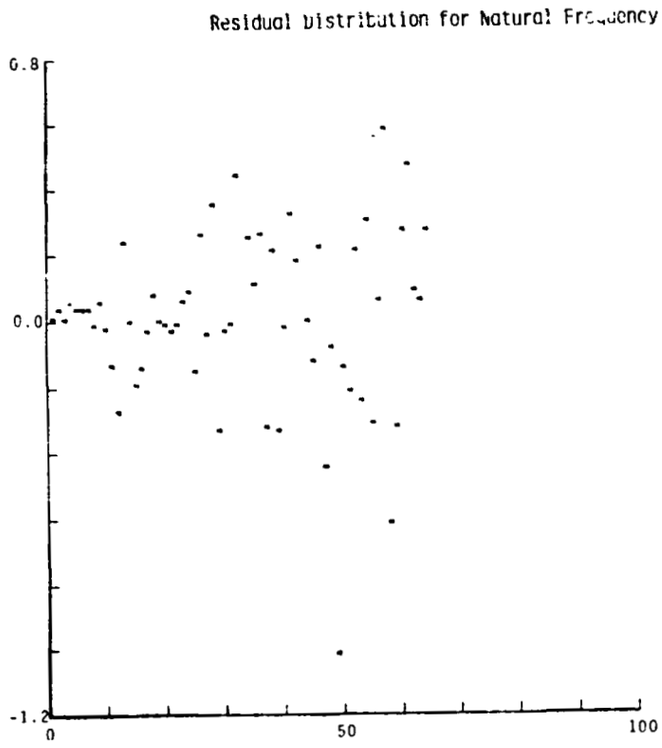

DYNAMIC CREEP BUCKLING: ANALYSIS OF SHELL STRUCTURES SUBJECTED TO TIME-DEPENDENT MECHANICAL AND THERMAL LOADING*

G.J. Simitses, R.L. Carlson, and R. Riff
Georgia Institute of Technology
Atlanta, Georgia 30332

The objective of the present research is to develop a general mathematical model and solution methodologies for analyzing the structural response of thin, metallic shell structures under large transient, cyclic, or static thermomechanical loads. Among the system responses associated with these loads and conditions are thermal buckling, creep buckling, and ratcheting. Thus geometric and material nonlinearities (of high order) can be anticipated and must be considered in developing the mathematical model.

A complete, true ab-initio rate theory of kinematics and kinetics for continuum and curved thin structures, without any restriction on the magnitude of the strains or the deformations, was formulated. The time dependence and large strain behavior are incorporated through the introduction of the time rates of metric and curvature in two coordinate systems: fixed (spatial) and convected (material). The relations between the time derivative and the covariant derivative (gradient) have been developed for curved space and motion, so the velocity components supply the connection between the equations of motion and the time rates of change of the metric and curvature tensors.

The metric tensor (time rate of change) in the convected material coordinate system is linearly decomposed into elastic and plastic parts. In this formulation a yield function is assumed that is dependent on the rate of change of stress, metric, temperature, and a set of internal variables. Moreover, a hypoelastic law was chosen to describe the thermoelastic part of the deformation.

A time- and temperature-dependent viscoplasticity model was formulated in this convected material system to account for finite strains and rotations. The history and temperature dependence were incorporated through the introduction of internal variables. The choice of these variables, as well as their evolution, was motivated by phenomenological thermodynamic considerations.

The nonisothermal elastic-viscoplastic deformation process was described completely by "thermodynamic state" equations. Most investigators (in the area of viscoplasticity) employ plastic strains as state variables. Our study shows that, in general, use of plastic strains as state variables can lead to inconsistencies with regard to thermodynamic considerations. Furthermore, the approach and formulation employed by all previous investigators lead to the condition that all the plastic work is completely dissipated. This, however, is in contradiction with experimental evidence, from which it emerges that part of the plastic work is used for producing residual stresses in the lattice,

---

*Work performed under NASA grant NAG3-534.

ANALYSIS OF SHELL-TYPE STRUCTURES SUBJECTED TO TIME-DEPENDENT MECHANCIAL AND THERMAL LOADING*

BY

G. J. SIMITSES
R. L. CARLSON AND R. RIFF
GEORGIA INSTITUTE OF TECHNOLOGY

* NASA GRANT: NAG3-534

FIRST YEAR EFFORT

- CONCENTRATED ON THE STUDY AND FORMULATION OF COMPLETE AND GENERAL MATHEMATICAL MODEL
- CENTRAL IDEAL: (i) CONSTRUCT TRUE RATE THEORY (RATE KINEMATICS, RATE OF VIRTUAL POWER, RATE OF CONSERVATION OF ENERGY)
  (ii) COMPOUNDED WITH THERMODYNAMICALLY CONSISTENT RATE CONSTITUTIVE EQUATIONS (FOR NONISOTHERMAL LARGE STRAIN, ELASTO-VISCOPLASTIC BEHAVIOR)

NO RESRICTION IS PLACED (INITIALLY) ON THE MAGNITUDE OF THE DEFORMATION GRADIENTS.

OBJECTIVES

1. DEVELOP A MATHEMATICAL MODEL (HIGHLY NONLINEAR GEOMETRICALLY AND IN MATERIAL BEHAVIOR).
2. DEVISE SOLUTION METHODOLOGIES, FOR ANALYZING (STRUCTURAL RESPONSE)
   - THIN SHELL-LIKE METALLIC STRUCTURES SUBJECTED TO
   - LARGE TRANSIENT, CYCLIC OR NOT, AND/OR STATIC THERMOMECHANICAL LOADS.

RESPONSE INCLUDES: THERMAL BUCKLING, CREEP BUCKLING AND RATCHETTING

KINEMATICS OF CONTINUUM

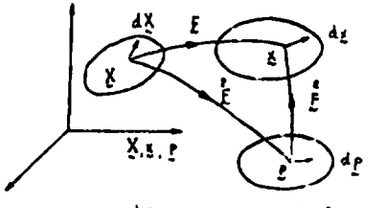

$$\underset{\sim}{F} = \frac{\partial \underset{\sim}{x}}{\partial \underset{\sim}{X}} \qquad \underset{\sim}{F} = \overset{e}{\underset{\sim}{F}}\,\overset{p}{\underset{\sim}{F}}$$

$$\underset{\sim}{L} = \partial \underset{\sim}{v}/\partial \underset{\sim}{x} = \dot{\underset{\sim}{F}}\,\underset{\sim}{F}^{-1}$$

$$\underset{\sim}{L} = \underset{\sim}{D} + \underset{\sim}{W}$$

$$\underset{\sim}{D} = \overset{e}{\underset{\sim}{D}} + \overset{e}{\underset{\sim}{F}}\,\overset{p}{\underset{\sim}{D}}\,\overset{e}{\underset{\sim}{F}}^{-1}\Big|_s + \overset{e}{\underset{\sim}{W}}\,\overset{e}{\underset{\sim}{F}}^{-1}\Big|_s$$

IN CONVECTED COORDINATES: $\underset{\sim}{D} = \overset{e}{\underset{\sim}{D}} + \overset{p}{\underset{\sim}{D}}$

which, when phenomenologically considered, causes hardening. Both limitations are not present in our formulation because of the inclusion of the "thermodynamic state" equations.

THIN SHELL-LIKE KINEMATICS

- THE THREE-DIMENSIONAL FORMULATIONS ARE UTILIZED TO DERIVE CONSISTENT KINEMATIC EQUATIONS FOR THIN SHELL-LIKE SYSTEMS (INCLUDING PLANE CURVE BEAMS) - FINITE STRAINS & ROTATIONS.

3-D	2-D(1-D)
VELOCITY GRADIENT (TENSOR: TIME RATE OF CHANGE OF DEFORMATION GRADIENT)	A NEW TENSOR (THAT INCLUDES THE CURVATURE).

5

FIVE DIFFERENT SHELL THEORIES (APPROXIMATIONS) [A,B,C,D,E] BASED ON KINEMATIC ASSUMPTIONS (I-V).

I. MAT'L POINTS REMAIN ON NORMAL AFTER DEFORMATION (FIRST KIRCHHOFF-LOVE HYPOTHESIS: TRANSVERSE SH.)
II. THE SHELL IS THIN ($t/R \ll 1$; LINEAR EXPANSION)
III. THE BOUNDING (UPPER AND LOWER) SURFACES REMAIN PARALLEL FOR ALL TIME.
IV. NORMALS ARE INEXTENSIONAL FOR ALL TIME (THIRD K-L)

A) I.; B) I + II; C) I + II + III; D) I + II + III + IV (CLASSICAL THEORY)
E) II - ONLY

6

CONSTITUTIVE EQUATIONS (INELASTIC)

THREE BASIC ELEMENTS ARE NEEDED (ELASTO-VISCOPLASTIC BEHAVIOR, NON-ISOTHERMAL, LARGE DEF.)

1) THE YIELD FUNCTION, $F(\tau_C^A, T, k, \ldots \alpha_C^A \ldots A_{BD}^{AC})$

τ_C^A: KIRCHHOFF STRESS
T : TEMPERATURE
k, α_C^A, A_{CD}^{AB} } VARIABLES CHARACTERIZE HARDENING, SOFTENING AND RECOVERY PHENOMENA

2) THERMODYNAMIC CONSIDERATIONS (PROCESSES CONSISTENT WITH THERMODYNAMIC LAWS)

3) PROPER CHOICE OF EXTERNAL AND INTERNAL THERMODYNAMIC VARIABLES (T, τ_C^A: EXTERNAL)

7

YIELD FUNCTION-ROLE, F

F = 0: BOUNDING DOMAIN OF PURE THERMO-ELASTIC BEHAVIOR (IN THE SPACE OF STRESS AND TEMPERATURE).

INELASTIC DEFORMATION OCCURS IF AND ONLY IF

I. $F(\tau_C^A, T, k, \ldots, \alpha_C^A, \ldots A_{BC}^{AC}, \ldots) = 0$ AND

$$\frac{\partial F}{\partial \tau_C^A} \overset{\nabla}{\tau}{}_C^A + \frac{\partial F}{\partial T} \dot{T} > 0$$

LOADING CONDITION

$\overset{\nabla}{\tau}{}_C^A$: JAUMAN STRESS RATE

FOR ELASTO-PLATIC MAT'L BEHAVIOR

II. $F(\tau_C^A, T, k, \ldots \alpha_C^A, \ldots, A_{BD}^{AC}, \ldots) > 0$

FOR ELASTO-VISCOPLASTIC MAT'L BEHAVIOR

8

THERMODYNAMIC CONSIDERATIONS (ELEMENTARY PROCESSES)

FIRST LAW: $\dot{u} = \dot{w} + \dot{q}$ (RATE OF SPECIFIC u-INTERNAL ENERGY, w-MECH. WORK, q-APPLIED HEAT)

WHERE $\dot{w} = \frac{1}{\rho_0}\tau_C^A d_C^{eA} + \frac{1}{\rho_0}\tau_C^A d_C^{pA} = \overset{e}{\dot{w}} + \overset{r}{\dot{w}}$

$\overset{I}{\dot{w}} = \overset{S}{\dot{w}} + \overset{D}{\dot{w}}$

($\overset{S}{\dot{w}}$: PART OF INELASTIC MECH. WORK THAT CHANGES THE INTERNAL STRUCTURAL-SLIP, DISLOCATIONS; $\overset{D}{\dot{w}}$: PART THAT IS DISSIPATED-NONRECOVERABLE)

. ONLY $\overset{D}{\dot{w}}$ ENTERS THE ENTROPY PRODUCTION

$$T\dot{s} = \dot{q} + \overset{D}{\dot{w}} \qquad (s: \text{ SPECIFIC ENTROPY})$$

SECOND LAW $\qquad \overset{D}{w} \geq 0$

9

THERMODYNAMIC CONSIDERATIONS (CONT'D)

. FOR IRREVERSIBLE PROCESSES SOME STATEMENTS ABOUT THE DEPENDENCE OF ENTROPY PRODUCTION ON THE THERMO-MECHANICAL PROCESS ARE NEEDED TO COMPLETE THE DESCRIPTION.

SINCE ENTROPY PRODUCTION IS CONNECTED WITH DISSIPATED MECHANICAL WORK (DURING INELASTIC DEFORMATION) WE MAY IN GENERAL ASSUME

$$\overset{D}{\dot{w}} = C_{CD}^{AB}\,\tau_A^C\,\overset{I}{d}{}_B^D \qquad (\geq 0) \qquad (2)$$

WHERE

$$C_{CD}^{AB} = C_{CD}^{AB}\left(\overset{E}{f}{}_C^A, T, k, \ldots \alpha_C^A, \ldots A_{CD}^{AB}\right)$$

EQS. (1) & (2) AND THE CONDITIONS ON F LEAD TO A SET OF CONSISTENT CONSTITUTIVE EQS. (FOR INELASTIC BEH.)

11

THERMODYNAMIC CONSIDERATIONS (CONT'D)

φ: SPECIFIC FREE ENERGY (HELMHOLTZ FCN)

$$\varphi = u - Ts = \overset{E}{\varphi}\left(\overset{E}{f}{}_C^A, T\right) + \overset{S}{\varphi}\left(T, k, \ldots \alpha_C^A, \ldots A_{CD}^{AB}, \ldots\right)$$

WHERE $\overset{E}{f}{}_C^A$: DEFORMATION GRADIENT

IT CAN BE SHOWN THAT

. $s = \partial\varphi/\partial T$

. $\overset{S}{\dot{w}} = \frac{\partial \overset{S}{\varphi}}{\partial k}\dot{k} + \ldots \frac{\partial \overset{S}{\varphi}}{\partial \alpha_C^A}\dot{\alpha}_C^A + \ldots + \frac{\partial \overset{S}{\varphi}}{\partial A_{CD}^{AB}}\dot{A}_{CD}^{AB}$ (1)

. $\tau_C^A = \rho_0 \overset{E}{f}{}_C^B \, \partial\overset{E}{\varphi}/\partial \overset{E}{f}{}_B^A$.

10

CONCLUSIONS

. A FORMULATION OF A RATE THEORY HAS BEEN DEVELOPED (LARGE DEFORM. & STRAINS: OR LARGE VELOCITIES & VELOCITY GRADIENTS)

. A PROCEDURE HAS BEEN ESTABLISHED FOR OBTAINING THERMODYNAMICALLY-CONSISTENT CONSTITUTIVE EQS (INELASTIC BEHAVIOR)

. THE THUSLY OBTAINED CONSTITUTIVE EQS ARE PHENOMENOLOGICAL IN NATURE AND WILL NEED EXPERIMENTAL SUPPORT (VERIFICATION AND EMPIRICAL EVALUATION OF EMPLOYED MATERIAL PARAMETERS)

12

N85-27960

STRUCTURAL TAILORING OF SSME BLADES (VANES)*

R. Rubinstein
Sverdrup Technology, Inc.
Middleburg Heights, Ohio 44130

The engine blade design optimization program STAEBL (Structural Tailoring of Engine Blades) is available at the NASA Lewis computer facility. The analysis capabilities of this program were extended to typical loading conditions for SSME turbopump blades including thermal and pressure loading. Input files for representative SSME blade designs were developed and sample optimization studies for these blades completed.

The structural tailoring program combines a general optimization package and a finite element blade analysis package. The analysis package's capabilities include natural frequency, maximum stress, and forced response computation, and fatigue life and flutter analysis.

Optimization is performed using the "feasible directions" method. The current design is modified by perturbing the design variables so that the design constraints are satisfied while the objective function, such as blade weight, is reduced at the maximum rate. The program's geometric design variables include blade thickness distribution, thickness to chord ratios, and root chord. Special design variables are included for composite and hollow blades. Typical design constraints include natural frequency margins imposed to avoid resonances near integral multiples of critical engine speeds, maximum stress limits, flutter margins, and forced response constraints imposed to avoid fatigue failure.

The program was designed for application to gas turbine fan blades. In order to extend the program's analysis capabilities to SSME blades, thermal and pressure load analyses, and the analysis of temperature dependent mechanical properties were added to the program. Optimization studies for flat plates and for compressor blades demostrated that such loads can cause significant increases in the weight of optimized designs. Pressure loads can greatly increase root stresses, and therefore require additional material at the blade root. Thermal loads influence the optimal design primarily by decreasing the blade's modulus of elasticity. This softening decreases the blade's natural frequencies and therefore requires higher blade weights in order to avoid resonances with engine speed.

SSME blade models provided by Lockheed and Rocketdyne were converted to the input format required by the structural tailoring program. Weight savings of approximately ten percent were achieved using optimized designs.

Design recommendations cannot, of course, be based on these calculations alone. Input from the SSME blade designers is crucial, especially to the formulation of constraints which correctly model the blade design requirements. However, the structure of the program is sufficiently flexible that any further program modifications required to accomodate SSME turbopump blade design requirements will surely be feasible.

---

*Work performed under NASA Lewis task number 84-52-01.

OBJECTIVE

MODIFY STRUCTURAL TAILORING PROGRAM (STAEBL) FOR APPLICATION TO SSME TURBOPUMP BLADES

STAEBL

OPTIMIZATION PROCEDURE

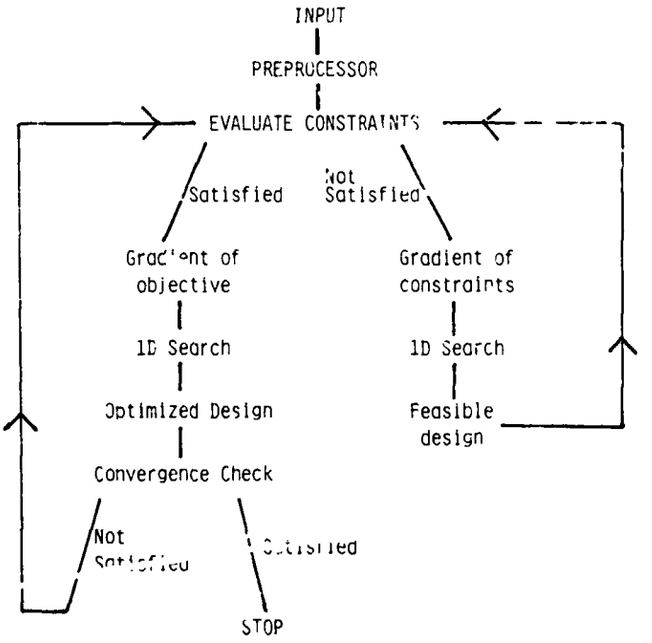

STAEBL

TYPICAL DESIGN VARIABLES

Thickness at 5 stations

Root chord

Thickness-to-chord ratio

TYPICAL CONSTRAINTS

Resonance margin for order number and root
(Campbell Diagram)

Maximum root static stress

Tip mode frequency margin

Forced response margin
(Goodman Diagram)

OPTIMUM BLADE DESIGN

Sixth Stage Compressor Blade

	INITIAL DESIGN			OPTIMIZED DESIGN			CONSTRAINT VALUES		
STAGE WEIGHT (LBS)		11.17			7.95				
PERCENT SPAN	0%	50%	100%	0%	50%	100%			
THICKNESS (IN)	.29	.20	.11	.24	.13	.08			
CHORD (IN)	2.8	3.1	3.6	1.7	1.9	2.2			
THICK/CHORD	.10	.06	.03	.14	.07	.04	.02 .15	.02 .12	.02 .10
CONSTRAINTS RESONANCE MARGINS									
MODE 1		.23			.05			> .05	
MODE 2		.21			1.3			> .05	
MODE 3		.24			1.6			> .05	
ROOT STRESS (KSI)		36			25			< 47	

OPTIMUM BLADE DESIGN

Sixth Stage Compressor Blade

EFFECT OF THERMAL AND PRESSURE LOADS

	NO THERMAL LOADS			THERMAL LOADS			THERMAL AND PRESSURE LOADS		
STAGE-WEIGHT (LBS)		7.95			8.24			9.69	
PERCENT SPAN	0%	50%	100%	0%	50%	100%	0%	50%	100%
THICKNESS (IN)	.24	.13	.08	.24	.15	.08	.48	.08	.08
CHORD (IN)	1.7	1.9	2.2	1.7	1.9	2.2	3.3	3.6	4.2
THICK/CHORD	.14	.07	.04	.14	.08	.04	.14	.02	.02
CONSTRAINTS RESONANCE MARGINS									
MODE 1		.05			.06			.05	
MODE 2		1.27			1.27			1.47	
MODE 3		1.65			1.65			1.67	
ROOT STRESS (KSI)		26			28			37	

OPTIMUM BLADE DESIGN

Lockheed SSME Blade

	INITIAL DESIGN			OPTIMIZED DESIGN High root stress			OPTIMIZED DESIGN Low root stress		
BLADE WEIGHT (LBS)		.046			.026			.038	
NUMBER OF BLADES		76			100			82	
PERCENT SPAN	0%	50%	100%	0%	50%	100%	0%	50%	100%
THICKNESS (IN)	.23	.15	.12	.17	.15	.06	.24	.13	.11
CHORD (IN)	1.0	.85	.81	.79	.64	.61	.96	.77	.74
THICK/CORD	.22	.18	.14	22	.23	.10	.25	.17	.15
CONSTRAINTS RESONANCE MARGINS									
MODE 1					2.3			2.9	
MODE 2					4.2			4.2	
MODE 3					8.1			8.6	
ROOT STRESS (KSI)					143			99	

STAEBL: Geometry Conversion

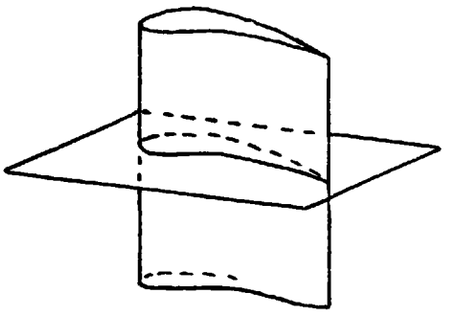

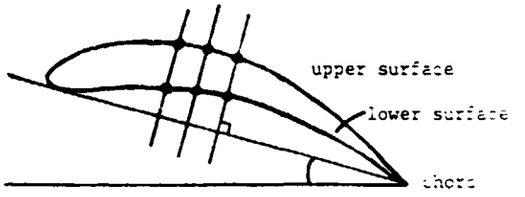

OVERVIEW OF FATIGUE, FRACTURE, AND CONSTITUTIVE MODELING PROGRAMS AT LEWIS

Gary R. Halford
National Aeronautics and Space Administration
Lewis Research Center
Cleveland, Ohio 44135

Because of the absolute requirement for having safe and durable reusable space propulsion systems and because of the extremely high performance required of such systems, the means must be available for accurately calculating the extent of usable mission lifetime. The design of reusable space propulsion systems is such that many of the critical components cannot avoid having very short lives. These lives must be reasonably well known in advance of committing a design to hardware because of the exceptionally high expense involved and the long time required for construction and certification. A minimum life must be attainable or the entire effort is not economically feasible. Being able to calculate expected lifetimes from expected loadings and structural analyses of the local stresses and strains enables the designer to alter details of a design to permit the maximizing of useful cyclic lifetime in conjunction with other design parameters such as performance, weight, and size. Knowledge of the possible design tradeoffs and their quantitative assessment will give rise to better designed systems.

Hence, the objective of the NASA Lewis Research Center's program in this durability area is to develop and verify cyclic constitutive stress-strain and life-prediction models for materials used in reusable space propulsion systems. The life-prediction models are aimed at accurately calculating the initiation and early growth resistance of cyclic cracks in materials used in hot-gas-path components. The development of cyclic crack propagation analysis and life-prediction methods by using fracture mechanics principles is being handled by my counterpart at the Marshall Space Flight Center, Carmelo Bianca.

Our approach to meeting the exceptionally rigorous demands of space propulsion systems is to start with the technology base developed in support of the aeronautics gas-turbine industry. Thus, life prediction and cyclic constitutive material models developed for aeronautics propulsion systems are being examined for deficiencies relative to reusable space propulsion systems.

Existing models are being modified and new ones will be developed as necessary to describe the evolutionary development of fatigue damage in terms of phenomenological variables and micromechanistic features of the materials involved. Crack initiation approaches are being addressed from experimental and theoretical points of view. Models will be subjected to rigorous verification at the subcomponent level to demonstrate their applicability to the unique conditions of reusable space propulsion hardware.

We are in the second year of the program and results are just now beginning to be realized. The early results will be presented by principal investigators from Lewis, universities, other Government laboratories, and industry.

INTERACTION OF HIGH-CYCLE AND LOW-CYCLE FATIGUE OF HAYNES 188 ALLOY AT 1400 °F

Peter T. Bizon, Dan J. Thoma, and Gary R. Halford
National Aeronautics and Space Administration
Lewis Research Center
Cleveland, Ohio 44135

The interaction of low-cycle fatigue (LCF) and high-cycle fatigue (HCF) was evaluated at the NASA Lewis Research Center on Haynes 188 alloy at 1400 °F. Completely reversed, axial-load, strain-controlled fatigue tests were performed to determine the baseline data for this study. Additional specimens for interaction tests were cycled first at a high strain range for various small portions of expected LCF life followed by a step change to a low strain range to failure in HCF. Failure was defined as complete specimen separation. The resultant lives varied between 10 and 5000 cycles for the low-cycle fatigue tests and between 4500 and 3 million for the high-cycle fatigue tests. For the interaction tests the low-cycle-life portion ranged from 30 and 1000 applied cycles while the high-frequency life ranged from 300 and 300 000 cycles to failure. The step change results showed a significant nonlinear interaction in expected life. Application of a small part of the LCF life drastically decreased the available HCF life as compared with what would have been expected by the classical linear damage rule (LDR).

The nonlinear cumulative damage rule proposed by Manson and Halford in 1981 and referred to as the "damage curve approach (DCA)" predicted the trends of the results. However, the presently observed interactions were more severe than anticipated, implying that the single universalized constant in the DCA has a different value than found for previous materials tested. A fractographic study of failed specimens showed that the fracture surfaces from interaction tests appeared to be essentially the same as surfaces from specimens tested in HCF only: the LCF portion of the cycling was not distinguishable on the interaction fracture surfaces.

NOMINAL PROPERTIES OF HAYNES 188 ALLOY

COMPOSITION (wt %)

COBALT	39%	IRON	3% MAX.
NICKEL	22%	MANGANESE	1.25% MAX.
CHROMIUM	22%	SILICON	0.4% MAX.
TUNGSTEN	14%		
CARBON	0.1%		
LANTHANUM	0.08%		

AT 1400 °F (TEST TEMPERATURE)

YIELD STRENGTH (0.2% OFFSET)	42 000 psi
ULTIMATE TENSILE STRENGTH	92 000 psi
TENSILE ELONGATION	43 %

V-2490

HOURGLASS SPECIMEN GEOMETRY

DIMENSIONS IN INCHES

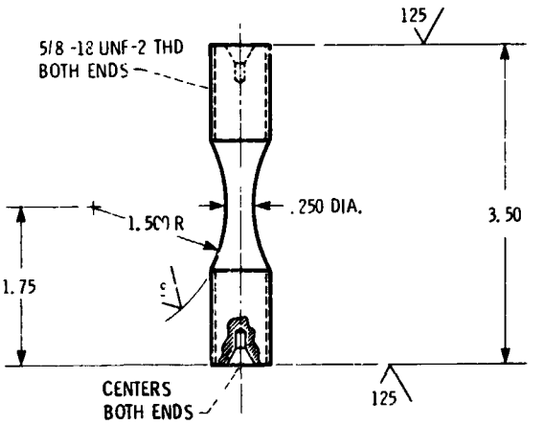

V-2485

CS-84-4506

TEST PARAMETERS

COMPLETELY REVERSED, AXIAL LOAD, STRAIN-CONTROL, FATIGUE TEST

TEMPERATURE	1400 °F
HEATING METHOD	SELF RESISTANCE
FREQUENCIES	0.4 AND 29 Hz
LOAD TRAIN ALIGNMENT	"WOODS-METAL SYSTEM"
MEASUREMENT:	
LOAD	FOUR-ARM STRAIN GAGE LOAD CELL
STRAIN	DIAMETRAL EXTENSOMETER USING LVDT
TEMPERATURE	OPTICAL DISAPPEARING-WIRE TYPE PYROMETER

V-2489

CS-84-4502

PROGRAM SCOPE

FATIGUE TESTS:

NUMBER OF TESTS	FREQUENCY (Hz)	LIFE (CYCLES)
9	0.4	13 → 4918
11	29	4500 → 3262300
10	0.4 → 29	33-925 → 300-310800

METALLOGRAPHIC STUDY:

TYPE OF TEST	LIFE (CYCLES)
LCF ONLY	2142
HCF ONLY	3262300
COMBINED LCF/HCF	51 → 76000

V-2488

CS-84-4503

SSME STRUCTURAL DURABILITY

LCF/HCF LOADING PATTERN

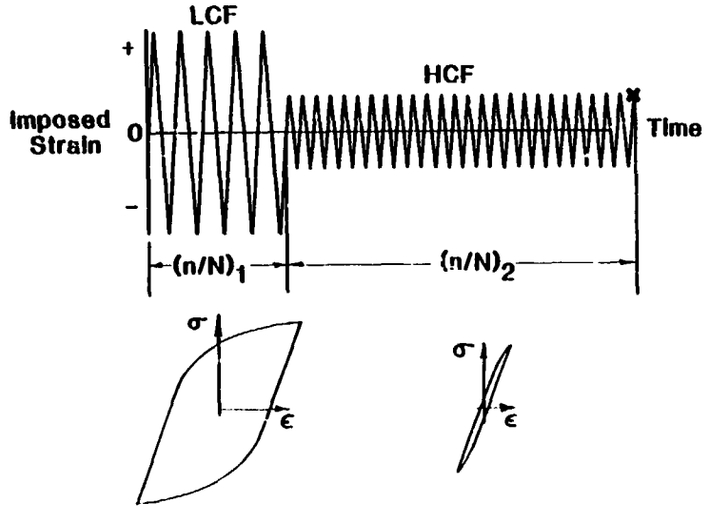

SSME STRUCTURAL DURABILITY

DAMAGE CURVE APPROACH

TWO LEVELS OF LOADING

N_1 & N_2

$$\frac{n_2}{N_2} = 1 - \left[\frac{n_1}{N_1}\right]\left[\frac{N_1}{N_2}\right]^{0.4}$$

INITIAL LIFE FRACTION

REMAINING LIFE FRACTION

SSME STRUCTURAL DURABILITY

DAMAGE CURVE APPROACH(DCA)

TWO LIFE LEVELS, N_{lo} AND N_{hi}

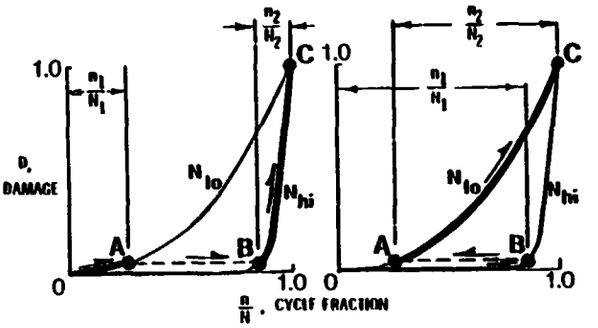

(a) $N_1 = N_{lo}$, $N_2 = N_{hi}$ (b) $N_1 = N_{hi}$, $N_2 = N_{lo}$

BASELINE FATIGUE DATA

HAYNES 188 ALLOY AT 1400 °F

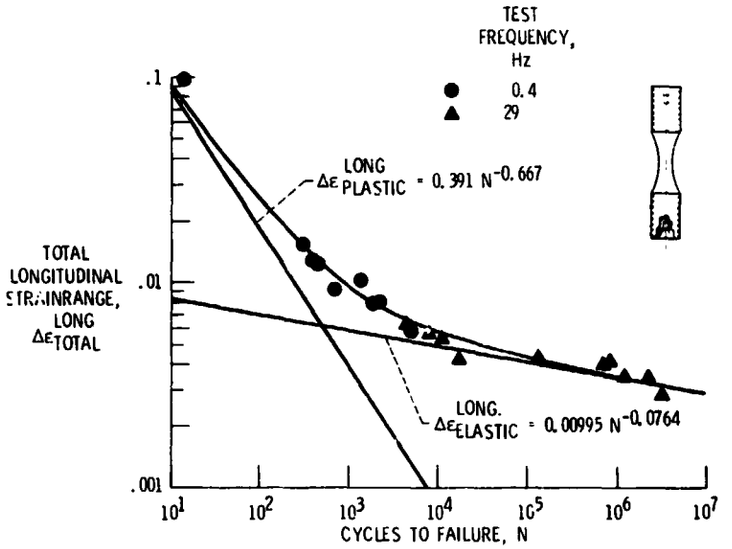

V-2486

CS-84-4505

LCF FOLLOWED BY HCF TO FAILURE

HAYNES 188 ALLOYS AT 1400 °F

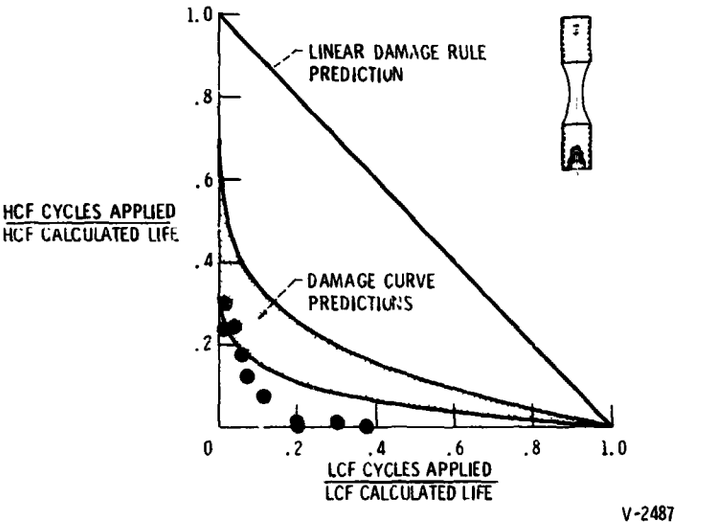

V-2487

CS-84-4504

1/4 INCH DIAMETER FAILED CROSS-SECTION

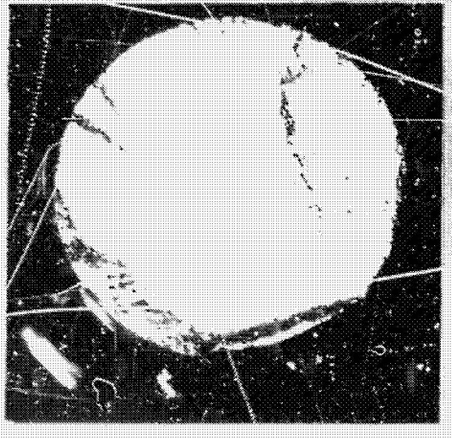

2142 CYCLES

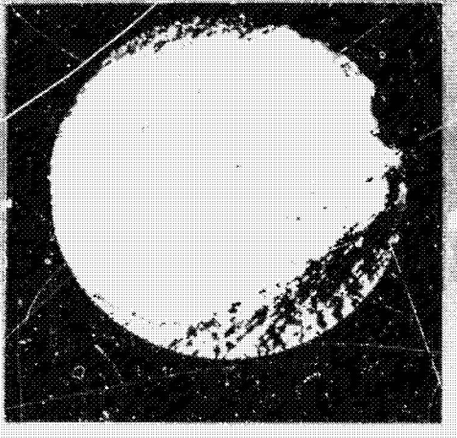

3262300 CYCLES

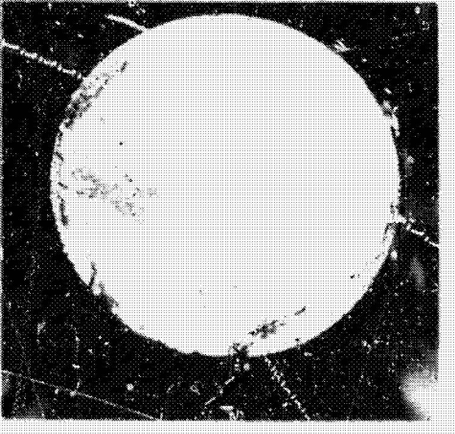

51/76000 CYCLES

V-2421

CS-84-4510

INITIATION SITE ON FAILED CROSS-SECTION

2142 CYCLES

3262300 CYCLES

31/76000 CYCLES

V-2482

CS-84-4511

LOW-MAGNIFICATION OF CENTER OF FAILED CROSS-SECTION

2142 CYCLES

3262300 CYCLES

5176000 CYCLES

V-2480

CS-84-4509

HIGH-MAGNIFICATION OF CENTER OF FAILED CROSS-SECTION

2142 CYCLES

326 300 CYCLES

51/76 000 CYCLES

(THIS MAGNIFICATION IS 1/2 THAT OF THE OTHER TWO PHOTOS)

CS-84-4508

V-2479

REEXAMINATION OF CUMULATIVE FATIGUE DAMAGE LAWS

Gary R. Halford
National Aeronautics and Space Administration
Lewis Research Center
Cleveland, Ohio 44135

S.S. Manson
Case Western Reserve University
Cleveland, Ohio 44106

Treatment of accumulated fatigue damage in materials and structures subjected to a history of nonsimple repetitive loadings has received a large amount of attention in recent years. The subject has been a popular one for more than half a century since Palmgren (ref. 1) first suggested what is now known as a "linear damage rule." After the same rule was later independently proposed by Langer (ref. 2) and Miner (ref. 3), it was recognized that, although the method has much merit for the simple treatment of complex loading history, it can result in unconservative predictions of material and structural behavior. An intense flurry of activity followed in the pursuit of alternative methods of analysis that would predict behavior more accurately. So many methods were introduced that it became necessary periodically to prepare review papers placing all the new methods into perspective, among them the ones by Newmark (ref. 4), Kaechele (ref. 5), Manson (ref. 6), O'Neill (ref. 7), Schive (ref. 8), and Laflen and Cook (ref. 9). Schive's study lists nearly 200 references while reviewing approaches to treat the problem and the numerous experimental programs that are relevant to the evaluation of the concepts. No truly comprehensive review has appeared of the considerable effort that has been made in the past dozen years since Schive's publication.

The current presentation is based on a few of the results contained in an extensive paper being prepared on the subject by Manson and Halford (ref. 10). Our primary goal is to review our own direct experience with this subject, to briefly mention some recent progress, and to express our current integrated view regarding the state of the art as it applies to our own efforts. Only incidentally shall we review the more recently proposed cumulative damage life prediction methods.

The double linear damage rule (DLDR), which has evolved in our laboratories over the past 20 years (refs. 11 to 13), is reexamined with the intent of improving its accuracy and applicability to engineering problems. Modifications are introduced to the analytical formulation to achieve greater compatibility between the DLDR and the so-called damage curve approach (ref. 13), which is an alternative continuous representation of the DLDR. For our present purposes we shall demonstrate the new formulation by using the recent HCF/LCF results generated by Bizon et al. (ref. 14) and presented at this conference. The constant in the new formulation are derived directly from the new data on the cobalt-base alloy Haynes 188. Once calibrated, the equations are used to predict lifetimes under complex, yet more realistic, simulated service conditions.

REFERENCES

1. Palmgren, Arvid: Die Lebensdauer von Kugellagern. VDI-Z (1857-1968), vol. 68, no. 14, Apr. 1924, pp. 339-341.

2. Langer, B.F.: Fatigue Failure from Stress Cycles of Varying Amplitude. J. Appl. Mech., vol. 4, no. 4, Dec. 1937, pp. A160-A162.

3. Miner, Milton A.: Cumulative Damage in Fatigue. J. Appl. Mech., vol. 12, no. 3, Sept. 1945, pp. A159-A164.

4. Newmark, N.M.: A Review of Cumulative Damage in Fatigue. Fatigue and Fracture of Metals, William M. Murray, ed., Wiley & Sons, New York, 1950, pp. 197-228.

5. Kaechele, L.: Review and Analysis of Cumulative-Fatigue-Damage Theories. Memorandum RM-3650-PR, Rand Corporation, Santa Monica, Aug. 1963.

6. Manson, S.S.: Interpretive Report on Cumulative Fatigue Damage in the Low Cycle Range. Welding Journal, Research Supplement, vol. 63, Aug. 1984, pp. 1-9.

7. O'Neill, M.J.: A Review of Some Cumulative Damage Theories. ARL/SM-REPORT-326, Aeronautical Research Laboratories, Melbourne, Australia, June 1970.

8. Schijve, J.: The Accumulation of Fatigue Damage in Aircraft Materials and Structures. AGARD-AG-157, AGARD, Paris, France, 1972.

9. Laflen, J.H.; and Cook, T.S.: Equivalent Damage: A Critical Assessment. (R82AEG533, General Electric Co.; NASA Contract NAS3-22534) NASA CR-167874, 1982.

10. Manson, S.S.; and Halford, G.R.: Re-Examination of Cumulative Fatigue Damage Analysis: An Engineering Perspective. To be presented at the Symposium on Mechanics of Damage and Fatigue, sponsored by the International Union of Theoretical and Applied Mechanics (IUTAM), (Haifa-Tel Aviv, Israel) July 1-4, 1985.

11. Manson, S.S.; Nachtigall, A.J.; and Freche, J.C.: A Proposed New Relation for Cumulative Fatigue Damage in Bending. Proc. Am. Soc. Test. Mater., vol. 61, 1961, pp. 679-692.

12. Manson, S.S.; et al.: Further Investigation of a Relation for Cumulative Fatigue Damage in Bending. J. Eng. Ind., vol. 87, no. 1, Feb. 1965, pp. 25-35.

13. Manson, S.S.; and Halford, G.R.: Practical Implementation of the Double-Linear Damage Rule and Damage Curve Approach for Treating Cumulative Fatigue Damage. Int. J. Fract., vol. 17, no. 2, Apr. 1981, pp. 169-192. (See also corrections in vol. 17, no. 4, 1981, pp. R35-R42.)

14. Bizon, P.T.; Thoma, D.J.; and Halford, G.R.: Interaction of High-Cycle and Low-Cycle Fatigue of Haynes 188 at 1400 °F. In this preprint.

DOUBLE DAMAGE CURVE APPROACH(DDCA)

$$D = \frac{n}{N_f}\left[g_1^{\gamma} + (1 - g_1^{\gamma})\left(\frac{n}{N_f}\right)^{\gamma(g_2 - 1)} \right]^{\frac{1}{\gamma}}$$

where

$$g_1 = \frac{0.35\left(\frac{N_{ref.}}{N_f}\right)^{\alpha}}{1 - 0.65\left(\frac{N_{ref.}}{N_f}\right)^{\alpha}}$$

$$g_2 = \left(\frac{N_f}{N_{ref}}\right)^{\beta}$$

γ = Small Integer as Required

Previous Work

$$\alpha = 0.25 \quad ; \beta = 0.40$$

Haynes 188 at 1400 F

$$\alpha = 0.35 \quad ; \beta = 0.60$$

CORRELATION OF HCF/LCF INTERACTION BY THE DOUBLE DAMAGE CURVE APPROACH(DDCA)

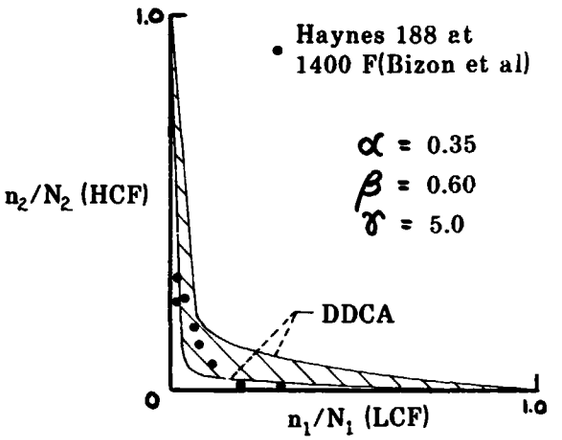

DOUBLE LINEAR DAMAGE RULE(DLDR)

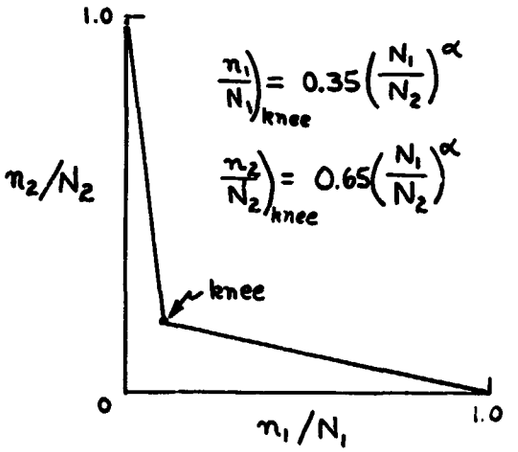

PHASE I ("Initiation")

$$\sum\left(\frac{n_1}{N_{I,1}} + \frac{n_2}{N_{I,2}}\right) = 1.0$$

PHASE II ("Propagation")

$$\sum\left(\frac{n_1}{N_{II,1}} + \frac{n_2}{N_{II,2}}\right) = 1.0$$

$$N_{I,1} = N_1 \times \left(\frac{n_1}{N_1}\right)_{knee}; \quad N_{II,1} = N_1 - N_{I,1}$$

$$N_{I,2} = N_2 - N_{II,2}; \quad N_{II,2} = N_2 \times \left(\frac{n_2}{N_2}\right)_{knee}$$

SIMULATED LOADING CASE(SSME LOX Post)

- HCF Freq. = 1000Hz
- Mission Duration = 500sec.
- LCF Life = 500 Cycles
- HCF Life = 50,000,000 Cycles

Mission Consists of 1 LCF Cycle at $N_1 = 500$ and 500,000 HCF Cycles at $N_2 = 50,000,000$

Based on Miner Linear Damage Rule,

$n/N_1 = 0.005$ and $n/N_2 = 0.01$

$0.005 + 0.01 = 0.015$

No. Missions = $1/0.015 = 67$

Based on DLDR for Haynes 188 at 1400 F

$N_{I,1} = 3$ $N_{I,2} = 49{,}400{,}000$

$N_{II,1} = 497$ $N_{II,2} = 578{,}000$

PHASE I

$$\frac{1}{3} + \frac{500{,}000}{49{,}400{,}000} = 0.343/\text{Mission}$$

$1/0.343 \Rightarrow 3$ Missions

PHASE II

$$\frac{1}{497} + \frac{500{,}000}{578{,}000} = 0.867/\text{Mission}$$

$1/0.867 \Rightarrow 1$ Mission

TOTAL = 4 Missions

EFFECT ON MISSION LIFE OF IMPROVING FATIGUE RESISTANCE

Baseline Fatigue Curve	—	4 Missions
Increase HCF Life by x 10, but Decrease LCF Life by x 2	—	5 Missions
Increase HCF Life by x 10	—	7 Missions
Increase LCF Life by x 2	—	9 Missions
Increase both HCF & LCF by x 10 & x 2 respec.	—	11 Missions
Increase HCF Life by x 100	—	23 Missions

INFLUENCE OF LCF/HCF DAMAGE RATIO

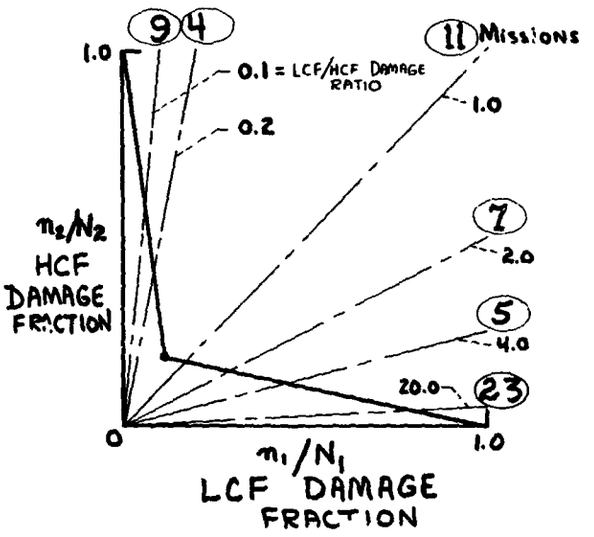

CYCLIC STRUCTURAL ANALYSES OF SSME TURBINE BLADES

Albert Kaufman and Jane M. Manderscheid
National Aeronautics and Space Administration
Lewis Research Center
Cleveland, Ohio 44135

Fuel turbopump components for reusable space propulsion systems experience extreme gas temperature and pressure environments. These operating conditions subject the high-pressure-stage turbine nozzles and blades to severe thermal transients that result in large inelastic strains and rapid crack initiation. To attain even the short lives required for these systems, anisotropic turbine blading alloys must be used. Assessing or improving the durability of these components is contingent on accurate knowledge of the stress-strain history at the critical location for crack initiation.

Nonlinear finite-element analysis techniques have become available in recent years for calculating inelastic structural response under cyclic loading. These methods are based on classical incremental plasticity theory with uncoupled creep constitutive models. Many of the nonlinear finite-element computer codes such as MARC (ref. 1) have the capability of handling materials with anisotropic properties. However, these codes are usually too costly and time consuming to use in the early design stages for aerospace applications. Costs are further increased by the geometrical complexity of high-pressure turbine blades, which necessitates three-dimensional analyses and sometimes substructuring for accurate solutions. Simplified procedures for more economically representing structural response under cyclic loading have been developed (refs. 2 to 4) to improve the design of engine hot-path components such as turbine blades.

This paper addresses the problems of calculating the structural response of high-temperature space propulsion components such as turbine blades for the fuel turbopump. The first high-pressure-stage fuel turbine blade (HPFTB) in the liquid-hydrogen turbopump of the space shuttle main engine (SSME) was selected for this study. In the past these blades have cracked in the blade shank region and at the airfoil leading edge adjacent to the platform. To achieve the necessary durability, these blades are currently being cast by using directional solidification. Single-crystal alloys are also being investigated for future SSME applications. The study evaluated the utility of advanced structural analysis methods in assessing the low-cycle fatigue lives of these anisotropic components.

The turbine blade airfoil of the high-pressure stage of the SSME fuel turbopump was analyzed because it has a history of rapid crack initiation. These uncooled airfoils have a span length of 0.33 cm and a span-to-chord width aspect ratio of approximately unity. The blades are cast from directionally solidified MAR-M 246 alloy. Temperature-dependent properties for this alloy were mainly provided by the Rocketdyne Division of Rockwell International Corporation. Material elastic properties are summarized in table I. Mean thermal coefficient of expansion data were converted to instantaneous values for MARC input. Poisson's ratio values of 0.143 and 0.391 were used for the longitudinal and transverse directions, respectively, and were assumed to be constant with temperature. Longitudinal stress-strain properties, summarized in table II, were used for the elastic-plastic region. A single-crystal MAR-M

246 alloy is also being considered for turbine blades in future SSME applications.

Cracking has occurred during service at the airfoil base near the leading edge and in the blade root shank area. These cracks apparently initiate during the first few mission cycles because of the severe thermal transients and are propagated by vibratory excitation. Since the primary purpose of this study was to compare nonlinear finite-element and simplified analytical methods, the blade root and platform were excluded from the analysis to reduce the size of the problem and therefore the computing time.

The mission used for the analysis is shown in figure 1 in terms of turbine inlet temperature, gas pressure, and blade rotational speed. This cycle is applicable to a factory test of the engine; it is also reasonably representative of a flight mission except for the foreshortened steady-state operating time. The major factors inducing rapid cracking are the transient thermal stresses and the inelastic strains caused by the sharp acceleration and deceleration transients.

Rudimentary transient and steady-state three-dimensional heat transfer analyses have been conducted using the MARC code. Film coefficients were obtained from preliminary information supplied by Rocketdyne. The gas sink temperature was assumed to be constant around the airfoil surface for each time step. Colder boundary conditions were assumed at the airfoil base to simulate the effects of the cooling of the blade-to-disk attachment region by the liquid-hydrogen fuel. Calculated metal temperatures at the leading edge at midspan and at the crack initiation site at the base of the airfoil (critical location) are presented in figure 2 as a function of elapsed time during the cycle. The assumed gas sink temperature around the airfoil is also plotted. Of particular note is that the leading-edge temperature is lower at the airfoil base than at midspan throughout the cycle. This seems reasonable because of the cooling of the blade-to-disk attachment region by the liquid-hydrogen fuel. The lower airfoil base temperatures induce tensile thermal stresses at the critical leading-edge location that are additive to the centrifugal stresses.

Elastic-plastic analyses are being conducted for the HPFTB airfoil with both the MARC code and a simplified analytical procedure developed at the NASA Lewis Research Center. The MARC analysis used the anisotropic material properties, while the simplified analysis used only Young's modulus and Poisson's ratio for the longitudinal (spanwise) direction.

A three-dimensional finite-element model of the airfoil (fig. 3) was constructed of eight-node isoparametric elements. The model consisted of 360 elements with 576 nodes and 1661 unsuppressed degrees of freedom. This model was a shortened version of a finite-element model created by Lockheed (ref. 5) for a NASTRAN elastic analysis of the HPFTB blade at rated power level; this work was done under contract to the NASA Marshall Space Flight Center. The main difference between the NASA Lewis and Lockheed models was that the blade base and most of the platform were omitted for the MARC nonlinear analysis to reduce the computing time and to run the problem in-core on the Cray computer system at Lewis. Boundary conditions were applied to constrain all nodes at the base of the model to lie on a plane. Additional boundary conditions were imposed to prevent rigid-body motion in this plane.

The MARC code has been used extensively at Lewis for inelastic analyses of aircraft turbine blades and combustor liners and of space power components. In conducting a cyclic analysis the loading history is divided into a series of incremental load steps, which are sequentially analyzed. The plasticity algorithm is based on a tangent stiffness approach in which the stiffness matrix is reformulated and reassembled for every plastic load increment. The incremental loads are modified by residual load correction vectors to ensure that the solution does not drift from a state of equilibrium. Convergence for the iterative plasticity analysis is indicated when the strain energy used in assembling the stiffness matrix approximately equals the energy change resulting from the incremental solution.

The mission cycle was subdivided into 129 increments. Incremental loading included centrifugal and gas pressure loads and metal temperature distributions as calculated from the heat transfer analysis. Approximately 1 million words of core storage on the Cray system were needed to run the problem. Each cycle of analysis required about 15 hours of computing time.

The directionality of the elastic material properties causes anisotropic constraints. Lekhnitskii (ref. 6) has derived the generalized elastic strain equations for an anisotropic body with a transverse plane of isotropy Matrix inversion of these equations to solve for the stresses results in the relationship

$$\begin{Bmatrix} \sigma_x \\ \sigma_y \\ \sigma_z \\ \tau_{yz} \\ \tau_{xz} \\ \tau_{xy} \end{Bmatrix} = a \begin{bmatrix} (1 - n\nu'^2) & (\nu + n\nu'^2) & \nu'(1 + \nu) & 0 & 0 & 0 \\ (\nu + n\nu'^2) & (1 - n\nu'^2) & \nu'(1 + \nu) & 0 & 0 & 0 \\ \nu'(1 + \nu) & \nu'(1 \quad \nu) & (1 - \nu^2)/n & 0 & 0 & 0 \\ 0 & 0 & 0 & G'/a & 0 & 0 \\ 0 & 0 & 0 & 0 & G'/a & 0 \\ 0 & 0 & 0 & 0 & 0 & G/a \end{bmatrix} \begin{Bmatrix} E_x \\ E_y \\ E_z \\ \gamma_{yz} \\ \gamma_{xz} \\ \gamma_{xy} \end{Bmatrix}$$

where $n = E/E'$ and $a = nE'/(1 + \nu)(1 - \nu - 2n\nu'^2)$. Here, E', G', and ν' denote Young's modulus, the shear modulus, and Poisson's ratio, respectively, for the longitudinal or span direction while E, G, and ν denote these constants with respect to any direction in the transverse plane of isotropy. This anisotropic stress-strain law was incorporated in the MARC user subroutine HOOKLW.

Plastic strain calculations were based on incremental plasticity theory using the von Mises yield criterion, the normality flow rule, and a kinematic hardening model. The material elastic-plastic behavior was specified by the yield strengths and work-hardening properties in the longitudinal direction; transverse properties were not available. Creep analyses are not being performed at the present time because of inadequate knowledge of the creep characteristics for the anisotropic blade material.

At the beginning of this study a steady-state MARC elastic-plastic analysis of the airfoil was conducted for rated power level (RPL). The temperature input was obtained from a NASTRAN steady-state heat transfer analysis performed by Lockheed. In contrast to the large temperature gradients calculated from the NASA heat transfer analysis, Lockheed had a maximum temperature variation in the airfoil of only 35 deg C. Effective stress distributions, as calculated

at the Gaussian integration points closest to the suction and pressure surfaces, are presented in figure 4. Since the airfoil was essentially at an isothermal state, the stresses primarily reflect the centrifugal and gas pressure loading and were entirely in the elastic range The maximum effective stress was only 40 percent of the yield strength. It is apparent that the analysis would not show a low-cycle fatigue problem if transient thermal effects were not considered. A MARC nonlinear finite-element analysis for the complete mission cycle was begun but has not been completed.

This work is still in a preliminary stage. A transient heat transfer analysis of the HPFTB airfoil has been completed. This analysis is rudimentary because of the inadequate definition of the heat transfer coefficients and omission of the cooled shank region in the finite-element model. However, it is sufficient for exercising and evaluating the structural analysis methods. A MARC cyclic stress-strain analysis has been started.

The simplified procedure will probably require further development for application to SSME turbopump blade problems - not only because of the use of anisotropic materials, but also because of the nonproportionality of the thermal and mechanical loading during the cycle. Experience has indicated that effective stresses and strains are not suitable criteria for relating multiaxial, nonproportional stress-strain states to uniaxial material properties.

REFERENCES

1. MARC General Purpose Finite Element Analysis Program. Vol. A: User Information Manual; Vol. B: MARC Element Library. MARC Analysis Research Corporation, Palo Alto, CA, 1981.

2. Kaufman, Albert: A Simplified Method for Elastic-Plastic-Creep Structural Analysis. NASA TM-83509, 1984.

3. Kaufman, Albert: Development of a Simplified Procedure for Cyclic Structural Analysis. NASA TP-2243, 1984.

4. Hwang, S.Y.; and Kaufman, A.: On Local Total Strain Redistribution Using a Simplified Cyclic Inelastic Analysis Based on an Elastic Solution. NASA TM-86913, 1985.

5. Hammett, W.C., et al : Space Shuttle Main Engine Powerhead Structural Modeling, Stress, and Fatigue Life Analysis, Vol. 3, (LMSC-HREC-TR-D867333-III, Lockheed Missiles and Space Co.; NASA Contract NAS8-34978.) NASA CR-171001, 1983.

6. Lekhnitskii, S.G.; and Brandstatter, Julius J.; (P. Fern, transl.): Theory of Elasticity of an Anisotropic Elastic Body. Holden-Day, San Francisco, 1983, pp.24-25.

TABLE I. - PHYSICAL PROPERTIES OF DIRECTIONALLY SOLIDIFIED MAR-M 246

Temperature, °C	Modulus of elasticity, GPa		Mean coefficient of thermal expansion, %/°C
	Longitudinal	Transverse	
21	131	183	-------
93	128	179	0.00113
204	125	173	.00130
316	124	173	.00133
427	119	166	.00141
538	114	162	.00148
649	109	156	.00149
760	103	149	.00156
871	97	142	.00160

TABLE II. - STRAIN PROPERTIES (LONGITUDINAL) OF DIRECTIONALLY SOLIDIFIED MAR-M 246

Plastic strain, percent	Stress, MPa, at -		
	21 °C	649 °C	816 °C
0.1	800	800	875
.2	830	855	930
.4	850	895	965
.6	855	930	970
.8	865	945	975
1.0	870	960	980

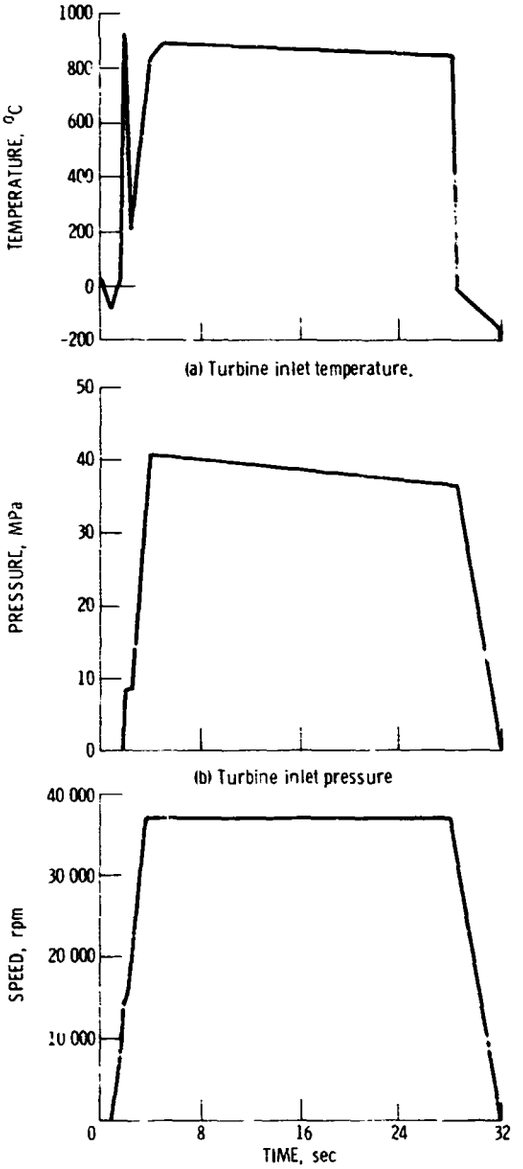

(a) Turbine inlet temperature.

(b) Turbine inlet pressure

(c) Blade rotational speed.

Figure 1. - Mission cycle used for analysis.

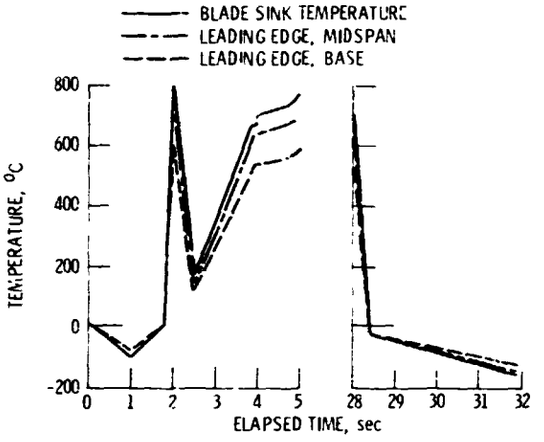

Figure 2. - Airfoil temperature cycle.

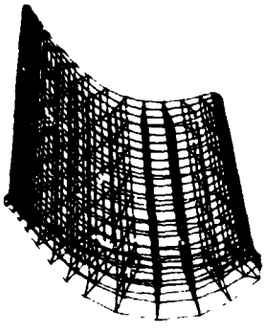

Figure 3. - Airfoil finite element model.

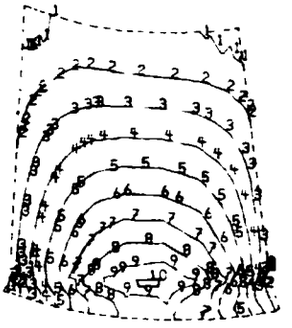

	STRESS, MPa
1	39.4
2	77.9
3	115.8
4	154.4
5	193.1
6	231.0
7	269.6
8	307.5
9	346.1
10	384.1

(a) Suction side.

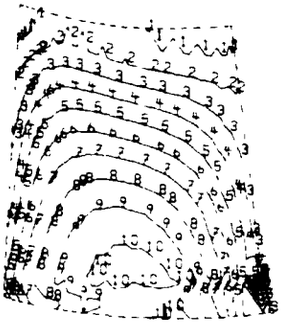

1	34.0
2	55.4
3	76.5
4	97.9
5	119.3
6	141.3
7	162.7
8	184.1
9	205.4
10	226.8

(b) Pressure side.

Figure -. - Airfoil effective stress distribution at RPL.

EFFECTS OF HIGH MEAN STRESS ON HIGH-CYCLE FATIGUE BEHAVIOR OF PWA 1480*

Saurin Majumdar
Argonne National Laboratory
Argonne, Illinois 60439

Steven Antolovich and Walter Milligan
Georgia Institute of Technology
Atlanta, Georgia 30332-0100

PWA 1480 is a potential candidate material for use in the high-pressure fuel turbine blade of the space shuttle main engine. As an engine material it will be subjected to high-cycle fatigue loading superimposed on a high mean stress due to combined centrifugal and thermal loadings. The present paper describes the results obtained in an ongoing program at the Argonne National Laboratory, sponsored by NASA Lewis, to determine the effects of a high mean stress on the high-cycle fatigue behavior of this material.

Straight-gauge high-cycle fatigue specimens, 0.2 inch in diameter and with the specimen axis in the [001] direction, were supplied by NASA Lewis. The nominal room temperature yield and ultimate strength of the material were 146 and 154 ksi, respectively. Each specimen was polished with 1-μm diamond paste prior to testing. However, the surface of each specimen contained many pores, some of which were as large as 50 μm. Testing was carried out at room temperature in the laboratory air environment. Future tests will be conducted at an elevated temperature in an inert environment.

In the initial tests, specimens were subjected to axial-strain-controlled cycles. However, very little cyclic plasticity was observed. For example, figure 1 shows the hysteresis loop at the tenth cycle of a 0 to 0.8 percent strain cycling test. The hysteresis loop has almost zero width, and very little cyclic mean stress relaxation occurred during the test. Since the majority of the tests were conducted at much lower strain ranges, where the hysteresis loops have no measurable width, it was decided to switch to load-controlled testing at a frequency of 20 Hz.

Figure 2 summarizes all of the tests run to date. Tests with mean stresses of 0, 60, and 120 ksi were carried out. The zero mean stress test data fall on a linear extrapolation of low-cycle fatigue test data for the same material at 1600 °F in a high-pressure hydrogen environment (ref. 1). Although the data are limited, the material seems to exhibit an endurance limit that is weakly dependent on the mean stress. Figure 3, for example, shows a Goodman diagram for a life of 10^6 cycles. It is evident that the high-cycle fatigue strength of the material is quite resistant to mean-stress effects.

Several specimens were analyzed by scanning electron and optical microscopy after fracture. Each specimen contained a large number of micropores

---

*Work supported by the National Aeronautics and Space Administration.

(fig. 4, top), and crack initiation always occurred from one of these micropores. Figure 5 shows crack initiation from a micropore in a specimen (#15-3) that was cycled at a stress range of 120 ksi with zero mean stress. A similar mode of crack initiation was also observed in a specimen (#112-3) that was cycled at a stress range of 38 ksi with a mean stress of 120 ksi (fig. 6). Crack propagation was crystallographic during most of the life; it apparently occurred along the {111} type of plane. In both specimens #112-3 and #15-3, the crack that led to failure was initiated by a crack on a different slip plane (figs. 4 and 5). Crack growth also appeared to preferentially follow microporosities (fig. 7). (The distinct slip band marks along the {111} type of plane in the figure are for a test with a rather large (0.8 percent) strain range. Such slip bands were not observed in the low-strain-range, high-cycle fatigue test specimens.)

Several slight differences were observed between specimen with zero and high mean stress. The specimen with high mean stress (#112-3) appeared to have cracks initiated at several sites, whereas the zero-mean-stress specimen (#15-3, fig. 5) had a single crack origin. The high-mean-stress specimen also had a rougher, more textured fracture surface, which may be indicative of a higher crack propagation rate. It also contained several "steps" on the fracture surface (fig. 4, bottom). These steps were probably caused either by the linking of two parallel cracks on the same type of octahedral plane or by the intersection of cracks on nonparallel octahedral planes.

REFERENCE

1. DeLuca, D.P.: Final Report on Mechanical Properties of Turbine Alloys in Hydrogen at Elevated Temperatures. Prepared for NASA George C. Marshall Flight Center by United Technologies Pratt & Whitney Aircraft, FR 14844, 1981.

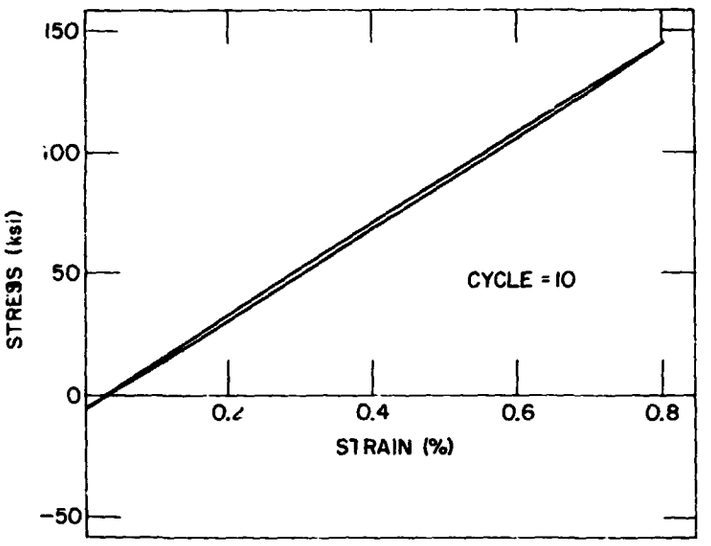

Figure 1. - Hysteresis loop at 10th cycle for PWA 1489 specimen subjected to cycling between 0 and 0.8 percent strain range at room temperature.

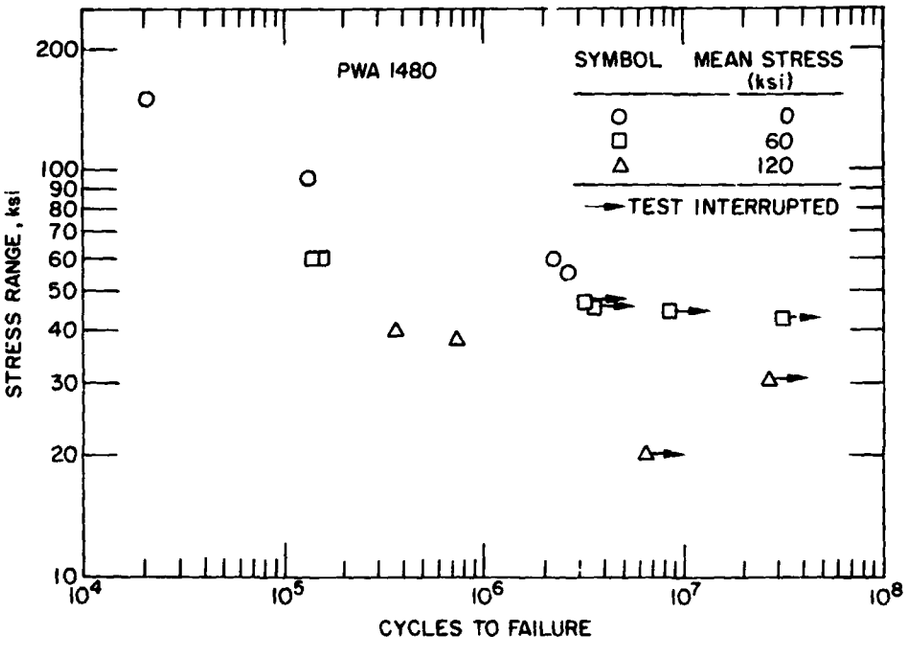

Figure 2. - Summary of high-cycle fatigue tests of PWA 1480 at room temperature at various mean stresses.

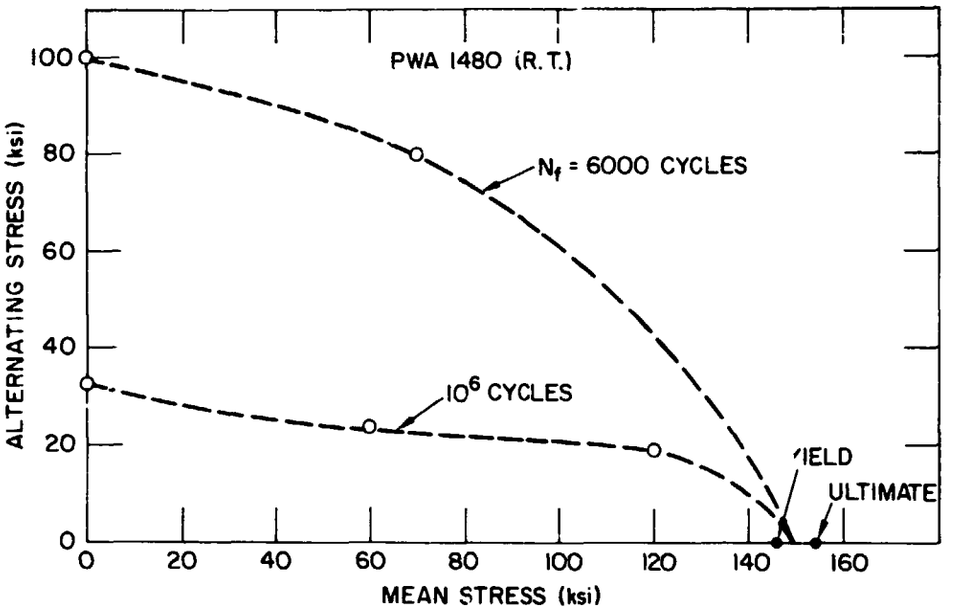

Figure 3. - Goodman diagram for PWA 1480 for lives of 6000 and 10^6 cycles at room temperature.

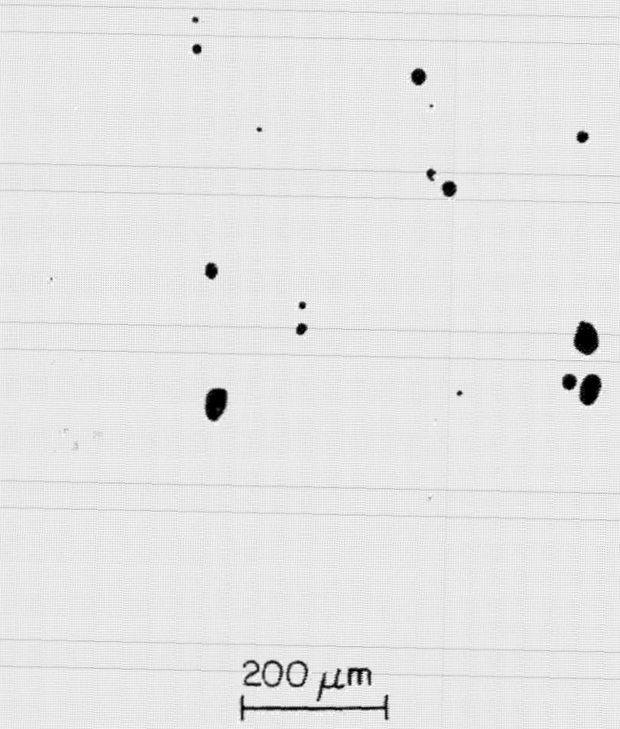

Figure 4. - Optical micrograph (top) illustrates typical micropore density in specimen #15-3 (unetched). Scanning electron micrograph (bottom) shows a "stepped" fracture surface in specimen #112-3, which was cycled at stress range of 38 ksi with mean stress of 120 ksi at room temperature.

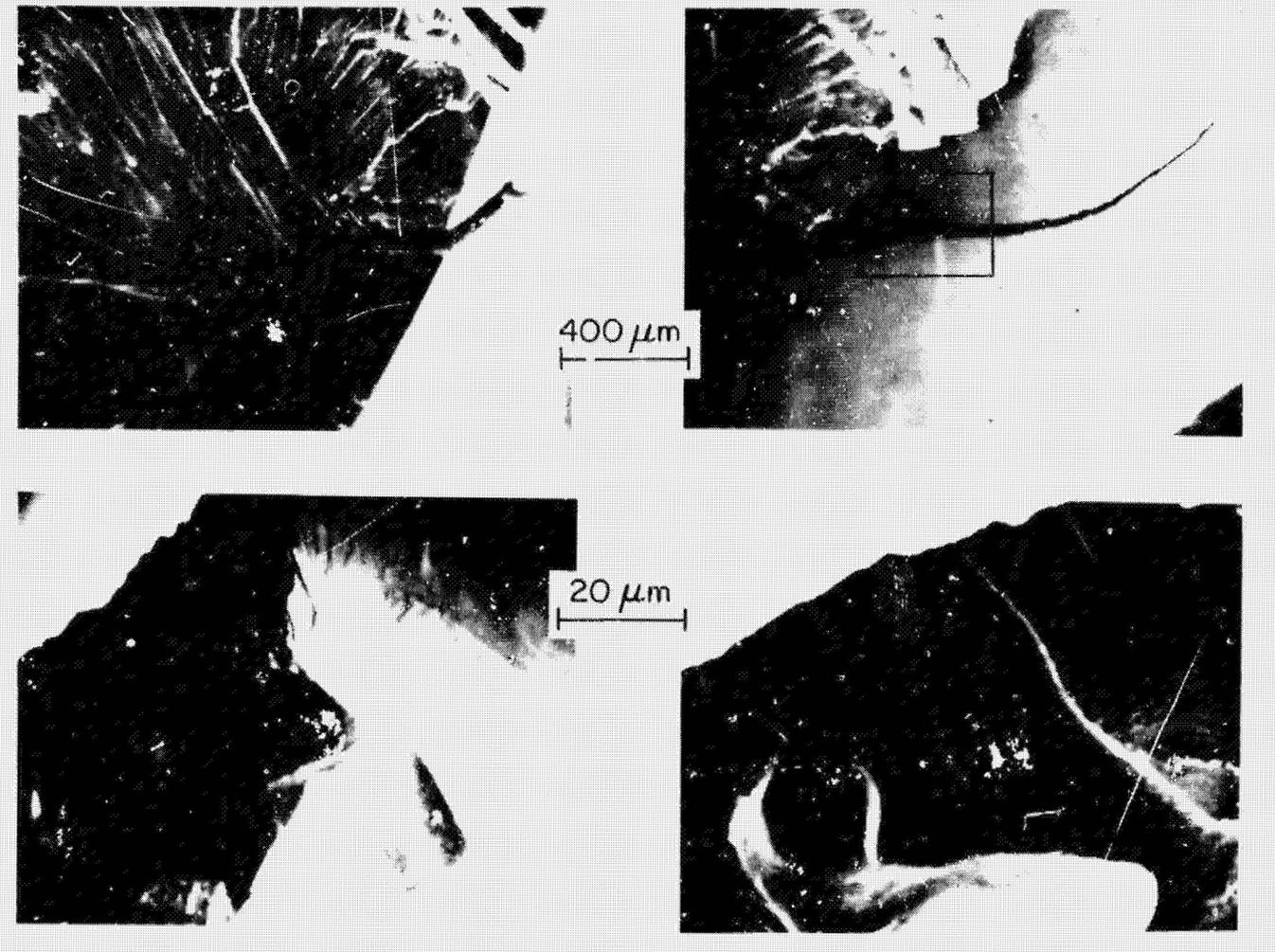

Figure 5. - Fracture morphology in specimen #15-3, which was cycled at stress range of 120 ksi with zero mean stress at room temperature. The micropore initiated two cracks on different planes; one of these cracks led to failure of the specimen.

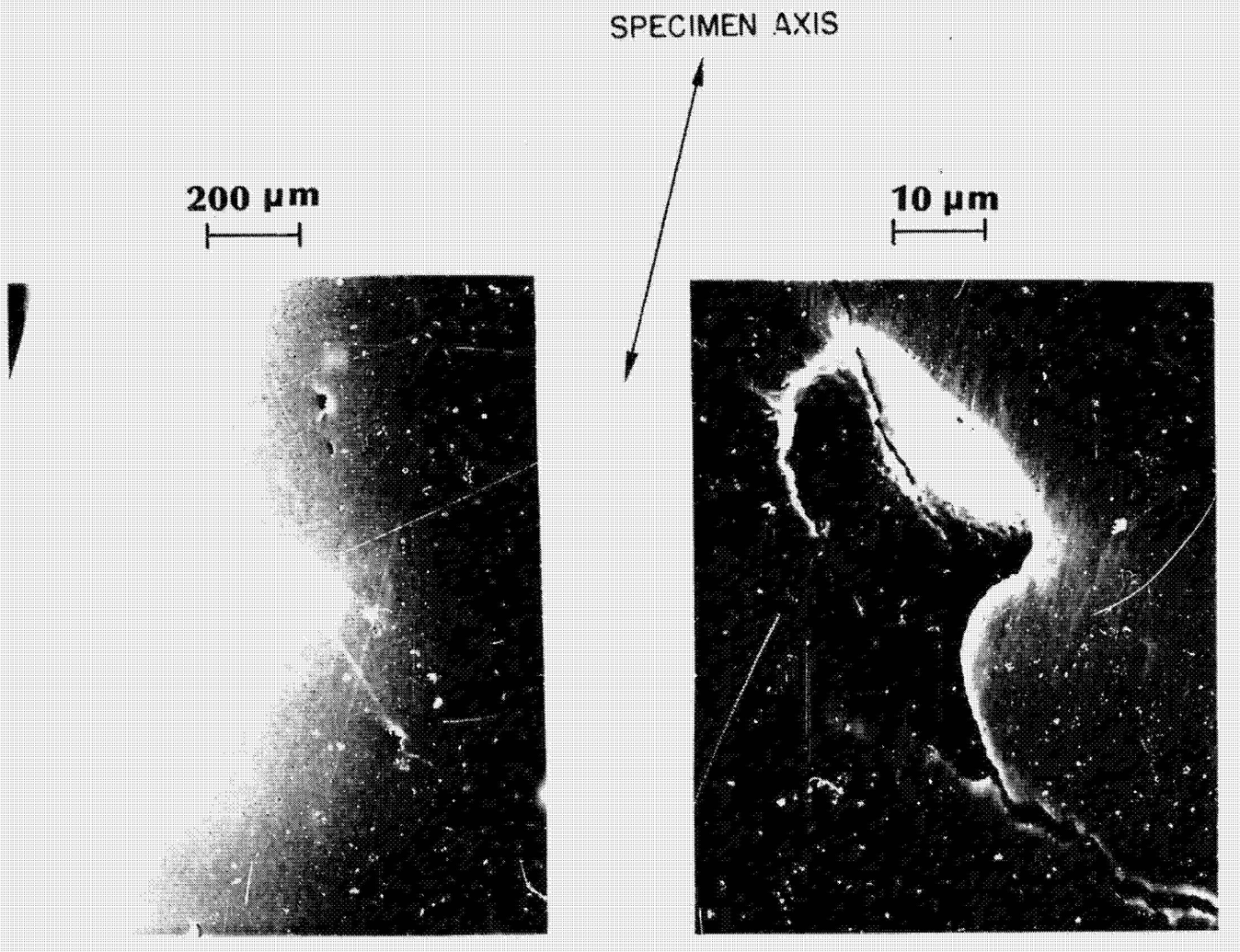

Figure 6. – Scanning electron micrographs showing surface pore from which crack was initiated under high-cycle fatigue loading with stress range of 38 ksi and mean stress of 120 ksi at room temperature.

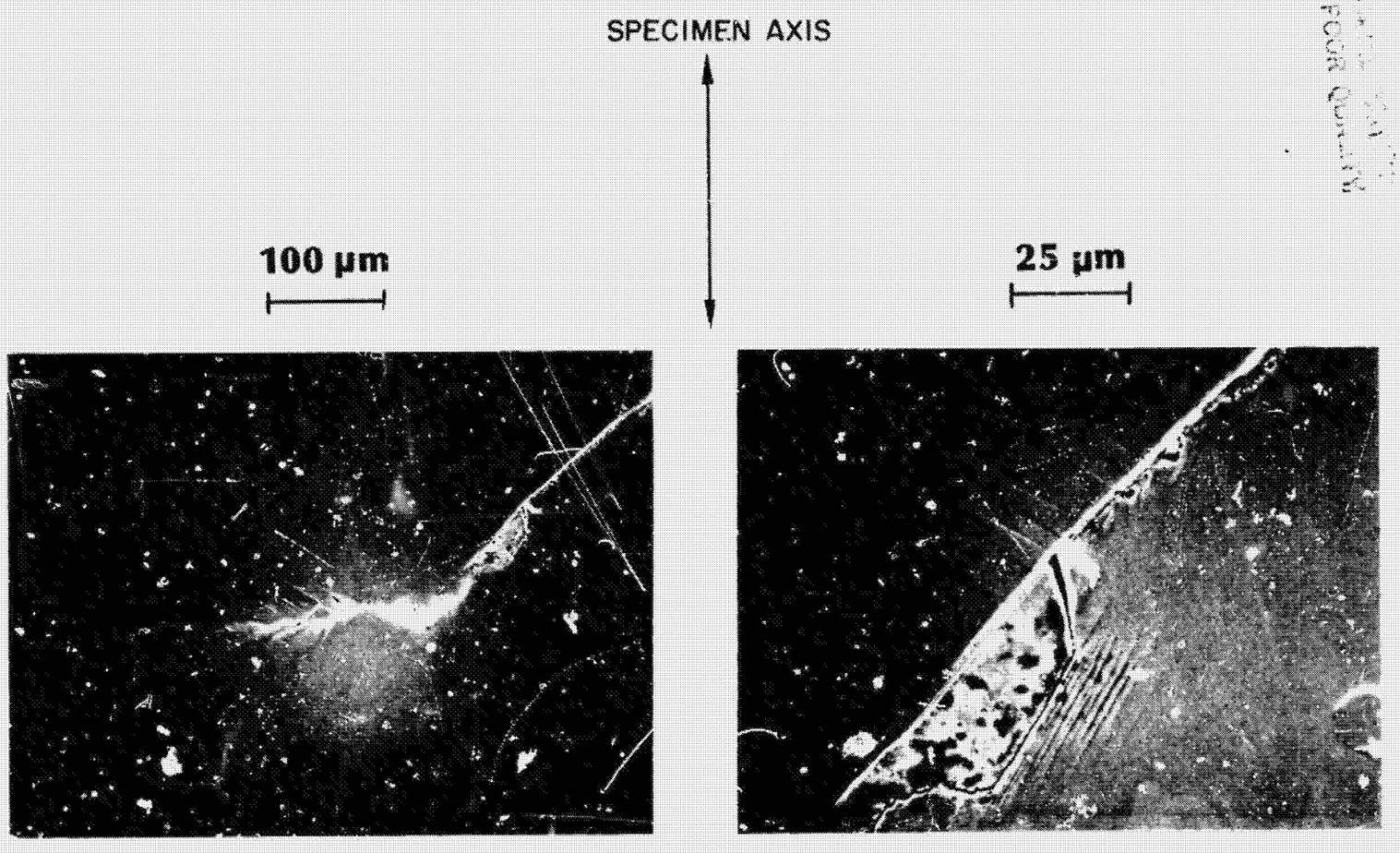

Figure 7. - Scanning electron micrographs showing crack propagation in PWA 1480 under 0 to 0.8 percent strain range testing at room temperature.

CONSTITUTIVE CYCLIC DEFORMATION BEHAVIOR IN SINGLE-CRYSTAL AND DIRECTIONALLY SOLIDIFIED SSME HIGH-PRESSURE FUEL TURBOPUMP AIRFOIL MATERIALS

Walter W. Milligan, Eric S. Huron, and Stephen D. Antolovich
Georgia Institute of Technology
Atlanta, Georgia 30332-0100

The major goal of the project is to correlate mechanical properties with microstructural deformation behavior and to develop models for constitutive response under a variety of monotonic and cyclic loading cycles, temperatures, strain levels, strain rates, and environments. The main areas of research to date have been the development of techniques for sample preparation and microstructural characterization. In addition, mechanical testing is being carried out and results will be reported.

Two alloys are being studied as candidate SSME turbine blade materials. The first is PWA 1480, which is a single crystal alloy whose nominal composition is reported in table I. As documented in figure 1, it is a two-phase γ/γ' alloy, with the γ' size averaging 0.75 μm after heat treatment. The dislocation density in the heat-treated material is very low. The alloy contains about 2 vol % microporosity (see abstract by S. Majumder et al.). The alloy also contains interdendritic γ/γ' eutectic. Several deformation microstructures are shown in figure 2.

The second alloy being studied is D.S. Mar-M 246 + Hf. This is a directionally solidified material, and its nominal composition is also reported in table I. Like PWA 1480, it is a two-phase γ/γ' alloy, with the γ' size averaging 0.5 μm (fig. 3). The precipitates contain a network of interfacial dislocations (fig. 3), an indication of a large mismatch with matrix. It also contains γ/γ' eutectic areas at the grain boundaries (fig. 4), large carbides (probably of the MC type) within the grains (fig. 4), fine carbides (probably M_6C or $M_{23}C_6$) in the grain boundaries (fig. 4), and submicroscopic carbides in the eutectic areas (fig. 3). This material contains very little microporosity.

The major areas of interest for the two materials will be slightly different. The single-crystal alloy lends itself well to fundamental deformation studies, since resolved shear stresses on slip planes are all known and only one grain is present. On the other hand, the D.S. material presents an excellent opportunity to study the effects of slightly misaligned grains on deformation behavior.

The two materials will be studied by using approximately the same test matrix, so a good degree of direct comparison will also be possible. In addition to contributing to fundamental understanding, the results of this study should have profound implications for design inasmuch as constitutive models (based on experimental observations) will be developed.

TABLE I. - ALLOY COMPOSITIONS

Element	PWA 1480	D.S. Mar-M 246
	Composition, wt %	
Cr	10	9
Co	5	10
Ai	5	6
Ti	1.3	1.5
W	4	10
Mo		2.5
Ta	12	1.5
Hf		1
C		0.15
B		0.015
Zr		0.05
Ni	Bal.	Bal.

(a)

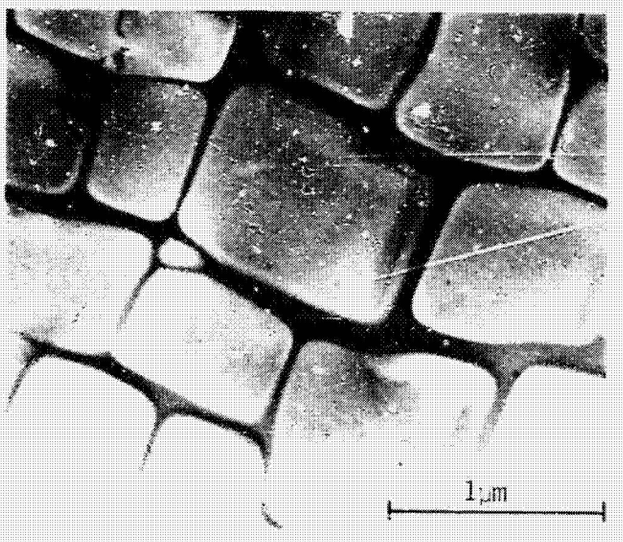

(b)

Fig. 1. TEM micrographs of the as-heat treated PWA 1480. (a) Bright field micrograph showing the γ' morphology and low dislocation density. <200> reflection, 8,000X. (b) Dark field micrograph of γ'. <300> superlattice reflection, 31,000X.

(a)

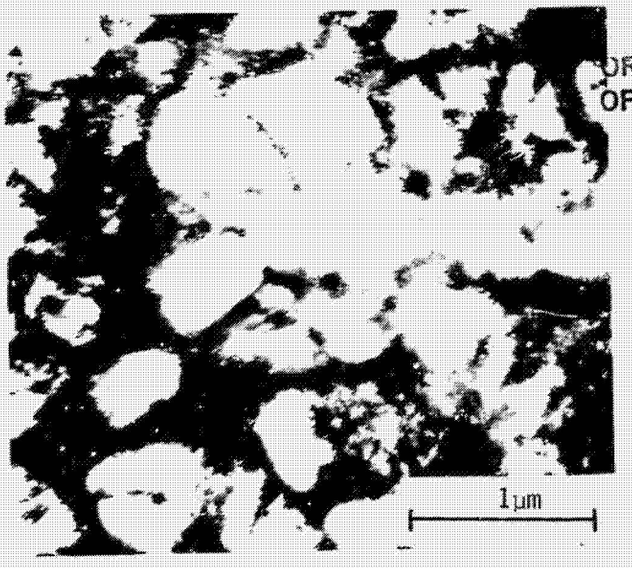

(b)

Fig. 2. TEM micrographs of deformation in PWA 1480. (a) Slip band in the as-heat treated condition. <111> reflection, 70,000X. (b) Extremely high dislocation density after tensile failure at 1200°F. The majority of dislocations appear to be in the matrix. <111> reflection, 27,000X.

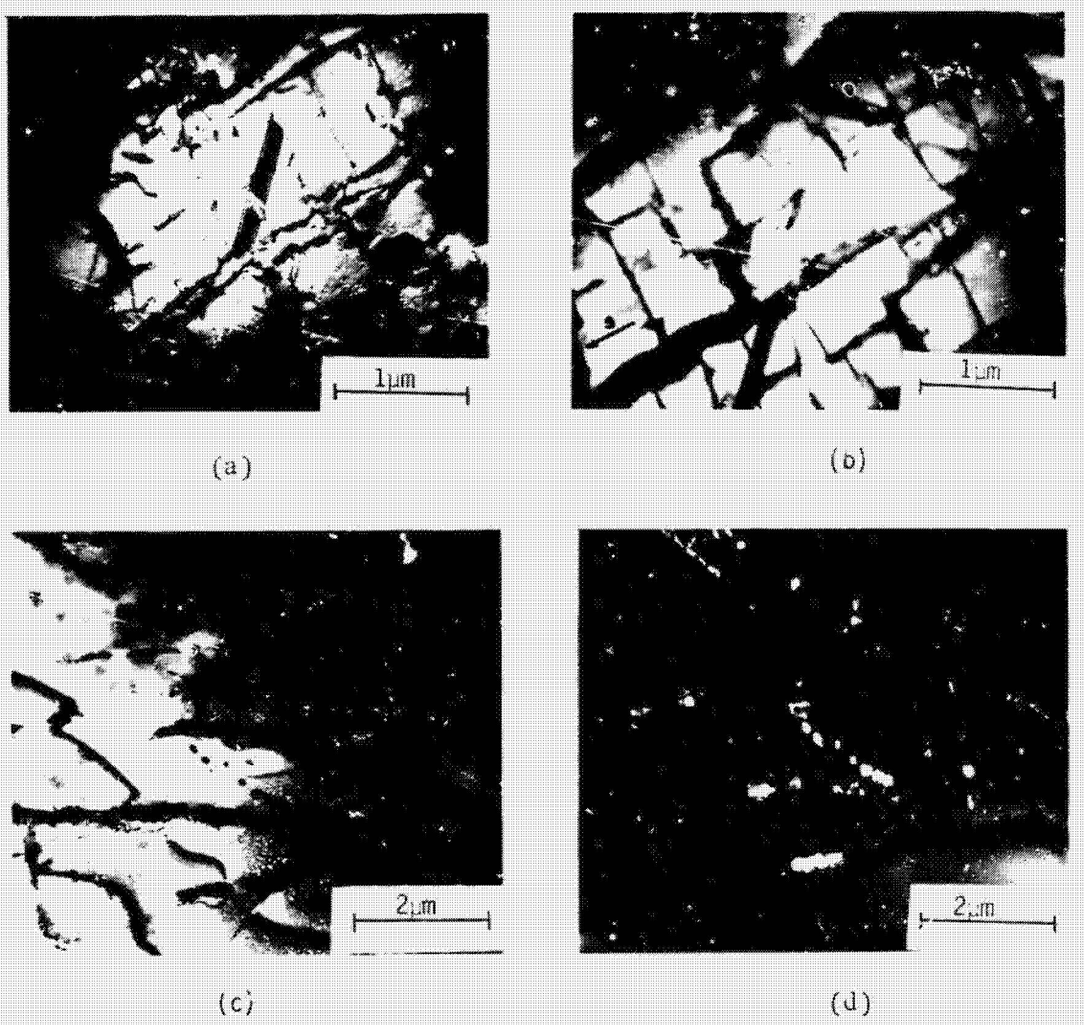

Fig. 3. TEM micrographs of as-heat treated DS Mar-M 246 + Hf. (a) Bright field micrograph showing interfacial dislocation networks and stacking faults. <200> reflection, 20,000X. (b) Dark field of the same area, slightly translated. <300> γ' superlattice reflection, 20,000X. (c) Bright field in a γ/γ' eutectic area. <200> reflection, 10,000X. (d) Dark field of the same area as "c", showing coherent carbides in the matrix.

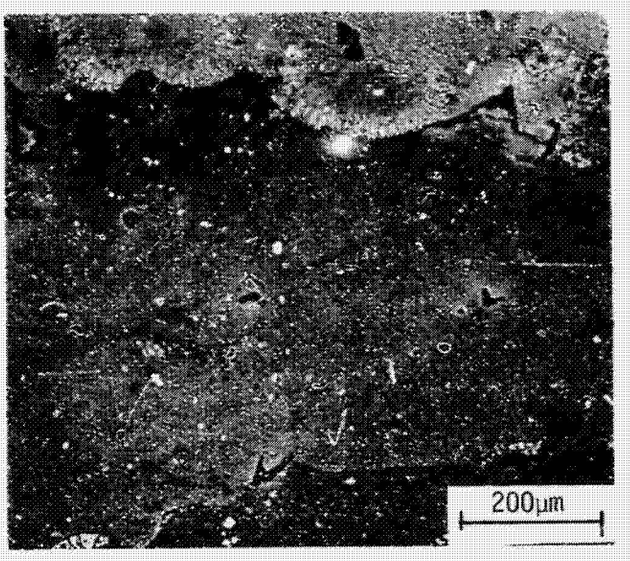

(a)

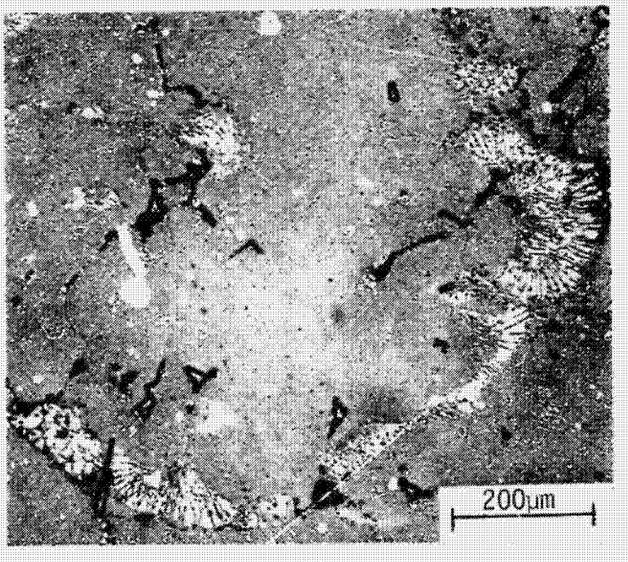

(b)

Fig. 4. Optical micrographs of the grain structure of DS Mar-M 246 + Hf. (a) Longitudinal (b) Transverse. Note Eutectic γ/γ' areas at grain boundaries and the irregular grain boundary shapes. 100X.

HIGH-THERMAL-GRADIENT SUPERALLOY CRYSTAL GROWTH

David D. Pearson, Donald L. Anton, and Anthony F. Giamei
United Technologies Research Center
East Hartford Connecticut, 06108

Single, [001]-oriented crystals of PWA 1480 were processed in alumina/silica shell molds in a laboratory high-gradient furnace. The furnace employs a graphite-resistance-heated element, a radiation baffle, and a water-cooled radiation trap below the baffle. All crystals were grown in vacuum (10 torr) and all heat transfer was radiative. The element is constructed with a variable cross section that is tapered just above the baffle to maximize heat input and therefore thermal gradient. A maximum alloy temperature of 1600 °C was used. A thermal gradient of 130 deg C/cm was recorded at 1370 °C just above the solidus of the PWA 1480 alloy. Crystal bars with 14.4- and 17.5-mm diameters were grown in alumina/silica shell molds similar to those used for producing gas turbine hardware. Each crystal was started from a 1.6-mm pencil seed at a rate of 76 mm/hr and slowly accelerated to a rate of 200 mm/hr under computer control. Volume percent porosity and average pore size were measured as functions of distance in representative bars. Low-cycle fatigue (LCF) behavior was determined at UTRC, and stress-rupture properties were determined at the NASA Lewis Research Center. UTRC will discuss the crystal growth, porosity measurements, and LCF behavior.

ROLE OF HYDROGEN AND STRUCTURE ON CMSX-2

C.L. Baker, J. Chene, W. Kromp, H. Pinczolitis,
S.M. Bernstein, and J.C. Williams
Carnegie-Mellon University
Pittsburgh, Pennsylvania 15213

Hydrogen environments have previously been shown to be deleterious to the properties of nickel-base superalloy single crystals. The goal of this study is to characterize and understand the detailed effect of hydrogen on the tensile and fatigue behavior of single crystals of CMSX-2.

Specimens were solutionized for 3 h at 1315 °C, air cooled, and then aged in one of two ways: 980 °C/5 h/air cool + 850 °C/48 h/air cool (standard heat treatment), or 1050 °C/16 h/air cool + 850 °C/ 48 h/air cool (ONERA heat treatment).

The resultant macro- and microstructure included a pronounced dendritic structure with numerous low angle boundaries in the interdendritic region and on the average a high level of porosity with a large variation in size and distribution. The microstructure consisted of 0.5-μm cuboidal γ' precipitates separated by thin continuous regions of matrix. The ONERA heat treatment led to slightly larger, more aligned, and more cuboidal γ' precipitates - a structure known to improve the creep strength of this alloy.

Hydrogen permeability and diffusivity in this material was found to be very low at room temperature. To enhance the extent of hydrogen penetration and embrittlement, hydrogen was introduced by cathodic charging at 150 °C in molten salt. This was expected to increase the permeability by 2 or 3 orders of magnitude. This treatment produced a 50-μm-deep embrittled layer in charged tensile and fatigue specimens that explicitly affected the fracture behavior. Knoop microhardness measurements of the hydrogenated surface showed a relative increase of about 25 percent, attributed to the lattice distortions associated with the steep hydrogen concentration gradient near the surface and consistent with the fracture appearance.

Hydrogen concentration studies on thin samples yielded values significantly higher than found for similar charging conditions in nickel and stainless steels. This implied a high effective hydrogen fugacity in molten salt and a strong trapping effect primarily at voids and γ/γ' interfaces. The existence of strong trapping at voids was inferred by the continued existence of an embrittlement effect and a large residual hydrogen concentration after desorption at 150 °C. Trapping at γ/γ' interfaces was suggested by the appearance of these interfaces on the fracture surfaces.

The tensile mechanical properties were found to depend on hydrogen concentration. Hydrogenation in molten salts enhanced hydrogen's effect on mechanical properties, particularly a significant decrease in strength and plasticity, with the greatest effect being decreased elongation, presumably an effect of hydrogen on crack initiation. Scatter in the tensile ductility of both charged and uncharged smooth tensile samples was observed, probably because of voids and slight differences in crystal orientation. No recovery of the mechanical properties was observed after aging for 7 days at room temperature, in agreement with the very low kinetics of hydrogen desorption at

20 °C. After desorption at 150 °C the remaining embrittlement was associated with hydrogen trapping in voids. Unlike previous studies, no influence of heat treatment on the extent of hydrogen embrittlement was seen in smooth tensile samples for these charging and testing conditions.

SEM observations of the brittle subsurface zone revealed a strong correlation between crack initiation sites and voids just beneath the surface. Preferential decohesion around the voids may have resulted from a hydrogen pressure buildup in such voids, while the very flat rupture features of the brittle zone indicated that the crack propagation was perpendicular to the stress axis, suggesting a preferential decohesion along the γ/γ' interfaces. In contrast uncharged samples showed a ductile tearing of the matrix throughout the cross section. The presence of numerous superficial transverse cracks in the brittle layer suggests that while cracks can initiate very easily in the outer zone, their propagation in the bulk is more difficult. Thus, a more dramatic loss in tensile ductility was not observed, particularly for smooth specimens, since the amount of hydrogenated material was small with respect to the total volume of the sample.

Fatigue tests at constant plastic strain amplitude were performed on samples with two different geometries: smooth solid specimens and hollow samples with similar external shapes. Similar to uniaxial testing, the accumulated strain to fracture in the hydrogen-charged samples was lower than in the uncharged ones; however, the ratio of the total strain (charged versus uncharged) was considerably lower in fatigue than in uniaxial tension. The decrease in the UTS of the charged sample is similar to uniaxial testing: about 10 percent lower than the uncharged ones.

The hollow and solid samples were compared to better understand the influence of increased charged volume on the fatigue behavior. As expected, the fatigue lifetime of the hollow samples was significantly shorter than that of the solid ones. In fact, the numbers of cycles to failure was about two times smaller while the ratio of the hydrogen-affected volume in the hollow versus solid specimens was approximately 4, suggesting a scaling relationship between the two. The fracture appearance was also similar to those of the tensile samples, especially the enhanced cracking around voids.

CONCLUSIONS

1. Significant hydrogen embrittlement of CMSX-2 can occur in high-fugacity cathodic environments.

2. Hydrogen accelerates the ease of crack initiation in both tension and fatigue.

3. Fatigue testing magnifies the extent of hydrogen embrittlement compared to tension.

4. Hydrogen embrittlement is enhanced by the presence of internal voids, which act as traps for hydrogen.

5. No effect of heat treatment on cathodically included hydrogen embrittlement of smooth tensile samples has been observed.

6. The dendritic structure deflects the crack path in hydrogenated specimens.

7. High concentrations of hydrogen affect the work-hardening behavior of CMSX-2.

8. Permeability of hydrogen is low in CMSX-2.

MICROSTRUCTURE

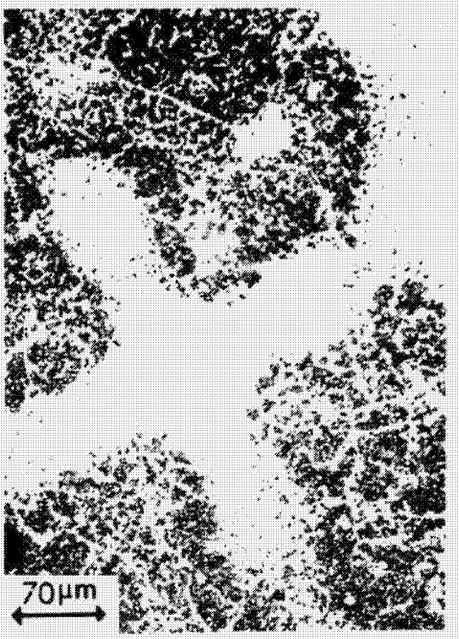

a) Dendritic structure remains evident after solutionizing and full heat treatment

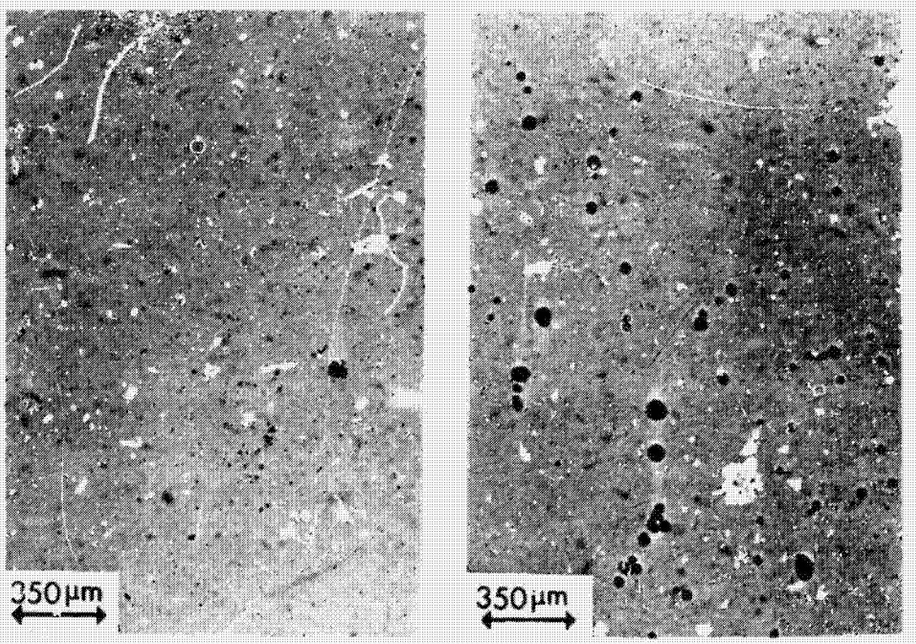

b) Porosity levels vary significantly

MICROSTRUCTURE VS. HEAT TREATMENT

γ' precipitate size and distribution vary with heat treatment

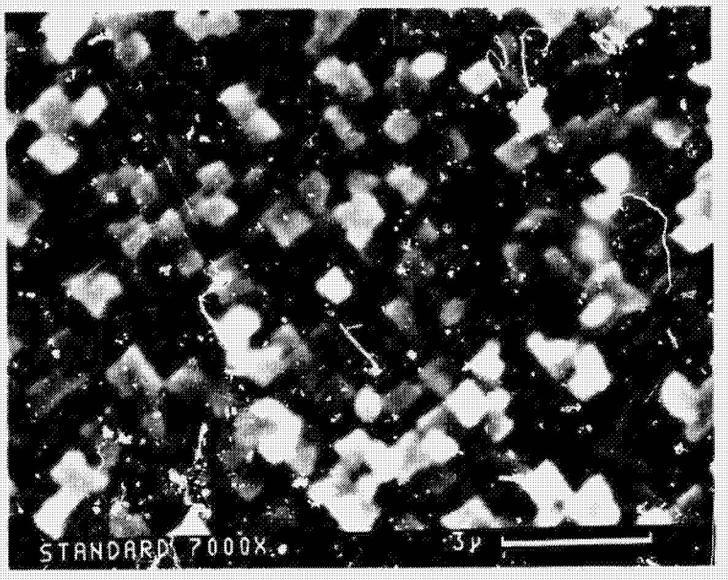

solution: 1215°C/ 3hr

primary age: 980°C/ 5hr

secondary age: 850°C/ 48hr

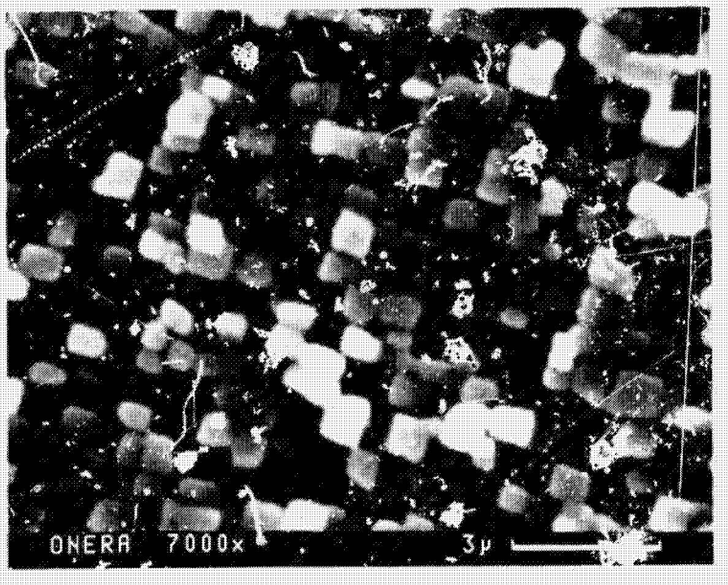

solution: 1315°C/ 3hr

primary age: 1050°C/ 16hr

secondary age: 850°C/ 48hr

Hydrogen Concentration Data and Microhardness Changes

Hydrogen introduced by cathodic charging

ONERA

Treatment	Thickness	H Conc (ppm wt)
Charge 5 hr/150°C/molten salts	500 µm	50 ppm
Charge 5 hr/150°C/molten salts	125 µm	503 ppm
Charge 5 hr/150°C/molten salts +desorb/5 hr/150°C/air	125 µm	185 ppm

STANDARD

Charge 5 hr/150°C molten salts	500 µm	100 ppm

Knoop Microhardness

	Uncharged	Charged	%increase
ONERA	392	474	21%
STANDARD	405	512	26%

TENSILE DATA (Tensile tests performed at 20°C in air $\dot{\epsilon}=2.10^{-4}s^{-1}$)

Heat Treatment	H Charging Conditions	E GPa	Yo.2 MPa	U.T.S. MPa	Eh %
As solutionized:	Uncharged	130	845	838	32.4
1315°C, 3h, air - forced cooled	Ch. 5h, 150°C Molten salts	130	825	782	20.8
Standard H.T.:	Uncharged	138	1126	1306	21.9
As sol. + 980°C 5h air cool + 850°C, 48h	Ch. 5h, 150°C Molten salts		948	1014	11.9
ONERA H.T.:	Uncharged	135	933	1129	14.3
As Sol. + 1050°C, 16h air cool + 850°C, 48h	Ch. 5h, 20°C H_2SO_4 1 N	126	929	1111	14.9
	Ch. 5h, 150°C Molten salts + aged 20°C, 7 days	132	938	909	7.0
	Ch 5h, 150°C Molten salts + aged 150°C, 5h	117	911	908	8.9

C-3

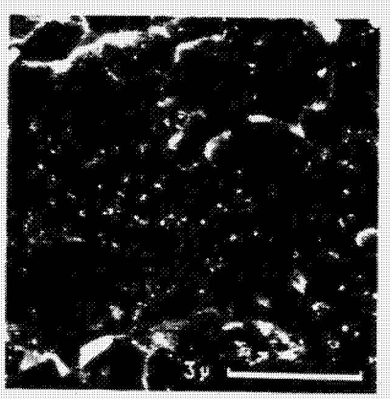

UNCHARGED : Fracture appears to occur by ductile tearing of the γ matrix

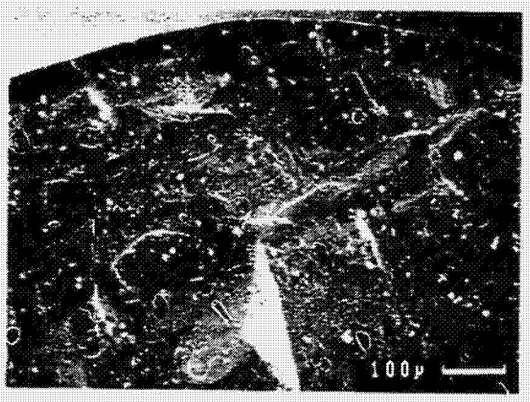

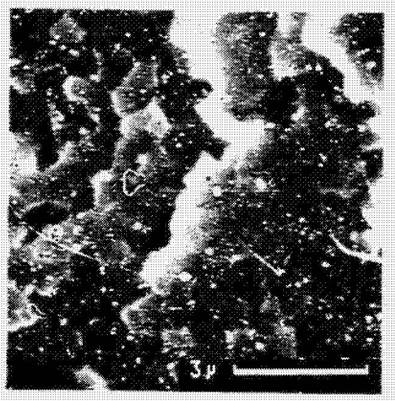

CHARGED : Outer embrittled region failure along (001) suggests a preferential decohesion along the γ/γ' interface

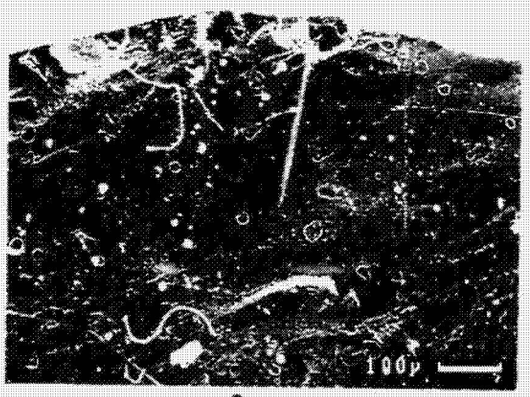

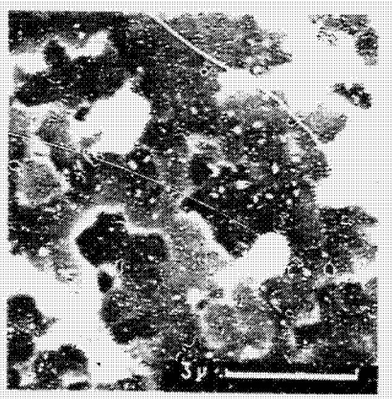

CHARGED + DESORB/15[illegible]°C : Embrittled regions continue to be evident but only in association with voids

SIDE VIEW OF FAILED TENSILE SAMPLES

ONERA HEAT TREATMENT

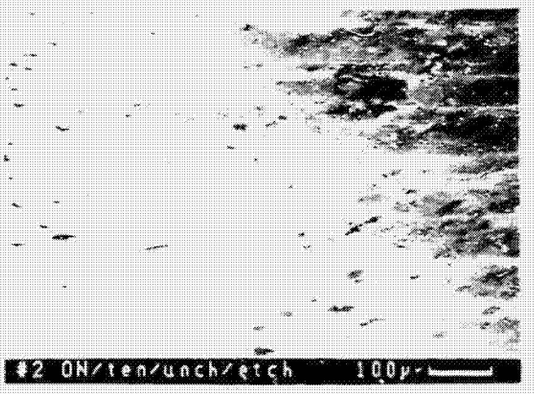

UNCHARGED: Very few cracks

CHARGED: Many transverse cracks

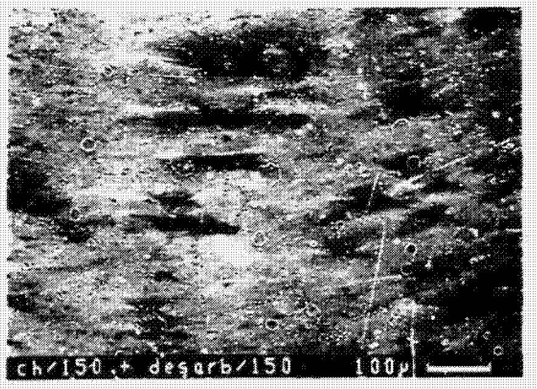

CHARGED + DESORB/ 150 C: Discontinuous cracking systematically associated with voids

Fatigue Data (ONERA H.T., test at 20°C in air, $\dot{\varepsilon} = 5.10^{-2} s^{-1}$, $\Delta\varepsilon_p$=constant, R=-1, n_u and n_c: number of cycles to fail of respectively uncharged and charged samples)

Sample Size	Charging and testing conditions	$\Delta\varepsilon_p$	E GPa	$Y_{0.2}$ MPa	UTS MPa	ε_p %	n	n_u/n_c
Bulk sample	Uncharged	0.4	130	1070	1440	22.3	57	
	Ch.5h,150°C Molten salts	0.4	146	1070	1220	6.4	16	3.56
Hollow sample	Uncharged	0.4	145	1040	1250	32.8	82	
	Ch.5h,150°C Molten salts	0.4	159	1100	1230	2.4	6	13.7
	Uncharged	0.4	157	1100	1290	20.4	51	
	Ch.5h,150°C Molten salts	0.4	161	1080	1030	4.8	12	4.25
	Uncharged	0.1	147	1060	1210	18.1	181	
	Ch.5h,150°C Molten salts	0.1	159	1080	1100	2.6	26	6.96

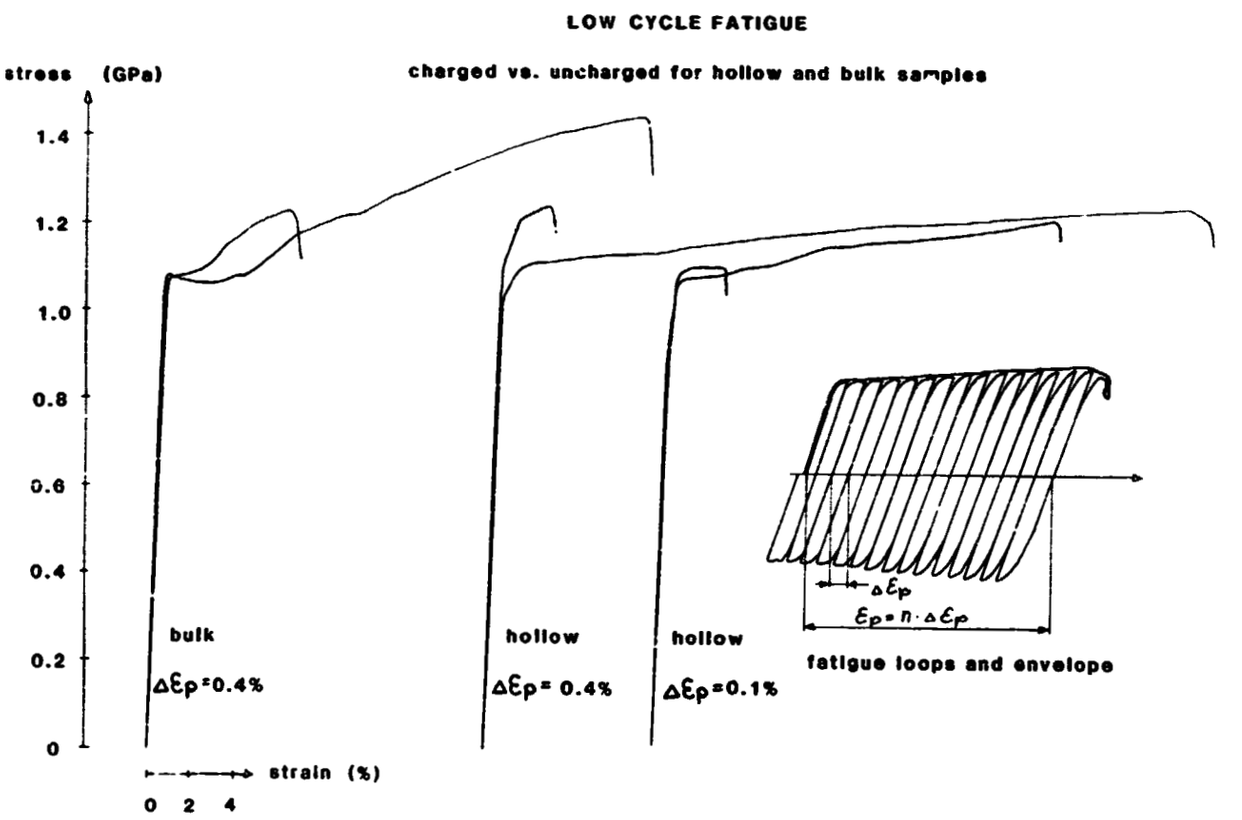

FRACTURE OF FATIGUE SPECIMENS WITH HYDROGEN

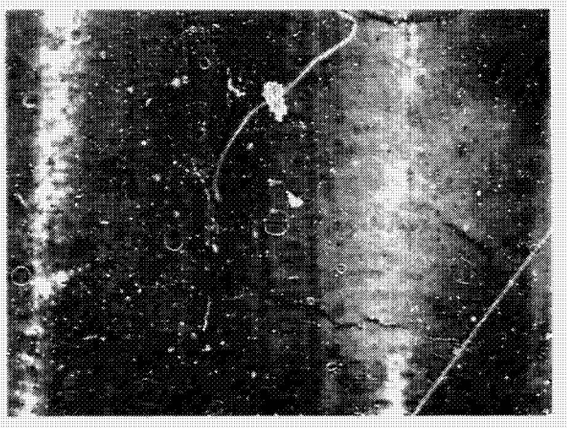

Change in crack path associated with the dendritic structure

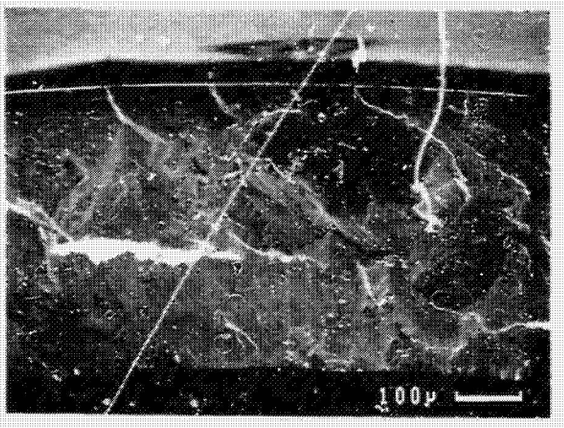

Outer embrittled region enhanced by voids

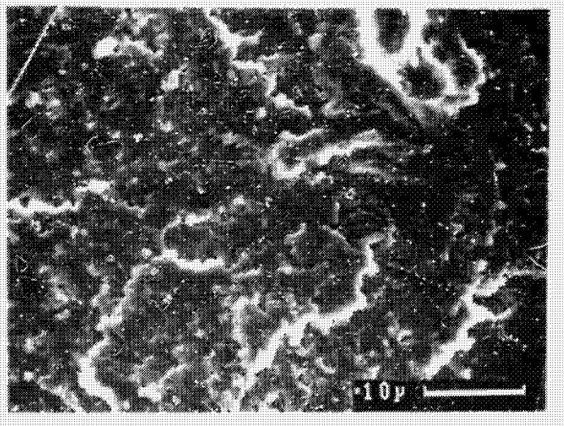

Fracture along the γ/γ' interface

OVERVIEW OF INSTRUMENTATION PROGRAM

William C. Nieberding
National Aeronautics and Space Administration
Lewis Research Center
Cleveland, Ohio 44135

A great deal of emphasis in the SSME durability program is being placed on the development of analytic codes for designing components and predicting their expected life. Before any faith can be placed in a code, there must be a series of benchmark experiments specifically designed and instrumented to verify the operating conditions that have been used as input to the code and to determine whether the code does indeed predict the correct results.

The instrumentation portion of the durability program is specifically aimed at developing those sensors and instrument systems necessary to verify the codes. In most cases this calls for developing sensors and systems that are minimally intrusive so as not to perturb the conditions being measured. In addition, since the codes tend to work with high-resolution maps of such parameters as flow, strain, and temperature, the instrument systems must produce data that are very high in both spatial and temporal resolution.

Much effort has already been put into developing such instrumentation for aircraft engines. This program is designed to extend this work to include the operating conditions and materials of the SSME. Indeed, some of these conditions are far more stringent than in aircraft engines, but other conditions are less stringent.

In this session you will hear four papers on the development of instrument sensors and systems aimed primarily at verifying the analytic codes being developed in the other parts of the durability program.

THIN-FILM SENSORS FOR SPACE PROPULSION TECHNOLOGY

Walter S. Kim and David R. Englund
National Aeronautics and Space Administration
Lewis Research Center
Cleveland, Ohio 44135

Specific needs in the space shuttle main engine technology are measurements of temperature, heat flux, and strain on the components to assess their structural integrity and durability. SSME components such as the turbine blades of the high-pressure fuel turbopump are subjected to rapid and extreme thermal transients that contribute to blade cracking and subsequent failure (ref. 1).

The objective of this work is to develop thin-film sensors for SSME components. Thin-film sensors have been developed for aircraft gas turbine engines and are in use for temperature measurement on turbine blades to 1800 °F (fig. 1). The technology established for aircraft gas turbine engines will be adopted to the materials and environment encountered in the SSME. Specific goals are to expand the existing in-house thin-film sensor technology, to continue developing improved sensor processing techniques via grants or contracts, and to test the durability of aircraft gas turbine engine technology in the SSME environment.

EXISTING TECHNOLOGY

Through a series of NASA contracts with Pratt & Whitney Aircraft, the thin-film temperature sensor technology was developed for aircraft gas turbine engines (refs. 2 to 4). In this technology the turbine blades coated with a proprietary NiCoCrAlY anticorrosion coating are oxidized to grow an adherent, electrically insulating surface film of aluminum oxide. This film is augmented with sputtered Al_2O_3 and then the thermocouple is sputter deposited (fig. 2). Junctions between the thin films and the lead wires are formed by hot-compression diffusion bonding. These thin-film sensors have performed successfully in engine tests to 1800 °F for over 60 hr with less than 0.02 percent drift per hour.

STATUS OF WORK

An initial goal is to augment the in-house capability in thin-film sensor technology. A thin-film sensor laboratory is being installed in a refurbished clean room, and new sputtering and photoresist exposure equipment is being acquired. Also, the procurement of material samples is in progress, and an effort is under way to put the initial coating on the samples. The MAR-M 200 (+Hf) and MAR-M 246 (+Hf) along with other materials are to be coated with NiCoCrAlY and NiCrAlY coatings.

In an on-going research activity through a grant with UCLA, various coatings and their insulating films are being investigated for use in sensor development. An impetus of this activity is to develop a generic coating material that is comparable to the proprietary MCrAlY coating. Some coating deposition methods such as activated reactive evaporation and chemical vapor deposition are being explored. The emphasis is on improving the processing techniques for greater processing yield.

Another activity is the testing of existing thin-film thermocouple technology in an SSME environment. Test blades will be made from MAR-M 200 (+Hf), for which the gas turbine type of thin-film sensor was developed. These blades are to be instrumented with two thin-film thermocouples deposited on one side of the airfoil and a wire thermocouple embedded from the other side of the blade (fig. 3). These instrumented blades will be tested in the turbine blade tester at the Marshall Space Flight Center (fig. 4). Besides testing the survivability of the aircraft turbine type of sensor in an SSME environment, this program will provide a measurement of the cyclic thermal gradient imposed on the blades.

FUTURE PLANS

Presently the SSME turbine blades are coated only with NiCrAlY bond coating, which provides minimal thermal protection. As more information on structural integrity and durability becomes available, the blade and the coating material may change. In anticipation of future improvements many varieties of alloys and coatings will be tested for compatibility with thin-film sensors.

The thin-film technology extends to other sensors such as the strain gauge. Figure 5 shows a thin-film strain gauge sputtered onto an aluminum oxide beam. This thin-film strain gauge will be tested in a high-temperature oven to determine the performance characteristics and adhesion properties of the sensor deposited on a ceramic surface.

REFERENCES

1. Holmes, R.R: Vacuum Plasma Coatings for Turbine Blades. Proceedings of MSFC Advanced High Pressure O_2/H_2 Technology Conference. June 1984.

2. Grant, H.P.; and Przybyszewski, J.S.: Thin Film Temperature Sensor. NASA CR-159782. 1980.

3. Grant, H.P.; Przybyszewski, J.S.; and Claing, R.G.: Turbine Blade Temperature Measurements Using Thin Film Temperature Sensors. NASA CR-165201, 1981.

4. Grant, H.P.; Przybyszewski, J.S.; Claing, R.G.; and Anderson, W.L.: Thin Film Temperature Sensors, Phase III. NASA CR-165476, 1982.

Figure 1. - Thin-film thermocouples on first-stage turbine blades after combustor exhaust gas-stream tests. Tests included 30 cycles to 1200 K on airfoil concave side, to 1100 K on airfoil convex side, and to 700 to 900 K on platform for a total of 56.6 hr. Arrow B denotes poor initial adherence.

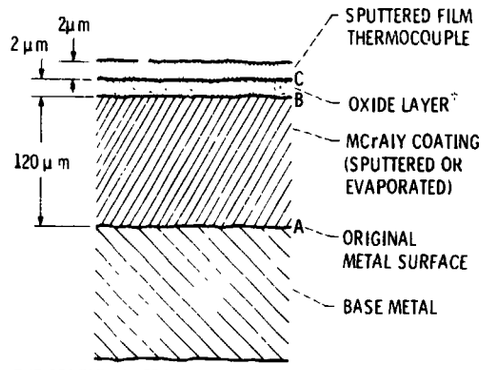

THE STABLE ADHERENT Al_2O_3 INSULATING LAYER IS OBTAINED BY AT LEAST 50-hr OXIDATION (AT 1300 K) OF THE COATING. FOLLOWED BY Al_2O_3 SPUTTERING.

Figure 2. - Thin-film temperature sensor on turbine blade.

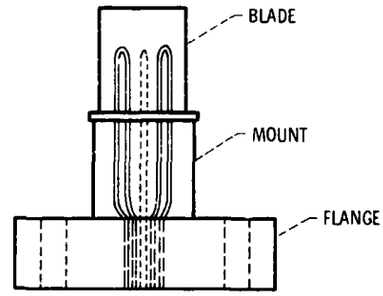

(a) Blade holder assembly. Three blades, each blade to have two thin-film thermocouples and one embedded-wire thermocouple.

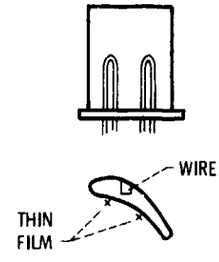

(b) Potential location. Two thin-film thermocouples on pressure or suction side, with wire thermocouple embedded from opposite side.

Figure 3. - Conceptual sketch of blade holder assembly.

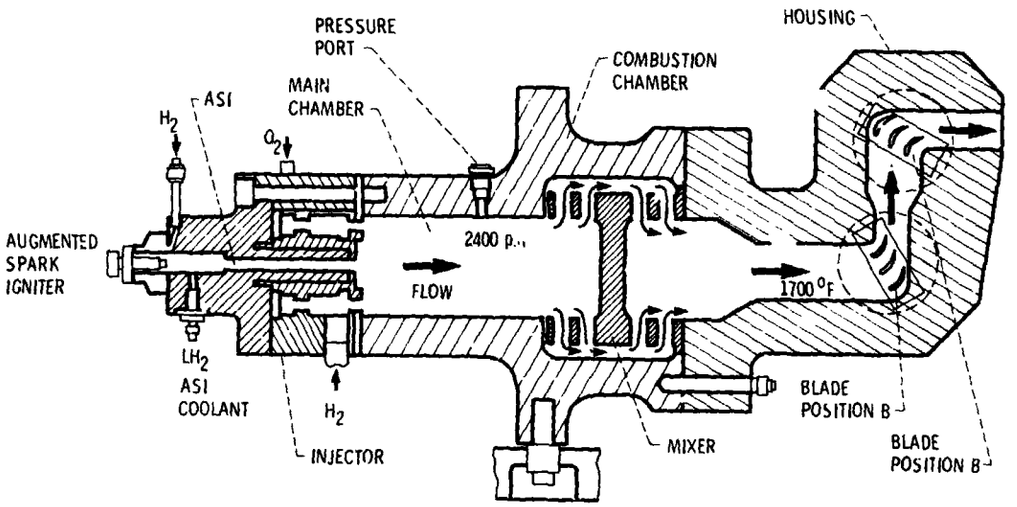

Figure 4. - Burner rig thermal cycling tester.

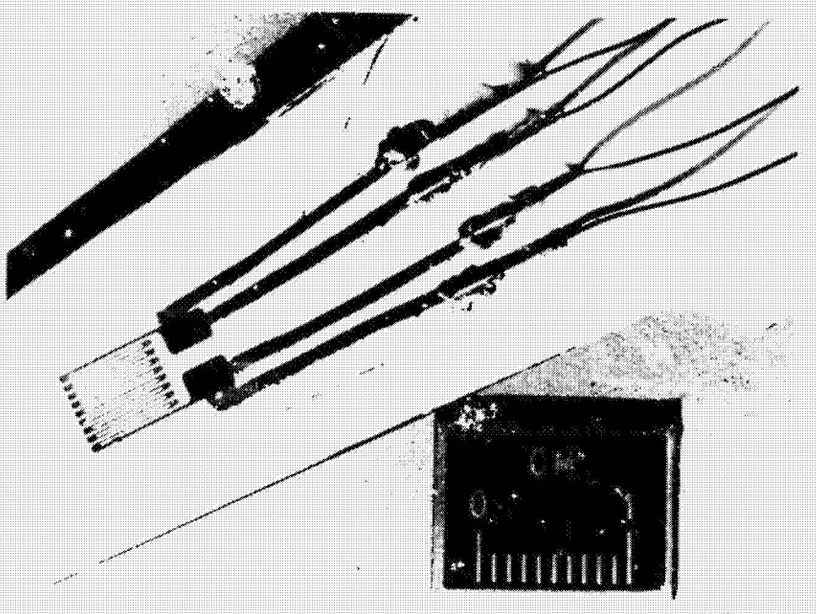

C-84-7482

Figure 5.- Thin-film strain gauge sputtered on aluminum oxide beam.

N85-27969

OPTICAL STRAIN MEASUREMENT SYSTEM DEVELOPMENT*

Christian T. Lant
Sverdrup Technology, Inc
Middleburg Heights, Ohio 44130

Investigations of physical phenomena affecting the durability of SSME components require measurement systems operational in hostile environments. The need for such instrumentation bore this contract to define and put into operation an optical strain measurement system. Sverdrup Technology, Inc., in cooperation with the Lewis instrument research laboratory, is currently developing this optical strain measurement system based on the speckle-shift method of Ichirou Yamaguchi (The Institute of Physical and Chemical Research, Japan). This is a noncontact, automatic method of measuring surface strain in one dimension that corrects for error due to rigid-body motion. It provides a gauge length of 1 to 2 mm and allows the region of interest on the test specimen to be mapped point by point. The output will be a graphics map of the points inspected on the specimen; data points will be stored in quasi-real time. This task is the first phase of a multiphase effort in optical strain measurement. Phase 2 will extend the technique to measure strain components in two dimensions.

BASIC PRINCIPLES

Theory shows that the difference between the speckle displacements for a pair of symmetrically incident laser beams is directly proportional to the surface strain parallel to the plane of incidence and independent of the translational and rotational components of motion. The speckle pattern created by the test specimen is interpreted as high-order interference fringes resulting from a random diffraction grating, being the natural surface roughness of the specimen. Strain induced on the specimen causes a change in spacing of the surface roughness, which in turn shifts the position of the interference pattern (speckles).

EXPERIMENTAL CONFIGURATION

In the experimental setup an argon-ion laser and a beam splitter provide the two symmetrical beams, which will each independently expose a linear photodiode array before and after stress is applied to the specimen. The "before" and "after" exposure patterns of the speckle in the array are cross-correlated for each beam to give the spatial shifts. After the shift from each beam is computed, the difference is taken to cancel out components due to rigid-body motion; the remaining shift is due to surface strain. The sensitivity of this strain gauge depends on the ratio of the pitch of the diodes in the linear array to the distance from the array to the test specimen.

The test specimen will be mounted on a stress fatigue testing machine, with specimen dimensions of approximately 100 mm x 20 mm x 1 mm. The center-to-center spacing of the diodes will be 15 μm with a sensor-to-specimen spacing of the order of a meter. Thus the resolution of the setup will be 10

---

*Work performed under Lewis task number 83-24-01.

to 20 microstrains, with an unlimited range because the incremental speckle displacements can be summed by using successive exposures. The system will be used for mechanically and thermally induced strain, and the experimentation will cover a temperature range of 20 to 600 deg Celsius. Testing will determine the amount of decorrelation of the speckle pattern at high temperatures. The upper temperature limit will be a function of this decorrelation. A gauge length of 1 to 2 mm corresponds to the spot size of the laser beams. The region of interest can be mapped by relocating the laser spots. Utilization of the natural surface structure of the specimen eliminates any need to artificially prepare the surface of the specimen before testing. However, for high-temperature strain measurements, cycling through the temperature range may be necessary to stabilize oxidation of the surface.

OPERATION

The system will be designed for a minimal amount of operator input; the procedure will be run by a microcomputer system. The operator will be required to position the laser spots through the terminal of the computer and to maintain this position with the aid of an area photodiode array. This area array will provide a graphics display of the test specimen and laser spots for a CRT and store location of the data points taken on the specimen. Motorized mirror mounts will be used to direct the beams onto the test specimen. This combination will ensure that relative movement between the test apparatus and the laser does not influence the accuracy of the strain measurement.

REFERENCE

1. Yamaguchi, I.: A Laser-Speckle Strain Gauge. J. Phys. E: Sci. Instrum., vol. 14, 1981. Printed in Great Britain.

SCOPE

Multi-task effort:

This task: One dimensional strain map

Future task: Measure strain of SSME components in two dimensions

TASK OBJECTIVES

Operationalize Yamaguchis' technique

- one dimensional strain measurement
- real or quasi-real time output of strain

OPTICAL STRAIN MEASUREMENT SYSTEM DEVELOPMENT

FEATURES

* Non-contacting measurement system
* Corrects for rigid body motion
* Gage length of 1 to 2 millimeters

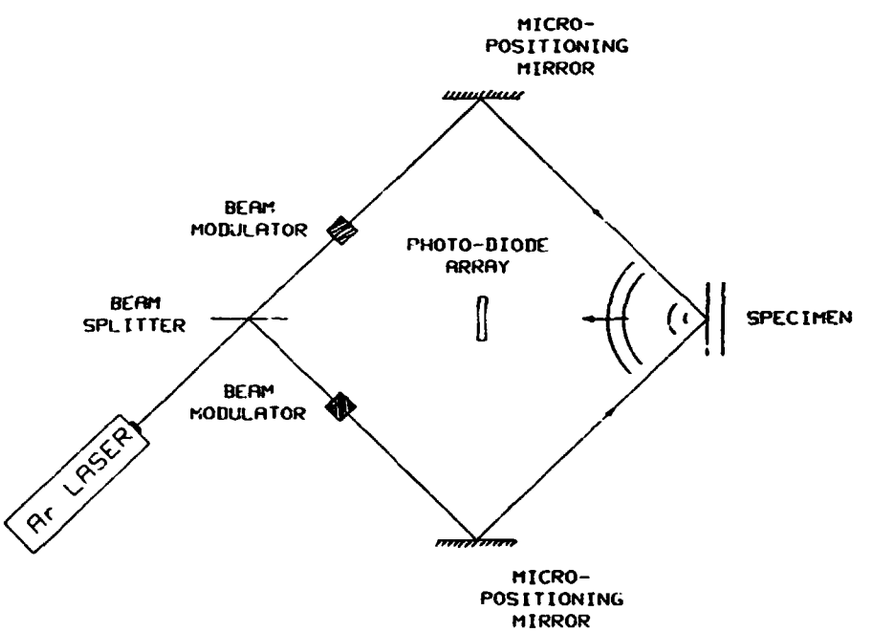

OPTICAL SYSTEM

Correlation Technique

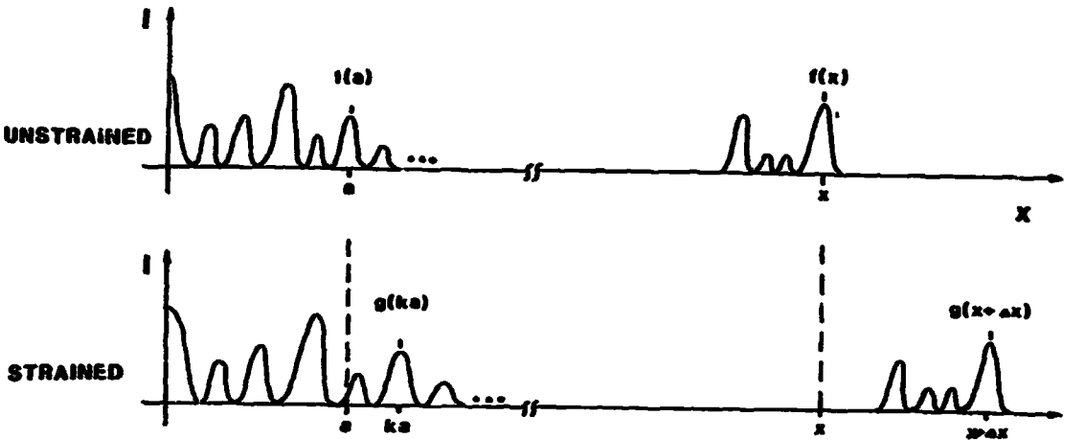

$$R = \lim_{T\to\infty} \frac{1}{T}\int_{a}^{a+T} f(x)\,g(x+\Delta x)\,dx$$

maxim. n of R ⇒ value of Δx

f(x)=g(x+Δx)

Δx=kx-x

STRAIN IS COMPUTED
FROM CORRELATION RESULTS :

1. Cross-correlation gives speckle displacement ΔX

2. Strain is directly proportional to ΔX :

$$\varepsilon = \frac{-\Delta X}{2L\sin\theta}$$

HEAT FLUX SENSOR CALIBRATOR

Curt H. Liebert
National Aeronautics and Space Administration
Lewis Research Center
Cleveland, Ohio 44135

The heat flux to space shuttle main engine (SSME) turbopump turbine blades may be as high as 10^7 W/m^2. This heat flux is 50 to 100 times that encountered in aircraft engines. The heat flux causes thermal transients that are of the order of 1 sec as temperature varies from perhaps 1500 K to 100 K. It is suspected that these transients cause durability problems in the turbine blades. To quantitatively evaluate the effect of these transients, heat flux sensors or gauges are needed to obtain data to verify analytical models (ref. 1). Because of these very high heat fluxes a new system must be developed for the calibration of heat flux sensors mounted on these blades.

OBJECTIVE

The objective of this effort is to design and fabricate a system for steady-state and transient calibration and durability testing of heat flux sensors for use in SSME turbine blades. Development will rely on experiment and analysis from many interdisciplinary fields of research including thin-film and wire thermocouples, materials, heat transfer, optics, and electric arc phenomena. Building on the techniques available in these fields, calibration and durability testing skills will be developed for measuring temperature and heat flux on SSME turbines.

LITERATURE SEARCH

The literature presents many methods for heat flux calibration. Most of the methods are based on the use of thermal radiation from solids; other methods are based on conduction or convection heat transfer modes (ref. 2). All of these methods are useful for calibration only at heat flux levels of one or two orders of magnitude less than those estimated for SSME turbopump blades. However, new developments in industrial electric arc engineering in the past several years have made electric arcs useful as a radiative heat source for calibration at the higher heat fluxes generated in SSME turbines. This development (fig. 1) is based on a patented electric arc lamp design (fig. 2, ref. 3) that produces optical radiation focused with a truncated elliptical mirror (ref. 4). The electric arc lamp design was based in part on research done at the Lewis Research Center during the 1960's and 1970's (ref. 5). Adjustable irradiances can be focused on the entire area of a pressure or suction surface of an SSME turbine blade at levels to 10^7 W/m^2 with a uniformity of 1 to 2 percent. The lamp will be remotely operated in either a pulsed or steady-state mode. Its performance is advertised as repeatable and independent of the operator or of the sensor being calibrated. Lamp life is several hundred hours.

CALIBRATOR DESIGN AND INSTALLATION

The calibrator will be used in a calibration and durability testing facility that includes equipment shown in figure 3. The calibrator consists of (1) the arc lamp, (2) a high-speed positioning table for placing standard and

special heat flux sensors in the incident beam of radiant heat flux, (3) provision for cooling the blade and special sensors inserted in the blade, (4) a computer for controlling the positioning table (local and remote), storing electrical output values from sensors, and calculating heat flux from these values, and (5) a pyrometer for measuring sensor surface temperatures.

CALIBRATION OF THE CALIBRATOR

The intensity of the arc will be calibrated with commercially available heat flux sensors that have been factory calibrated by techniques traceable to those used by the National Bureau of Standards.

DEMONSTRATION TESTS

Facility tests will include measurement of sensor electrical output as a function of known radiant heat flux input. Both transient and steady-state tests will be performed.

Heat transfer analysis and thermal stress experiments are proceeding for the design and fabrication of, and the reduction of data from, special heat flux sensors mounted in turbopump airfoils. The special sensors will be used with the calibrator and other equipment to demonstrate the operational aspects of the facility.

REFERENCES

1. Liebert, Curt H., Gaugler, Raymor E.; and Gladden, Herbert J.: Measured and Calculated Wall Temperatures on Air-Cooled Turbine Vanes with Boundary Layer Transition. NASA TM-83030, 1983.

2. Liebert, Curt H., et al.: High Temperature Thermocouple and Heat Flux Gauge Using a Unique Thin Film - Hardware Hot Junction. NASA TM-86898, 1984.

3. Vortek Industries, Ltd.: 100,000-W Arc Lamp (Model 107). Industrial Research and Development. vol. 25, no. 10, Oct. 1983, p. 107.

4. Camm, D.M.: Optimal Reflectors for Coupling Cylindrical Sources and Targets of Finite Dimensions. Applied Optics, vol. 23, no. 4, Feb. 15, 1984, pp. 601-606.

5. Decker, Arthur J.; and Pollack, John L.: 400 Kilowatt Argon Arc Lamp for Solar Simulation. NASA TM X-68042, 1972.

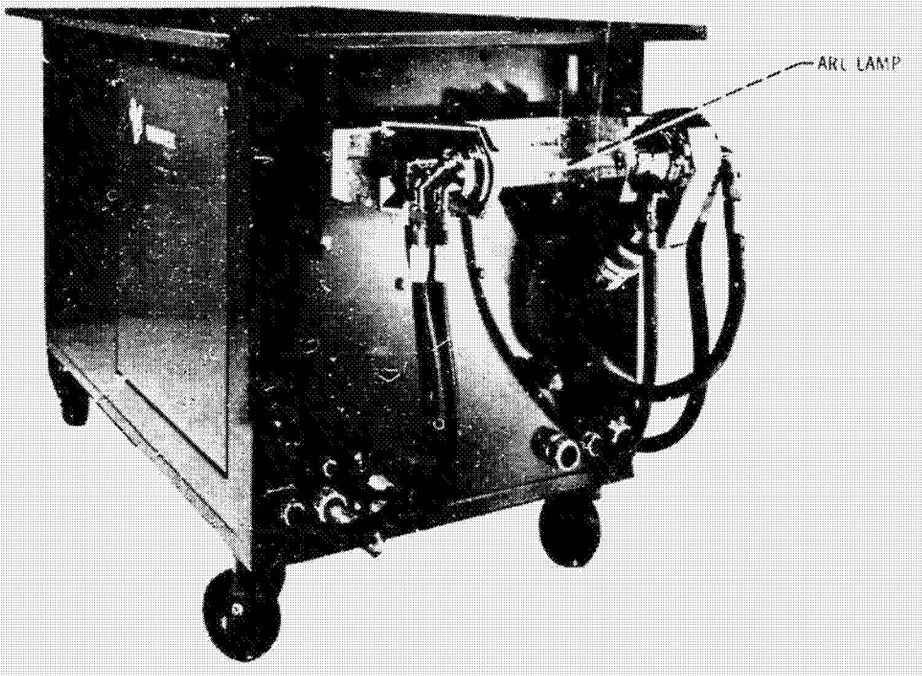

Figure 1. - Vortex lamp

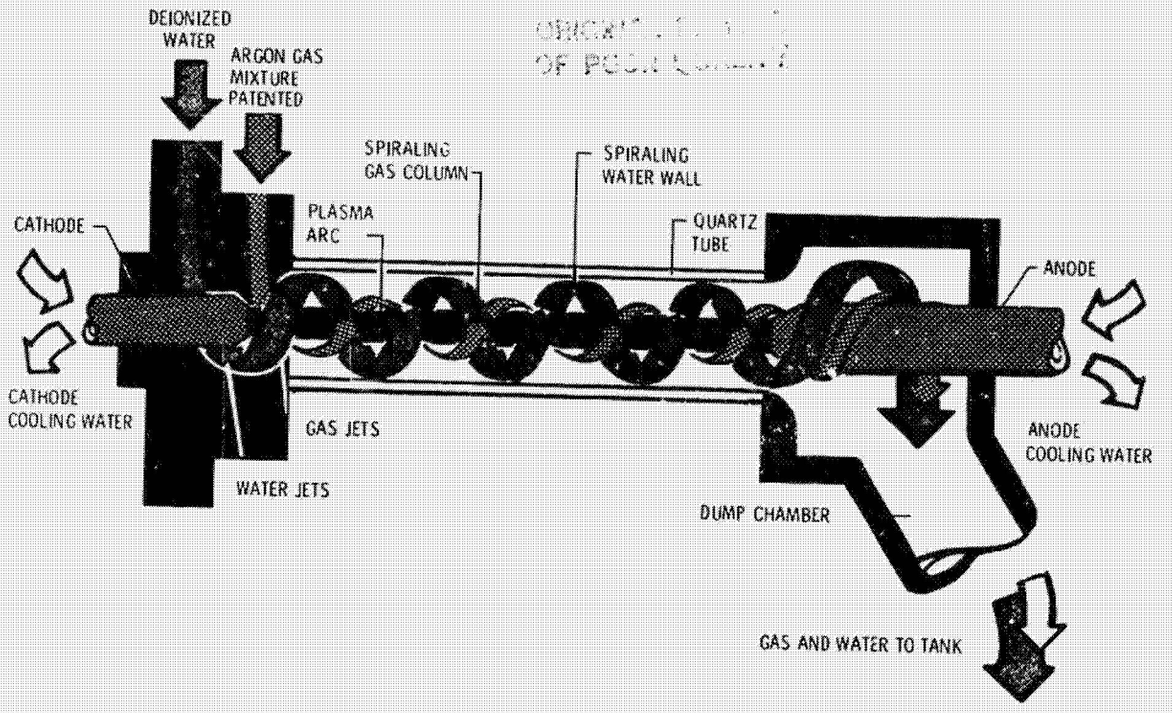

Figure 2. - Arc lamp

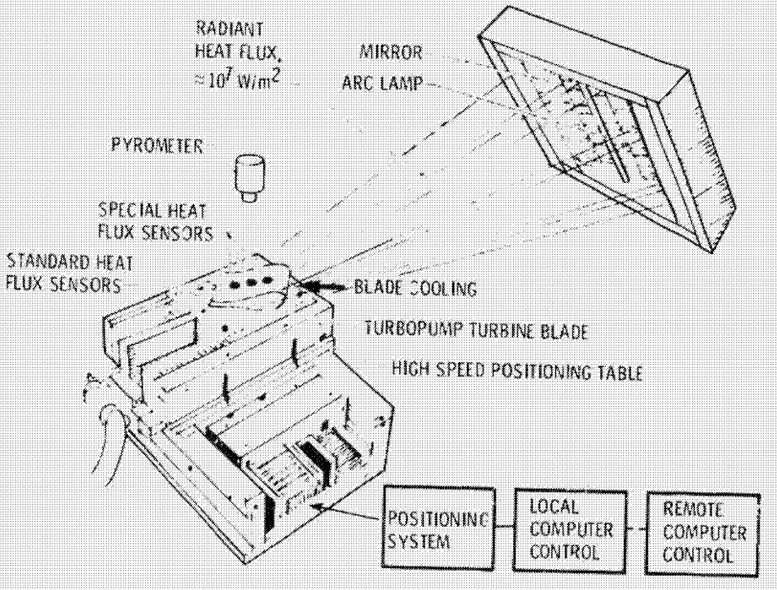

Figure 3. - Schematic for calibration of heat flux input versus sensor electrical output.

N85-27971

FEASIBILITY OF MAPPING VELOCITY FLOW FIELDS IN SSME POWERHEAD BY LASER ANEMOMETRY TECHNIQUES*

D.G. Pelaccio, L.K. Sharma, T.V. Ferguson,
J.M. Maram, and S. Pinkowski
Rockwell International
Canoga Park, California 91304

The requirements of higher performance for the space shuttle main engine (SSME) and future Earth-to-orbit propulsion systems dictate the use of efficient liquid-fueled rocket engines with cycles that require lightweight, high-pressure, compact powerhead configurations. These configurations typically exhibit complex, nonuniform hot-gas internal flows. Such propulsion systems must be designed with an emphasis on long life, high reliability, and minimum maintenance. In-depth characterization and understanding of the powerhead flow field is essential for optimal design of this key engine component. NASA is currently planning hot-fire engine tests for the SSME Component Enhancement Technology Program to establish a detailed data base from which to address powerhead flow issues and to verify advanced, three-dimensional, fluid-dynamic analysis models currently under development.

Because of the flow environment associated with the SSME powerhead pressure (3000 psia), temperature (1900 °R), and mechanical complexity and the high-vibration test stand environment, detailed flow measurements are at best difficult to make. During the past year the NASA Lewis Research Center initiated a study with Rocketydne that addresses the feasibility of using laser anemometry techniques to map velocity flow fields in an SSME powerhead. This is in support of the proposed model verification experiments.

In the on-going study three engine powerhead component flow environments - (1) the high-pressure fuel turbopump preburner, (2) the fuel turbopump turbine rotor and stator region, and (3) the 180° turnaround duct - are being considered. Flow parameters to be measured by the anemometry techniques are time-averaged values of the velocity magnitude and flow direction, turbulence intensity, velocity component correlations, integral time scale, and turbulence spectrum.

Key technical issues such as identifying feasible means of optical access to the high-pressure, high-temperature measurement flow regions, and measurement system compatibility with the test environment are addressed. At the conclusion of the study a measurement system is to be defined that will include layout sketches and specifications of component hardware that will be compatible with mapping the flow field in one of the regions of interest.

---

*Work performed under NASA contract NAS3-24356.

1. Report No.	2. Government Accession No.	3. Recipient's Catalog No.
NASA CP-2381		

4 Title and Subtitle	5. Report Date
Structural Integrity and Durability of Reusable Space Propulsion Systems	May 1985
	6. Performing Organization Code 553-13-00
7. Author(s)	8. Performing Organization Report No. E-2554
	10. Work Unit No
9. Performing Organization Name and Address National Aeronautics and Space Administration Lewis Research Center Cleveland, Ohio 44135	11. Contract or Grant No.
	13. Type of Report and Period Covered Conference Publication
12. Sponsoring Agency Name and Address National Aeronautics and Space Administration Washington, D.C. 20546	14. Sponsoring Agency Code

15. Supplementary Notes

The workshop was sponsored by NASA Headquarters and the NASA Lewis Research Center.

16. Abstract

A two-day conference on the structural integrity and durability of reusable space propulsion systems was held on June 4 and 5, 1985, at the NASA Lewis Research Center. Presentations were made by industry, university, and government researchers organized into four sessions: aerothermodynamic loads; structural dynamics, fatigue, fracture, and consititutive modeling; and instrumentation. The principal objectives of the conference were to disseminate research results to date and future plans in each of the four areas. This publication contains the extended abstracts and the visual material presented during the conference.

17. Key Words (Suggested by Author(s))	18. Distribution Statement
Earth-to-orbit propulsion; Reusable rocket systems; Aerothermodynamic loads; Fatigue; Constitutive modeling; Instrumentation	Unclassified - unlimited STAR Category 20

19. Security Classif. (of this report)	20. Security Classif. (of this page)	21 No. of pages	22. Price*
Unclassified	Unclassified		

*For sale by the National Technical Information Service, Springfield, Virginia 22161